

Inaugural dissertation

for
obtaining the doctoral degree
of the
Combined Faculty of Mathematics, Engineering and Natural
Sciences
of the
Ruprecht - Karls – University
Heidelberg

Presented by

Carolin Schunke (M.Sc.)

born in Alfeld (Leine), Germany

Oral examination: 04.04.2025

Phosphorylation-Dependent Remodeling
of the FRQ-FRH-CK1a Complex
in the *Neurospora crassa* Circadian Clock

Referees:

Prof. Dr. Michael Brunner

Prof. Dr. Thomas Höfer

Besser als die Unwissenden sind
diejenigen, die Bücher lesen;
besser als diese – diejenigen,
die das Gelesene behalten;
besser als diese – diejenigen,
die das Gelesene verstehen;
besser als diese – diejenigen,
die ans Werk gehen.

Indische Weisheit

Acknowledgements

First of all, I would like to thank Michael for accepting me as a PhD student in his lab and letting me join the Brunner group. Thank you for the fascinating project that began with WCC and then led me through FRQ to FRH. Thank you for the many fruitful discussions that revolved around my project, science in general, and even vacations.

Thank you to everyone who is or has been part of the Brunner lab: Axel, thank you for your help in experimental setups and your interest and discussions about my results. Sabine, thank you for giving me motivational talks in the morning (Bergfest) and helping me with *Neurospora* experiments and sharing your seemingly endless knowledge about technical setups. A big thank you also goes to Martina, first, for your relentless efforts and helping me organize my paperwork and secondly thank you for reminding me to always focus on the essentials and not to lose sight of the image of toasting together. Bianca, thank you for your help in cell culture, great tips and good talks in the Monday-Wednesday lunch club. Thomas, thank you for your help with everything technical, for the many incredible conversations on a number of topics I am not versed in, especially weapons, chemistry and laws. Gabi, for always having a sympathetic ear and having good talks in the early morning.

I am also deeply grateful to the former members of the lab: Michael Oehler, Anton Shostak and Marina Pelzl, who helped me get used to the lab and shared many protocols. Anna, thank you for making me feel welcome in our shared lab (522!) and sharing many nerdy talks about gaming, anime, series and music (#TheWallOfGlassNeverStoppedUs). Dani, I cannot thank you enough for your guidance (especially in the beginning). Thank you for helping me with my thesis and always being open to discussing lab-related topics, finances, or even amazing podcast recommendations. Min, thank you for being on the same ship, struggling alongside each other on our projects (We can do it). Thank you also for always sharing the best food recommendations. Fidel, thank you for good talks and giving helpful advice, especially regarding data processing and the writing process.

Reshmika, thank you for the fun conversations in our shared lab and giving me a small introduction into Indian culture, food and music. Ming, thank you for your bubbly optimism that creates a good atmosphere and our entertaining lunch talks. To the both of you: all the best for your projects, keep at it. At one point, all of the work will pay off!

Outside the lab, I want to thank the friends I made in Heidelberg. Thank you Briyanka, Nathalie, Tom, Robin and Ramon for the enjoyable company, fun evenings, PubQuiz nights and in general the good time. A special thanks also goes to the 'inner circle'. Thank

you Michelle and Jenny for making my time here as enjoyable as it was (and I hope for more good times to come in the future of course). Thank you for all the good talks, discovering Heidelberg together, shared times, participating in (mostly) fun yoga classes and finding the most interesting books to read and discuss together while enjoying bubble tea or ice cream (though Jenny always chose the best flavor).

Bella, thank you for being my best friend through all these years. Thank you for introducing me to gaming all this time ago and supporting me during my ups and downs during my PhD and staying by my side even without being physically present. Kati, we got to know each other during our first day of our Bachelors and it stuck! Many thanks for sticking through this whole journey of Bachelor, Master and PhD/ Ref together and becoming best friends on the way!

Bella and Kati, looking back, it's amazing how much we've grown, and I'm excited for the decades of memories we'll continue to create.

Last but not least I want to thank my family. I am more grateful for you than I could ever express on these pages. Mama and Papa, without your endless support I would not be at the point in my life that I am. Both of you allowed me to walk my path and guided me to pursue my goals. Thank you.

Sarah, even though our relationship as sisters had its ups and downs, I am glad that I have you in my life and I am grateful to you that you support me and my life choices. Thank you Oma Anni and Opa Karl for being there for me and being more excited about me finishing my PhD than even I. You always stood behind me and my goals. Thank you!

Table of Contents

List of Figures	V
List of Tables	VI
Abbreviations.....	VII
Abstract.....	1
Zusammenfassung	2
1. Introduction.....	3
1.1 The evolution of circadian clocks	3
1.2 The circadian clock of <i>Neurospora crassa</i> (<i>N. crassa</i>).....	4
1.3 The Mammalian circadian clock.....	6
1.4 Intrinsic disorder in clock proteins.....	7
1.5 The pacemaker of the circadian clock, FRQ.....	10
1.6 Helicase FRH is the homologue of Mtr4	13
1.7 CK1a	14
1.8 Heterodimeric transcription factor WCC is involved in light and dark response of the circadian clock.....	15
1.9 Aim of the thesis	18
2. Methods	19
2.1 Microbiological methods	19
2.1.1 Preparation of bacterial DMSO stocks	19
2.1.2 Cultivation of <i>E.coli</i>	19
2.1.3 Transformation of chemocompetent <i>E. coli</i>	19
2.1.4 Cultivation of <i>N. crassa</i>	19
2.1.5 Transformation of <i>N. crassa</i>	20
2.2 Molecular biological methods	20
2.2.1 Determination of DNA and protein concentrations.....	20
2.2.2 Extraction of plasmid DNA from <i>E. coli</i>	21

2.2.3 Native protein extraction from <i>N. crassa</i>	21
2.2.4 Polymerase chain reaction (Q5)	21
2.2.5 Site-directed mutagenesis.....	23
For the introduction of mutations, site-directed mutagenesis PCR was employed. The system of QuikChange II XL Site-Directed Mutagenesis Kit was developed by Agilent (CAT# 200521). The kit was mostly used according to the manufacturer's instructions. The conditions for the PCR can be found in table 2.2.5a and 2.2.5b.	
2.2.6 Purification of PCR products	24
2.2.7 Restriction enzyme free cloning (cloning with overlapping regions).....	24
2.2.8 Cloning with restriction enzymes.....	25
2.3. Mammalian cell culture and sample preparation	26
2.3.1. Cell culture maintenance	26
2.3.2. Transient transfection with plasmids.....	26
2.3.3. Protein extraction from mammalian tissue culture	27
2.3.4 Incucyte Zoom analysis.....	27
2.3.5 Leptomycin B treatment.....	28
2.4 Biochemical and analytical methods.....	28
2.4.1 Agarose gel electrophoresis	28
2.4.2 SDS-PAGE.....	28
2.4.3 Western blotting	29
2.4.4 Luciferase reporter assay (<i>in vivo</i>)	29
2.5 Protein biochemical methods	30
2.5.1 Immunoprecipitation	30
2.5.2 Gel filtration (Size exclusion chromatography)	30
2.5.3 In vitro phosphorylation	31
3. Materials.....	32
3.1 Plasmids	32
3.1.1 Cell culture plasmids	32

3.1.2 <i>Neurospora</i> plasmids	32
3.2 Oligonucleotides	33
3.2.1 Oligonucleotides for mammalian vectors	33
3.2.2 Oligonucleotides for <i>Neurospora</i> vectors.....	37
3.3 Antibodies.....	37
3.4 Solutions and buffers for biochemical methods	38
3.5 Media and solutions for the handling of <i>E. coli</i>	41
3.6 Media and solutions for the growth and transformation of <i>N. crassa</i>	41
3.7 Enzymes, chemicals, disposals and kits.....	44
3.8 Machines, devices and reuseables	49
3.9 Service providers, web services and software	51
4. Results.....	52
4.1 The overexpression of FRQ, WCC and FRH in U2OS T-REx cells allows for the screening of the clock proteins without the influence of other factors.....	52
4.2 FRQ-FRH and WCC co-localization: validation in U2OStx cells.....	54
4.2.1 FRH prevents the accumulation of FRQ in nuclear foci	55
4.2.2 FRQ has three functional NLS sequences	58
4.2.3 FRQ has three functional NLS in <i>N. crassa</i> of which one is essential for clock function	61
4.2.4 WC-2 supports nuclear accumulation of WC-1.....	63
4.3 Dissecting the FFC-WCC interaction in circadian regulation: impact of FRH ...	64
4.3.1 Investigating the role of FRH in FRQ and WCC co-localization and interaction	64
4.3.2 FRQ and WCC exhibit co-localization in nuclear foci independently of FRH.....	66
4.3.3 The C-terminus of FRQ interacts with WC-1.....	68
4.3.4 FRQ and WC-2 co-localize in nuclear foci	69
4.3.5 FRH does not interact with WCC in absence of FRQ.....	70

4.4 FRH disrupts FRQ interaction with WC-1 and WC-2	71
4.4.1 FRH and WC-1 binding to FRQ: mutually exclusive interactions in the C-terminal region	71
4.4.2 FRH prevents the interaction of FRQ with WC-2.....	73
4.5 Phosphorylation-driven regulation of FRQ-FRH interaction may have an impact on WCC binding.....	75
4.5.1 Phosphorylation of FRQ by CK1a induces its dissociation from FRH and nuclear export.....	75
4.5.2 Native FFC dissociates upon phosphorylation of FRQ by CK1a	78
5. Discussion	81
5.1 Studying the FFC complex: a technical question.....	81
5.2 FRH is anchored to the C-terminal part of FRQ and disrupts FRQ self-interaction.....	82
5.3 FRH dissociates from phosphorylated FRQ.....	84
5.4 The subcellular localization of FRQ is regulated by three NLSs and one NES....	85
5.5 FRH masks the WCC binding-site	89
5.6 Model	93
5.7 Conclusion and outlook.....	95
6. References	97
7. Appendix	108

List of Figures

- Figure 1.4 The core components of the circadian clock contain intrinsically disordered regions
- Figure 1.5 AlphaFold-derived model of FRQ
- Figure 1.6 Comparison of the crystal structure of FRH and Mtr4p
- Figure 4.1 Transient expression and localization of fluorescently tagged *N. crassa* clock proteins in U2OStx cells
- Figure 4.2.1a The C-terminus of FRQ is not essential for foci-formation
- Figure 4.2.1b Saturating amounts of FRH binding to FRQ prevent FRQ nuclear foci-formation in U2OStx cells
- Figure 4.2.2 FRQ contains three NLSs
- Figure 4.2.3 NLS1, NLS2 and NLS3 of FRQ affect circadian phase and period length
- Figure 4.2.4 WC-2 recruits WC-1 to the nucleus
- Figure 4.3.1 Saturating amounts of FRH interfere with binding of FRQ to WCC
- Figure 4.3.2 FRQ interacts with WCC in the absence of FRH
- Figure 4.3.3 FRQ can interact with WC-1 and WC-2 individually
- Figure 4.3.5 FRH does not interact with WCC
- Figure 4.4.1 FRH interferes with binding of FRQ^{C-term} to WC-1
- Figure 4.5.1a CK1a phosphorylates FRQ, FRQ^{6B2} and FRQ⁹ in U2OStx cells over the course of time
- Figure 4.5.1b Phosphorylation of FRQ by CK1a triggers its dissociation from FRH and nuclear export
- Figure 4.5.2a Hyperphosphorylated FRQ does not interact with FRH in *Neurospora*
- Figure 4.5.2b Phosphorylation of FRQ by CK1a triggers its dissociation from FRH
- Figure 5.4 Prediction of coiled-coil domains in FRQ using npsa-prabi
- Figure 5.6 Model of our current understanding of the modulation of FRQ by CK1a and FRH
- Figure S1 Overview of FRQ constructs
- Figure S2 Subcellular localization of FRH
- Figure S3 Saturating amounts of FRH interfere with binding of FRQ to WCC
- Figure S4 FRH and FRH^{R806H} compete with the binding of WC-1 to FRQ
- Figure S5 CK1a phosphorylates FRQ, FRQ^{6B2} and FRQ⁹ in U2OStx cells over the course of time
- Figure S6 Phosphorylation of FRQ by CK1a triggers its dissociation from FRH and nuclear export
- Figure S7 Phosphorylation of FRQ by CK1a triggers its dissociation from FRH

List of Tables

Table 2.2.4a	PCR reaction mix
Table 2.2.4b	PCR cycling conditions for Q5 polymerase
Table 2.2.5a	Pfu ultra PCR reaction mix
Table 2.2.5b	PCR cycling conditions for Pfu ultra mutagenesis
Table 2.2.7	2-step Q5 PCR program
Table 2.2.8	Restriction digestion for cloning with restriction enzymes
Table 2.3.2	Volumes for Xfect transfection
Table 3.1.1	Plasmids used for expression in U2OStx cells
Table 3.1.2	Plasmids used for transformation of <i>N. crassa</i>
Table 3.2.1	Oligonucleotides for mammalian vectors
Table 3.2.2	Oligonucleotides for <i>Neurospora</i> vectors
Table 3.3	Antibodies applied in Western blotting and Co-IP
Table 3.4.1	Phosphate buffered saline (PBS) pH 7.4
Table 3.4.2	Solutions for native <i>Neurospora</i> protein extraction (PEX)
Table 3.4.3	Solutions for native <i>Neurospora</i> protein extraction with NP40 (PEX +NP40)
Table 3.4.4	TAE (Tris-Acetic acid-EDTA)
Table 3.4.5	Laemmli sample buffer (Laemmli 1970)
Table 3.4.6	SDS gel mix
Table 3.4.7	SDS running buffer for SDS-PAGE
Table 3.4.8	Ponceau S staining solution
Table 3.4.9	Tris buffered saline (TBS) pH 7.4
Table 3.4.10	Luminol mix
Table 3.4.11	Gelfiltration buffer
Table 3.5.1	Super optimal broth (SOB)/ SOB with catabolite repression (SOC)*
Table 3.5.2	LB Medium and LB Agar plates
Table 3.6	Supplements
Table 3.6.2	Vogel's solution* (Vogel 1956)
Table 3.6.3	FGS (fructose-glucose-sorbose) solution
Table 3.6.4	Top agar
Table 3.6.5	Bottom agar
Table 3.6.6	Slant and flask medium*/**
Table 3.6.7	Composition of Luciferase plate medium
Table 3.6.8	Trace elements
Table 3.7.1	Enzymes
Table 3.7.2	Chemicals, beads and ladders
Table 3.7.3:	Disposals
Table 3.7.4	Kits
Table 3.8	Devices, machines and reusables
Table 3.9	Websites, Providers and Software

Abbreviations

aa	Amino acid
amp	Ampicillin
APS	Ammonium persulphate
ATP	Adenosine tri phosphate
BMAL1	Brain and Muscle ARNT like 1
bp	Base pairs
BSA	Bovine serum albumin
ccg	Clock controlled gene
CAMPK-1	Calcium/calmodulin dependent protein kinase I
CIP	Calf intestinal alkaline phosphatase
CK	Casein Kinase
CLK	CLOCK
CRY	CRYPTOCHROME
DMEM	Dulbecco's Modified Eagle Medium
DMSO	Dimethyl sulfoxide
DNA	Deoxyribonucleic acid
dsDNA	Double stranded DNA
DSHCT	Dead-box Spreading Helicase C-terminal Tail
DTT	DL-dithiothreitol, Cleland's reagent
EDTA	Ethylenediaminetetraacetic acid
<i>E. coli</i>	<i>Escherichia coli</i>
FBS	Fetal bovine serum
FCD	FRQ-CK1a interaction domain
FFD	FRQ-FRH interaction domain
FGS	Fructose-glucose-sorbose solution
FRH	FRQ interacting RNA helicase
FRQ	Frequency
GAM	Goat-anti-mouse secondary antibody
GAR	Goat-anti-rabbit secondary antibody
HEPES	N-(2-hydroxyethyl)piperazine-N'-(2-ethanesulfonic acid)
h	hour
HPR	Horseradish peroxidase
IDP	Intrinsically disordered protein
IDR	Intrinsically disordered region
IP	Immunoprecipitation/ immunoprecipitate
KO	Knock-out
Lae	Laemmli buffer = SDS
LB	Luria-Bertani medium
LOV	Light-oxygen-voltage domain
Luc	Luciferase
Min	Minutes
mK2	mKATE2

VIII

mNG	mNeonGreen
mRNA	Messenger ribonucleic acid
mut	Mutagenesis / mutagenized
MW	Molecular weight
<i>N. crassa</i>	<i>Neurospora crassa</i>
N-Medium	<i>N. crassa</i> standard growth medium
NES	Nuclear export signal
NLS	Nuclear localization signal
NP40	4-Nonylphenyl-polyethylene glycol
OD	Optical density
ON	Over night
ORF	Open reading frame
PAS	Per-Arnt-Sim domain
PBS	Phosphate buffered saline
PCR	Polymerase chain reaction
pdp	Phosphate-dependent phosphorylation
PER	PERIOD
PEST	Proline, aspartate, glutamate, serine, and threonine rich region
PEX	Native protein extraction under non-denaturing conditions
pip	Phosphate-independent phosphorylation
PKA	Protein kinase A
PMSF	Phenylmethylsulfonyl fluoride (inactivates serine hydrolases)
PP2A	Protein phosphatase 2A
QA	Quinic acid
rcf	Relative centrifugal force
RT	Room temperature
SOB	Super optimal broth
SCN	Suprachiasmatic nucleus
SD	Standard deviation
SDS	Sodium dodecyl sulphate
SDS-PAGE	SDS polyacrylamide gel electrophoresis
SEM	Standard error of mean
SOC	Super optimal broth with catabolite repression
TB	Terrific broth
TBS	Tris buffered saline
TCA	Trichloroacetic acid
Tris	Tris(hydroxymethyl)aminomethane
Triton X-100	Polyethylene glycol tert-octylphenyl ether
TTFL	Transcription-translation feedback loop
WC-1	White Collar 1
WC-2	White Collar 2
WCC	White Collar complex
WT	Wild-type

Abstract

The circadian clock of the filamentous fungus *Neurospora crassa* (*N. crassa*) is based on a negative transcriptional-translational feedback loop (TTFL), in which the transcriptional activator White Collar Complex (WCC) activates expression of *frequency* (*frq*), the central negative regulator of the clock. FRQ, together with FRQ-interacting RNA helicase (FRH) and casein kinase 1a (CK1a), forms the FRQ-FRH-CK1a complex (FFC), which inhibits the transcriptional activator of FRQ, WCC, by phosphorylation, thus completing the transcription-translation feedback loop (TTFL). CK1a, which is anchored to FRQ, hyperphosphorylates FRQ at its intrinsically disordered regions (IDRs) in a slow, temperature-independent manner, forming a module suitable for molecular time measurement. However, the molecular processes triggered by the hyperphosphorylation of FRQ and the way in which time is measured are not yet fully understood.

The present work aims at understanding this mechanism in more detail and therefore focuses on the role of phosphorylation in the remodeling of the FRQ-FRH-CK1a complex. For this purpose, fluorescently tagged versions of the central clock proteins of *N. crassa* were heterologously overexpressed in cultured mammalian cells and their interaction and subcellular dynamics were investigated by live cell imaging. A major result of this work is the discovery of a new and unexpected function of FRH within the framework of the circadian clock. FRH like its *Saccharomyces cerevisiae* homolog, Mtr4p, has an essential role as a helicase in the exosome complex in RNA metabolism. In the circadian clock, FRH protects its interaction partner FRQ from premature degradation. In this work, I uncovered a new role of FRH. My data show that FRH decodes the phosphorylation state of FRQ, triggering a two-step remodeling of the FFC complex. The FRQ dimer binds initially two FRH molecules. This hetero-tetrameric complex is inactive because binding of FRH blocks the interaction of FRQ with WCC. Slow phosphorylation of FRQ leads with a delay to the dissociation of one bound FRH molecule, resulting in activation of FRQ by exposure of a WCC binding. The complex interacts with WCC and supports its phosphorylation and inactivation by FRQ-bound CK1a. Further phosphorylation of FRQ leads eventually to the release of the second FRH. The FRQ dimer is then rapidly exported from the nucleus and degraded in the cytosol. These mechanisms ensure precise activation and inactivation of FRQ and emphasize the central role of FRH as a decoder of time-dependent signals in the circadian rhythm of *Neurospora*.

Zusammenfassung

Die zirkadiane Uhr des filamentösen Pilzes *Neurospora crassa* (*N. crassa*) basiert auf einer negativen transkriptionell-translationalen Rückkopplungsschleife (TTFL), in der der Transkriptionsaktivator White Collar Complex (WCC) die Expression von *Frequency* (*frq*), dem zentralen negativen Regulator der Uhr, aktiviert. Das FRQ-Protein bildet zusammen mit der FRQ-interagierenden RNA-Helikase (FRH) und der Casein-Kinase 1a (CK1a) den FRQ-FRH-CK1a-Komplex (FFC), der den WCC durch Phosphorylierung hemmt und so die Transkriptions-Translations-Rückkopplungsschleife vervollständigt.

CK1a, das an FRQ verankert ist, hyperphosphoryliert FRQ an seinen intrinsisch ungeordneten Regionen (IDRs) auf langsame, temperaturunabhängige Weise und bildet so ein Modul, das sich für molekulare Zeitmessungen eignet. Die molekularen Prozesse, die durch die Hyperphosphorylierung von FRQ ausgelöst werden, und die Art und Weise, wie die Zeit gemessen wird, sind jedoch noch nicht vollständig verstanden.

Die vorliegende Arbeit zielt darauf ab, diesen Mechanismus genauer zu verstehen und konzentriert sich daher auf die Rolle der Phosphorylierung beim Umbau des FRQ-FRH-CK1a-Komplexes. Zu diesem Zweck wurden fluoreszenzmarkierte Versionen der zentralen Uhrenproteine von *N. crassa* in kultivierten Säugetierzellen heterolog überexprimiert und ihre Interaktion und subzelluläre Dynamik mittels Live-Cell Imaging untersucht. Ein wichtiges Ergebnis dieser Arbeit ist die Entdeckung einer neuen und unerwarteten Funktion von FRH im Rahmen der zirkadianen Uhr. FRH spielt wie sein Homolog Mtr4p aus *Saccharomyces cerevisiae* eine wichtige Rolle als Helikase im Exosomenkomplex des RNA-Stoffwechsels. In der zirkadianen Uhr schützt FRH seinen Interaktionspartner FRQ vor vorzeitigem Abbau. In dieser Arbeit habe ich eine neue Rolle von FRH entdeckt. Meine Daten zeigen, dass FRH den Phosphorylierungszustand von FRQ dekodiert und dadurch einen zweistufigen Umbau des FFC-Komplexes auslöst. Zunächst binden zwei FRH-Moleküle an das FRQ-Dimer. Dieser Hetero-Tetramer ist inaktiv, da die Bindung von FRH die Interaktion von FRQ mit WCC blockiert. Eine langsame Phosphorylierung von FRQ führt mit zeitlicher Verzögerung zunächst zur Dissoziation eines der gebundenen FRH-Moleküls und damit zur Aktivierung von FRQ durch Exposition einer WCC-Bindungsstelle. Der Komplex interagiert mit WCC und unterstützt dessen Phosphorylierung und Inaktivierung durch FRQ-gebundenes CK1a. Die weiter fortschreitende Phosphorylierung von FRQ führt schließlich zur Freisetzung des zweiten FRH-Moleküls. Das FRQ-Dimer wird dann rasch aus dem Zellkern exportiert

und im Zytosol abgebaut. Diese Mechanismen gewährleisten eine präzise Aktivierung und Inaktivierung von FRQ und unterstreichen die zentrale Rolle von FRH als Decodierer zeitabhängiger Signale im zirkadianen Rhythmus von *Neurospora*.

1. Introduction

1.1 The evolution of circadian clocks

The circadian clock (Latin “circa” and “dies” meaning “about a day”) was first measured in 1729 by Jean-Jacques d'Ortous de Mairan who noted that plants showed rhythmic leaf movement that persisted even in darkness (de Mairan 1729, Gardner et al. 2006). Since then, circadian clocks have been discovered in many eukaryotes and several prokaryotes, highlighting clocks as a fundamental cellular feature across a wide range of organisms (Kondo et al. 1993, Bhadra et al. 2017, Sartor et al. 2023). The influence of the circadian clock on an organism can range from subtle effects, such as influencing photosynthesis rhythms to more extreme and more obvious outputs like controlling the sleep-wake cycles of mammals or spore production in filamentous fungi (Bell-Pedersen et al. 1996, Gardner et al. 2006, Wijnen and Young 2006). The primary function of the circadian clock is thought to be the orchestration of physiological responses and to synchronize these with environmental changes as well as to anticipate the latter, therefore creating a selective advantage for the organism (Pittendrigh 1960, Woelfle et al. 2004, Dodd et al. 2005).

Circadian clocks have fascinating properties: they maintain a period of approximately 24 h even under constant environmental conditions. Furthermore, the clocks can be entrained by rhythmically recurring environmental cues, known as “Zeitgebers” (German for time givers), which include factors like light, temperature, and food (Aschoff 1954). They also exhibit temperature compensation, ensuring that the period length remains relatively stable across a physiological temperature range (Aronson et al., 1994). Together, these properties enable robust oscillations in biochemical, physiological, and behavioral processes, aligning them with the day-night cycle (Pittendrigh 1960, Aschoff 1981).

Edgar and colleagues (2012) proposed that cellular timekeeping co-evolved with homeostatic redox mechanisms in response to the Great Oxidation Event (GOE) around 2.5 billion years ago. During this period, oxygen began to accumulate in the atmosphere due to the activity of photosynthetic bacteria, posing a significant threat to life forms that

had, until then, lived in an anaerobic environment. As the production of oxygen by photosynthetic bacteria is dependent on light, organisms had to adapt to the diurnal rhythm of oxygen production and its toxic by-products by evolving mechanisms to eliminate reactive oxygen species (ROS). Consequently, rhythmic oxidation-reduction cycles and their peroxiredoxin proteins, conserved across different phylogenetic kingdoms, evolved under similar selective pressures (O'Neill and Reddy 2011, Edgar et al. 2012, Fischer et al. 2016).

The circadian clocks of different phyla and kingdoms - including humans, insects, fungi, plants and bacteria - are based on a transcription-translation feedback loop (TTFL). While the TTFL mechanism is conserved, its core components vary widely, suggesting that circadian clocks have likely evolved independently throughout evolutionary history (Bünning 1959, Aschoff 1965, Konopka and Benzer 1971, Kondo et al. 1993, Sartor et al. 2023). TTFLs are auto-regulatory negative feedback loops which include positive elements such as transcription factors which directly or indirectly promote the expression of *clock controlled genes (ccgs)*. Among the *ccgs* are also the negative elements of the clock that promote the inhibition of the positive element and thus lead to the inhibition of their own expression resulting in negative feedback (Reischl and Kramer 2011, Diernfellner and Brunner 2020).

1.2 The circadian clock of *Neurospora crassa* (*N. crassa*)

The filamentous fungus *N. crassa* is an important model organism in chronobiology. Its circadian clock has been subject of extensive studies, making *N. crassa* an important system for understanding circadian rhythms (Beadle and Tatum 1941, Horowitz 1991, Galagan et al. 2003, Cha et al. 2015). *N. crassa* can sense environmental cues such as light, nutrients and temperature and use this information to generate molecular responses that optimize its adaptation to recurrent environmental changes (He et al., 2002). In particular, light synchronizes the *N. crassa* clock to environmental rhythms, inducing conidiation, and initiating chromophore production (Nelson et al. 1989, Olmedo et al. 2010).

The heterodimeric transcription factor White Collar Complex (WCC) and its inhibitor Frequency (FRQ) are the central element of the TTFL in *N. crassa*. The key transcription factor and thus the positive element of the TTFL is the heterodimeric WCC, consisting of

the two GATA-type zinc finger proteins White Collar-1 (WC-1) and White Collar-2 (WC-2) (Harding and Turner 1981, Degli-Innocenti and Russo 1984). The heterodimer is formed through their Per-Arnt-Sim domains (PAS) (Ballario et al. 1998, Cheng et al. 2002). Dimerization is important, because WC-1 alone is unstable and is stabilized by its interaction with WC-2 (Cheng et al. 2001, Cheng et al. 2002).

Once activated and bound to its target genes, the WCC supports transcription of *ccgs*. Hurley et al. estimated that up to 40% of all transcribed genes are under circadian control, categorized into daytime-activated genes for catabolism and nighttime-activated genes for growth (Hurley et al. 2014). Most important for the function of the circadian clock, WCC also drives the transcription of the circadian pacemaker gene *frequency* (*frq*).

The translated FRQ protein forms a homodimer, which recruits Casein Kinase 1a (CK1a) and FRQ-interacting RNA helicase (FRH). The resulting FRQ-FRH-CK1a (FFC) complex comprises the negative element of the TTFL. CK1a, anchored to FRQ via two FRQ-CK1a-interacting domains (FCD1 and FCD2), inhibits WCC's transcriptional activity by phosphorylating and inactivating it, initiating the negative feedback loop (Talora et al. 1999, Froehlich et al. 2003, He et al. 2003, Schafmeier et al. 2005, He et al. 2006, Querfurth et al. 2011).

Although, there is an interplay of phosphorylation and dephosphorylation by phosphatases, such as PP2A and PP4, phosphorylation of WCC accumulates over time (Schafmeier et al., 2008; Cha et al., 2005). Eventually, WCC becomes hyperphosphorylated, leading to its inactivation and stabilization, completing the feedback cycle (Schafmeier et al. 2005). Meanwhile, FRQ also undergoes progressive phosphorylation by CK1a, which initially leads to its inactivation and subsequently targets it for degradation via the ubiquitin-proteasome pathway (He and Liu 2005, Baker et al. 2009, Tang et al. 2009).

After FRQ degradation, WCC is slowly dephosphorylated and reactivated, then re-enters the nucleus, and regains transcriptional activity. The WCC exhibits a rhythmic oscillation in binding to the *frq* promoter. This oscillation generates rhythmic FRQ expression, which characterizes the circadian clock of *N. crassa*.

1.3 The Mammalian circadian clock

The mammalian circadian clock shares similarities with the *Neurospora* clock, especially in regulatory mechanisms involving post-translational modifications. In both systems, phosphorylation plays a critical role, particularly by CKI δ and CK1 ϵ in mammals, which are essential for maintaining the 24-h cycle (Akashi et al. 2002, Eide et al. 2005, Hirano et al. 2016). The stability of the mammalian PER protein, which functions analogously to FRQ in *Neurospora*, is also regulated by phosphorylation (Dunlap & Loros, 2017). Similar to FRQ, hyperphosphorylation of PER promotes its polyubiquitination and degradation (Eide et al. 2002, Eide et al. 2005, Shirogane et al. 2005, Reischl et al. 2007, Reischl and Kramer 2011).

The mammalian circadian clock is hierarchically organized, with a "master clock" in the suprachiasmatic nucleus (SCN) of the hypothalamus coordinating cellular clocks in peripheral organs. The SCN receives zeitgeber cues via the retinohypothalamic tract from light-sensitive retinal ganglion cells, adjusting the clock based on environmental light (Moore and Eichler 1972, Stephan and Zucker 1972, Inouye and Kawamura 1979, Berson et al. 2002, Warren et al. 2003).

The mammalian circadian system operates through a primary TTFL and several secondary feedback loops. The primary TTFL is driven by a core transcription activator. Circadian Circadian Locomotor Output Cycles Kaput (CLOCK) and Brain and Muscle ARNT like 1 (BMAL1) form a heterodimeric transcriptional activator via their PAS protein interaction domains, which promotes the transcription of clock-controlled target genes containing E-box *cis*-regulatory elements (Gekakis et al. 1998; Hogenesh et al. 1998). This includes key genes like PERIOD (PER1-3) and CRYPTOCHROME (CRY1 and CRY2), which form a feedback complex that inhibits CLOCK-BMAL1, similar to *Neurospora*'s FFC complex. (Kume et al. 1999, Bunger et al. 2000, Zheng et al. 2001, Sato et al. 2006, Andreani et al. 2015).

In addition to the primary TTFL, there are several secondary feedback loops in mammals (Lowrey and Takahashi 2004, Yin et al. 2010, Solt et al. 2011, Kato et al. 2014). Despite its increased complexity, the mammalian and *Neurospora* circadian clocks are based on similar regulatory mechanisms, underscoring similarities in circadian control even though the clocks are not evolutionarily conserved.

1.4 Intrinsic disorder in clock proteins

Many proteins, such as FRH, have a well-defined three-dimensional structure that determines their function (Ward et al. 2004, Conrad et al. 2016) (Figure 1.4). However, many proteins contain intrinsically disordered regions (IDRs) that allow them to switch between different conformational states, giving them functional flexibility. A large number of proteins with IDRs have been shown to undergo liquid-liquid phase separation (LLPS) *in vitro*, with examples documented in the LLPS database (LLPSDB; Li et al., 2020). Peng et al. estimated that 20.5% of the eukaryotic proteome is unstructured, with long disordered segments predicted for 17.4% of proteins (Peng et al. 2015).

These disordered regions are characterized by low complexity sequences in which charged and polar amino acids, such as serine, tyrosine, glutamine, glycine and asparagine, are overrepresented, while aromatic, aliphatic and hydrophobic residues are underrepresented (Alberti et al. 2019). This unique composition provides flexibility and allows intrinsically disordered proteins (IDPs) to interact with multiple molecules, often adopting different conformations depending on the binding partner. This flexibility is especially important for signal transduction junctions and regulatory proteins (French-Pacheco et al. 2022).

In recent years, LLPS has been linked to various biological processes, including RNA metabolism, gene regulation, and signal transduction (Boehning et al. 2018, Zhang et al. 2018, Tatavosian et al. 2019). For instance, the RPB1 domain of RNA polymerase II (Pol II) contains a C-terminal low-complexity domain (CTD) that is intrinsically disordered and capable of phase separation. This CTD is crucial for pre-mRNA synthesis and co-transcriptional processing (Zaborowska et al., 2016). Recent research has highlighted LLPS as a fundamental mechanism for the intracellular organization of membrane-less organelles (MLOs). Prominent examples of MLOs include stress granules, P-bodies, and the nucleolus (Banani et al. 2017, Boeynaems et al. 2018).

LLPS and intrinsic disorder are highly relevant and important mechanisms that can explain how the densely packed cellular space is organized to allow control over complex biochemical reactions in space and time (Banani et al. 2017).

Taking a closer look at the proteins of the circadian clock, intrinsic disorder has been described for all components of the mammalian circadian clock, such as the negative central elements PER and CRY as well as the transcriptional activators CLOCK and

BMAL1 (Gustafson and Partch 2015, Dunlap and Loros 2018). Intrinsic disorder has also been described for *Neurospora crassa*'s FRQ protein. Predictions assume that 85.5% of its sequence is intrinsically disordered with only few regions that form secondary structures marking it as an intrinsically disordered protein (IDP; Figure 1.4) (Hurley et al. 2013, Pelham et al. 2020). Recently, FRQ was also shown to phase separate *in vivo* in *Neurospora* (Tariq et al. 2024), highlighting that LLPS also seem to play a crucial role in the circadian clock.

FRH, a primarily structured protein with a helicase function, contains an intrinsically disordered region (IDR) at its N-terminus (Figure 1.4, second panel). This IDR plays a key role in binding to FRQ, distinguishing it from the structured domains associated with its helicase activity (Guo et al. 2010, Cha et al. 2011, Hurley et al. 2013, Conrad et al. 2016).

To carry out its biological function as a kinase, CKI employs a catalytic domain that is fully structured. However, it also contains an intrinsically disordered region (IDR) in its C-terminal tail, which provides structural flexibility (Figure 1.4, third panel). This C-terminal tail is associated with auto-phosphorylation and auto-inhibition, which regulate the kinase activity of CKI (Carmel et al. 1994, Graves and Roach 1995, Xu et al. 1995).

Prediction tools, such as MobiDB, estimate WC-1 to be approximately 60% disordered, featuring only a few structured functional domains, including its LOV domain, coiled-coil (CC), zinc finger (ZnF), and Per-Arnt-Sim (PAS) domains. Likewise, WC-2 is predicted to be about 63% intrinsically disordered, with structured regions limited to its PAS, CC, and ZnF domains (Figure 1.4, 4. and 5. panel).

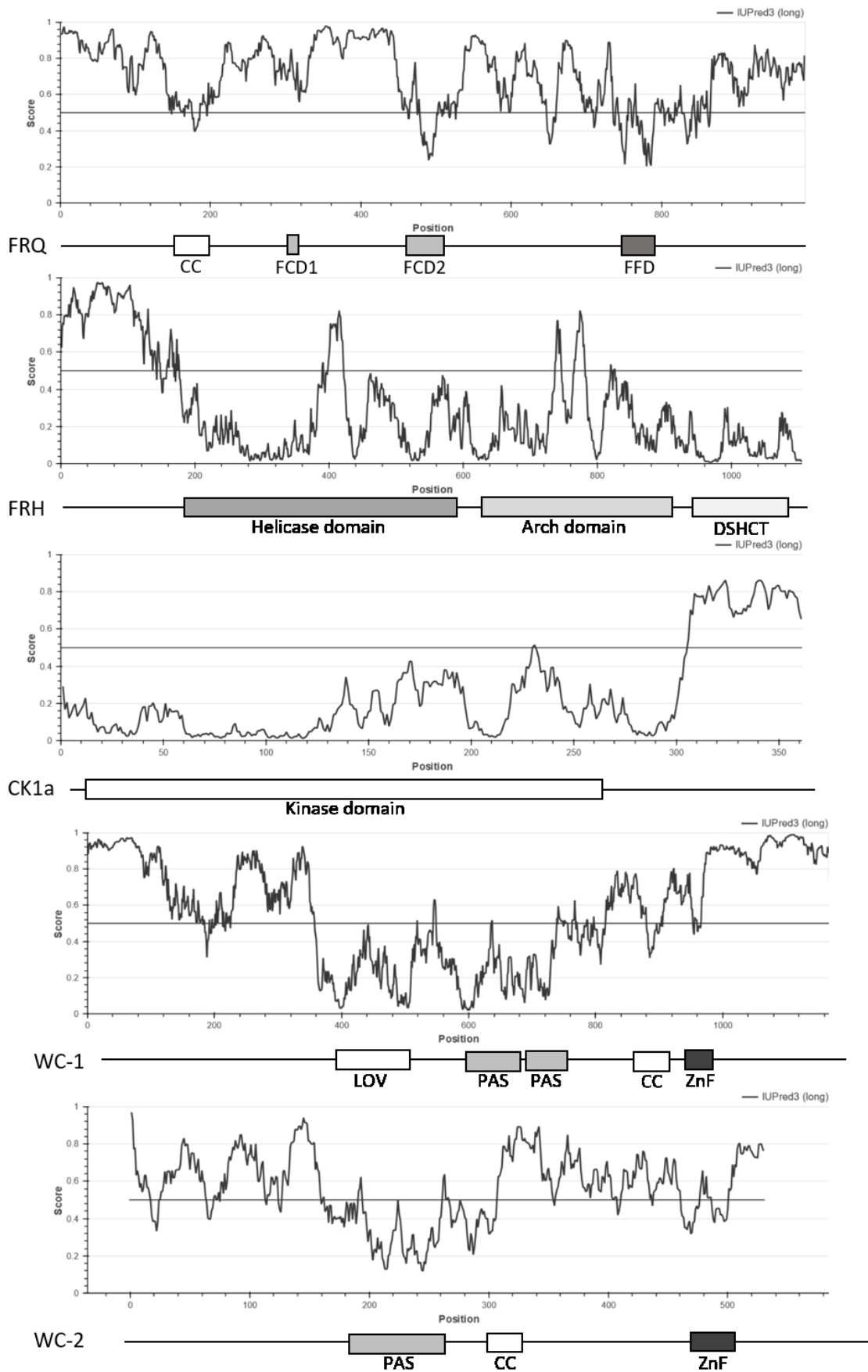


Figure legend on next page

Figure 1.4: **The core components of the circadian clock contain intrinsically disordered regions.**

FRQ is an intrinsically disordered protein, with approximately 85.5% disorder. Secondary structure predictions loosely align with binding sites (CC = coiled-coil domain, FCD1/FCD2 = FRQ-CK1a interaction domain, FFD = FRQ-FRH interaction domain). FRH has a disordered N-terminus, while the helicase, arch and Dead-box Spreading Helicase C-terminal Tail (DSHCT) domain remain structured. CK1a has a disordered C-terminus, while its kinase domain is structured. WC-1 and WC-2 show high disorder. But they also contain domains like PAS (Per-Arnt-Sim) and LOV (light-oxygen-voltage sensing). Disorder propensities were assessed using IUPred version 3 (Erdos et al. 2021).

1.5 The pacemaker of the circadian clock, FRQ

In 1973, Feldman and Hoyle discovered the importance of FRQ for the circadian clock in *Neurospora crassa*. By generating mutations in the *frq* locus, they observed altered period lengths under constant conditions, from the normal ~22.5 h periods shifted to anywhere between 16 and 35 h, making FRQ the first circadian clock protein identified in *Neurospora* (Feldman and Hoyle 1973). Mutations at the *frq* locus produced either a prolonged circadian period, as seen in *frq-3*, *frq-7*, and *frq-8*, or a shortened period, as in *frq-1*, *frq-2*, *frq-4*, and *frq-6* (Feldman and Hoyle 1973, Gardner and Feldman 1980). In *frq-9*, which is truncated at amino acid 663, *frq* mRNA levels remain high, indicating a disruption in the negative feedback loop and resulting in a completely arrhythmic clock (Loros et al. 1986, Dunlap 1999). Another mutation, *frq-10*, includes a deletion of most of the *frq* reading frame, disrupted both rhythmicity and temperature compensation of the circadian clock (Loros and Feldman 1986, Aronson et al. 1994). Moreover, artificially modifying FRQ expression, such as introducing a constitutive promoter, also leads to arrhythmicity (Aronson et al. 1994). Additionally, disrupting FRQ degradation by deleting *fwd-1*—which encodes the F-box/WD-40-repeat-containing protein 1, a substrate-recruiting subunit of the ubiquitin ligase responsible for FRQ ubiquitination and degradation—also abolishes the circadian rhythm (He and Liu 2005). These findings highlight the importance of rhythmic expression and degradation of FRQ for proper clock function.

FRQ is a 108 kDa protein, which functions as the core protein of the negative regulator complex, formed together with FRH and CK1a (Baker et al. 2012). FRQ inhibits its own transcription (discussed in detail in section 1.2) at a specific circadian phase, likely influenced by phosphorylation (Aronson et al. 1994, Mellow et al. 1997).

The structure of FRQ is intrinsically disordered (as discussed in section 1.4) with only few functional and structured regions. Co-immunoprecipitation experiments suggest that FRQ forms a homodimer initiated by the coiled-coil domain at FRQ's N-terminus (Cheng et al. 2001, Görl et al. 2001). Other important structured parts of FRQ include FCD-1 and 2 used for CK1a binding as well as the FRQ-FRH interaction domain (FFD). The minimal interaction site for FRH on FRQ includes the 6B2 and 6B5 regions, as identified by Guo and colleagues through co-immunoprecipitation studies (Guo et al. 2009). However, recent findings indicate that two arginine residues at positions 783-784 also contribute to the FRQ-FRH interaction, highlighting the importance of charge to the FRQ-FRH interaction (Cheng et al. 2005, He et al. 2006, Guo et al. 2010, Querfurth et al. 2011, Jankowski et al. 2024). Recently, Tariq published an AlphaFold predicted model of FRQ, which impressively showcases the disorder of FRQ (Tariq et al. 2024). We had a similar result when running an AlphaFold prediction on the FRQ structure (Figure 1.5). Here, secondary elements form structure-like elements for predicted structures like coiled-coil domain (green), FCD1 and 2 (blue and cyan respectively) and FFD (yellow), which also includes the 6B2 site (red), which was shown to be essential for FRH interaction (Guo et al. 2010).

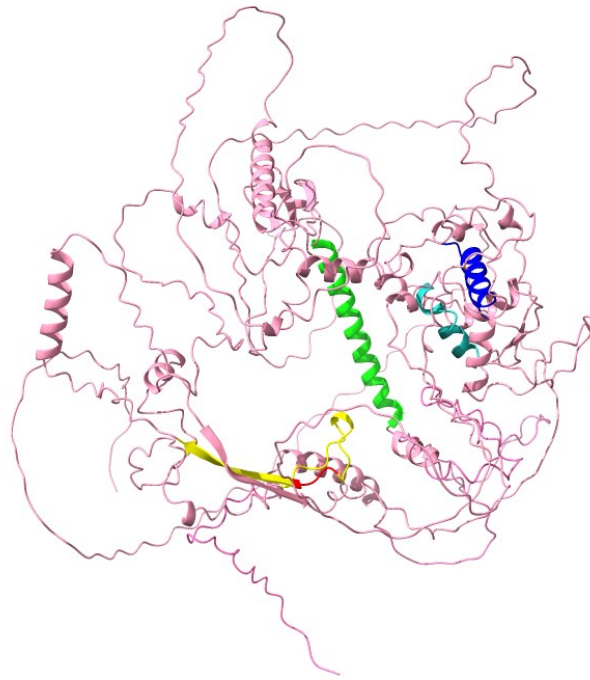


Figure 1.5: **AlphaFold-derived model of FRQ**

The AlphaFold prediction for FRQ shows a substantial amount of unstructured regions, consistent with the IUPred 3 prediction (Figure 1.4). Few secondary structures are shown. Key structured elements including the coiled-coil domain (green), FCD1 (blue), FCD2 (cyan) and the FFD (yellow, with the 6B2 region in red) are highlighted.

FRQ is regulated through multiple mechanisms, including transcriptional, post-transcriptional, translational, and post-translational modifications (Baker et al. 2009, Baker et al. 2012). Notably, over 100 phosphorylation sites have been identified for FRQ, emphasizing the critical role of phosphorylation in its regulation (Baker et al. 2009, Tang et al. 2009). Various kinases contribute to this process, with CK1a serving as the primary kinase essential for FRQ phosphorylation. Other kinases, including CK2, PERIOD-4 (PRD-4), CAMK-1, and protein kinase A (PKA), also participate in modulating FRQ's phosphorylation state. Additionally, the phosphatases PP1, PP2A, and PP4 have been identified dephosphorylating FRQ, thereby balancing its phosphorylation levels (Schafmeier and Diernfellner 2011, Baker et al. 2012).

FRQ is phosphorylated in clusters and there has been no specific phosphorylation event identified that acts as a functional switch, indicating that not individual phosphorylation sites are important but the amount of phosphorylation. Recently, our group demonstrated that slow and progressive phosphorylation of FRQ is essential for time keeping (Marzoll

et al. 2022b). These findings shift the perspective from focusing on specific phosphorylation sites as functional switches to understanding phosphorylation as a cumulative and gradual process critical for clock regulation.

1.6 Helicase FRH is the homologue of Mtr4

FRH was the last core clock protein identified. Using inducible *frh*-RNAi, Cheng and colleagues demonstrated that reduced FRH expression leads to decreased FRQ levels and arrhythmicity, suggesting that FRH serves as a stabilizer or “nanny protein” for FRQ. They also observed that low FRH expression increased *frq* mRNA levels, implicating FRH in the negative feedback loop of the circadian clock (Cheng et al. 2005).

Beyond its stabilizing role, the specific function of FRH within the circadian clock remains unclear. A point mutation in FRH, FRH (R806H), renders the clock of *Neurospora* arrhythmic but viable, unlike *frh* knockouts (KO), which are lethal. This mutation results in elevated FRQ levels, as well as a reduced and hypophosphorylated WCC, thereby disrupting the negative feedback mechanism due to elevated WCC activity and subsequent degradation (Schafmeier et al. 2006, Schafmeier et al. 2008, Shi et al. 2010). These findings underscore FRH’s role in the circadian clock’s negative feedback loop, which also indirectly impacts the positive feedback loop.

While FRH plays a significant role in the circadian mechanism, its interaction with FRQ depends on its intrinsically disordered N-terminus, which is not essential for the viability of *Neurospora*. FRH’s helicase function is essential for cellular survival but not required for the clock (Guo et al. 2009, Conrad et al. 2016).

FRH belongs to the DExH-box RNA helicase family, with nuclear homologue Dob1p/Mtr4p and cytosolic homologue Ski2p in *Saccharomyces cerevisiae* (de la Cruz et al. 1999, Mitchell and Tollervey 2000, van Hoof et al. 2000, Hilleren and Parker 2003). Mtr4p is a key nuclear cofactor for the yeast exosome complex involved in RNA metabolism, which impacts procession and degradation of RNAs in the 3’-5’ direction (Allmang et al. 1999, LaCava et al. 2005, Houseley et al. 2006). The function of the exosome in RNA metabolism is often compared to the proteasome’s role in protein degradation (Lorentzen and Conti 2006).

The helicase core of FRH and Mtr4p shows 67% sequence identity, resulting in high structural similarity between FRH and Mtr4p (Putnam and Jankowsky 2013, Conrad et al. 2016). In 2016, Conrad and colleagues solved the structure of FRH (as shown in Figure 1.6), identifying five distinct domains analogous to those in Mtr4p. These include the RecA-1 and RecA-2 domains, which are typical DExH/Dc-box helicase domains containing an ATPase domain for ATP binding in RecA-1 and a nucleotide binding fold in RecA-2 (Ye et al. 2004). What follows these domains is the arch domain, which forms an arm-like structure with the "stalk" acting as an arm and elbow and the KOW region as a "fist." Beyond the arch domain lies the winged-helix domain, which connects to the DExH-box Spreading Helicase C-terminal Tail (DSHCT) domain, aligning with RecA-2 to complete the RNA-binding cleft, essential for nucleotide hydrolysis (Ye et al. 2004, Mohr et al. 2008, Putnam and Jankowsky 2013, Rudolph and Klostermeier 2015, Conrad et al. 2016).

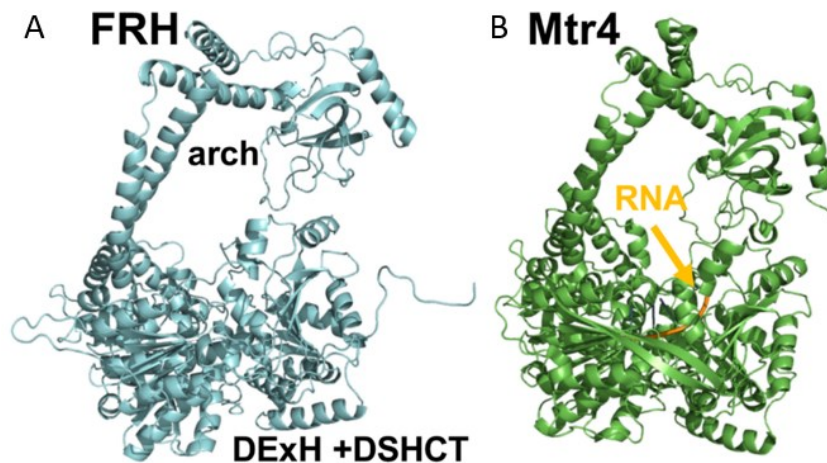


Figure 1.6: Comparison of the crystal structure of FRH and Mtr4p

The structures of FRH (PDB5E02; cyan) and Mtr4 (PDB2XGJ, green, RNA backbone in orange) are highly similar and differ primarily in the orientation of the arch domain (Figure from Conrad et al. (2016)).

1.7 CK1a

As mentioned previously, FRQ is phosphorylated by several kinases, but CK1a is the kinase primarily responsible for progressive FRQ phosphorylation and is also part of the negative regulator complex. CK1a belongs to the Casein Kinase 1 family, a highly

conserved class of kinases across eukaryotes containing homologues from fungi to mammals (Etchegaray et al. 2009). CK1 kinases are monomeric kinases that phosphorylate serines and threonines with a preference for substrates that have pre-phosphorylated motifs (Flotow et al. 1990, Songyang et al. 1996). A distinctive feature of CK1 kinases is that they are constitutively active and require no prior phosphorylation in their activation segment, which is a prerequisite for the activation of most other kinases (Johnson et al. 2013, Fulcher and Sapkota 2020).

The crystal structure of CK1 was solved 1995 by Xu and colleagues. The structure of CK1 was found to include a conserved kinase domain, which is essential for ATP loading, substrate binding, and phosphorylation. In addition to the conserved kinase domain, CK1 contains an unstructured C-terminal tail that varies between CK1 isoforms. This tail plays a role in regulating substrate specificity and kinase activity (Graves and Roach 1995, Xu et al. 1995) (Figure 1.4).

Through substrate phosphorylation, kinases such as CK1 regulate numerous aspects of substrate function, including changes in activity, stability, or subcellular distribution (Fulcher and Sapkota 2020). Over 140 CK1 substrates have been identified so far, highlighting the central role of these kinases in various biological processes. These include membrane trafficking, cytokinesis, vesicular transport, ribosome biogenesis, apoptosis, DNA repair, signal transduction pathways, and circadian rhythms (the role of CK1 in circadian rhythms is discussed in detail in sections 1.2 and 1.3). In particular, CK1's involvement in cell signaling, growth, and apoptosis underscores its importance in maintaining cellular homeostasis. The dysregulation of CK1 activity has been linked to a variety of diseases, including cancer and neurological disorders. This underscores the critical role of CK1 in maintaining health and has therefore become a focus of research (Knippschild et al. 1997, Knippschild et al. 2005, Cheong and Virshup 2011, Schitteck and Sinnberg 2014, Zemp et al. 2014).

1.8 Heterodimeric transcription factor WCC is involved in light and dark response of the circadian clock

The WCC in *Neurospora* is a heterodimer consisting of WC-1 and WC-2 proteins. The circadian clock transcriptional activator complex was discovered in the 1980s and named after the white growth phenotype of WC-1 or WC-2 mutants, which results from the lack

of expression of carotenoid pigment synthesis genes (Harding and Turner 1981, Degli-Innocenti and Russo 1984, Chen et al. 2010).

WC-1 is the larger subunit of the complex with 127 kDa. WC-1 contains a PAS-like light-oxygen-voltage (LOV) domain functioning as a blue light photoreceptor, two PAS domains, a positively charged DNA-binding domain (DBD), and a GATA-type zinc finger (ZnF) domain required for site-specific DNA binding (Ballario et al. 1996, Lee et al. 2000, Linden 2002) (Figure 1.4). The smaller subunit, WC-2, with a molecular weight of 57 kDa, contains one PAS domain and a ZnF domain (Linden 2002) (Figure 1.4).

The WCC assembles through the PAS domains of WC-1 and WC-2, which are essential for the formation of the complex. Cheng and colleagues found in 2002 that when WC-2 is deleted or the PAS domains are disrupted, WC-1 levels are significantly reduced, which suggests that WC-2 is necessary to stabilize WC-1 through interaction with the Pas domains (Cheng et al., 2002). The active transcription factor WCC is localized predominantly in the nucleus (Schafmeier et al. 2008, Wang et al. 2015a).

Neurospora utilizes two primary pathways to adapt its cellular physiology to environmental cues: an inner circadian clock regulating expression of ccgs (dark pathway) and a pathway regulation gene expression in response to light (light pathway) (Aronson et al. 1994, Crosthwaite et al. 1997). In the dark, the ZnF domains of WC-1 and WC-2 are crucial for binding to the clock-box (C-box) in the promoters of target genes, such as *frq*, to activate their transcription and drive circadian oscillations. Deletion of either ZnF domain impairs this binding, disrupting transcriptional activation and consequently perturbing the circadian clock (Crosthwaite et al. 1997, Cheng et al. 2002, Collett et al. 2002, Cheng et al. 2003, Froehlich et al. 2003). In light, the LOV domain of WC-1 undergoes a conformational change upon the formation of a photoadduct, where flavin adenine dinucleotide (FAD) covalently binds to a cysteine residue within the domain. This triggers dimerization of the LOV domain, leading to the formation of the light-induced WCC homodimer (Salomon et al. 2000, Swartz et al. 2001, He et al. 2002, Malzahn et al. 2010). For light-activated transcription, only the ZnF domains of WC-2 are required (He et al. 2002). The ZnF domains bind to proximal light-regulatory elements (PLREs) to activate the transcription of target genes, such as *frq* (Cheng et al. 2003, Malzahn et al. 2010, Wang et al. 2015a).

The activity of the WCC is regulated through phosphorylation and dephosphorylation mainly facilitated through kinases CK1a and CK2 as well as phosphatases PP4 and PP2A (He et al. 2006, Huang et al. 2007, Cha et al. 2008, Tataroğlu et al. 2012). In a study from Wang and colleagues, 80 phosphorylation sites in WC-1 and 15 in WC-2 were identified (Wang et al. 2019). The phosphorylation and inactivation of WCC is facilitated through interaction with FRQ, which leads to the accumulation of inactivated WCC (Schafmeier et al. 2005, Schafmeier et al. 2006, Wang et al. 2015b, Wang and Dunlap 2023).

Multiple sites have been identified that influence the interaction between FRQ and WCC, though no single specific site has been pinpointed. The DBD domain of WC-1 has been shown to influence interaction of FRQ and WCC (Wang et al. 2015b). Moreover, recently, three Aspartic acid / Glutamic acid (Asp/Glu) clusters in FRQ were found to be indispensable for FFC–WCC complex formation (Wang and Dunlap 2023).

1.9 Aim of the thesis

Although much is known about the proteins that form the core of *Neurospora crassa*'s clock, the molecular mechanism by which time is measured remains unclear.

Important questions in unravelling the mechanism of circadian timekeeping include how FRH protects FRQ from degradation, why a separate protein is required for this process, and how FRH affects the interaction of FRQ with the WCC. Perhaps most importantly, what is the role of multisite phosphorylation of the intrinsically disordered regions (IDRs) of FRQ and what conformational changes does it induce? To date, these questions remain unanswered, and progress in understanding these mechanisms is hindered by several challenges. CK1a is a conserved and essential serine/threonine kinase and is involved in many essential biological processes. Similarly, FRH has a vital function as an RNA helicase within the exosome complex. Therefore, both proteins have essential roles beyond their roles in the clock, rendering their inactivation impossible. Moreover, FRQ and WC-1 are unstable without their binding partners, FRH and WC-2, respectively, and therefore cannot be adequately studied on their own. Furthermore, the dense hyphal networks and motile nuclei of *Neurospora* make imaging studies of subcellular protein dynamics difficult. The role of the WCC as a light receptor further complicates real-time observations of clock proteins. These obstacles have significantly slowed progress in understanding the circadian clock of *Neurospora*.

In this thesis, I aim to overcome these limitations by overexpressing fluorescently tagged *Neurospora* clock proteins in a heterologous system. Therefore, I expressed the proteins of interest in inducible U2OS_{tx} cells and analyzed their interactions and subcellular dynamics using live-cell imaging. This approach allowed me to analyze processes that are difficult to study in *Neurospora* by circumventing the difficulties mentioned above. The insights I gained enabled us the design of specific experiments in *Neurospora* that would otherwise have been difficult to devise.

Utilizing this strategy allowed me to make new interesting discoveries about molecular timekeeping by the core clock: I found that the phosphorylation state of the IDRs of FRQ is decoded by the interaction with its folded partner, FRH. This interaction drives the stepwise remodeling of the FFC complex and regulates the interaction between FRQ and WCC, nuclear export and degradation, shedding new light on the mechanism of molecular timekeeping.

2. Methods

2.1 Microbiological methods

2.1.1 Preparation of bacterial DMSO stocks

Bacterial strains were stored as DMSO stocks. 900 μL of an overnight (ON) culture was added to 100 μL of 100% DMSO in a sterile 2 mL cryo tube and mixed. Stocks were stored at $-80\text{ }^{\circ}\text{C}$. For inoculation, frozen stocks were scraped with a sterile inoculation loop and streaked out on the desired plate.

2.1.2 Cultivation of *E. coli*

For the isolation of plasmid DNA, *E. coli* cultures were cultivated ON in LB liquid medium supplemented with ampicillin (100 $\mu\text{g}/\text{mL}$; Table 3.5.2) with agitation at 180 rpm and $37\text{ }^{\circ}\text{C}$. In case of solid cultures from petri dishes, single colonies were picked for inoculation of 5 mL liquid LB-medium containing ampicillin (100 $\mu\text{g}/\text{mL}$).

2.1.3 Transformation of chemocompetent *E. coli*

The chemocompetent cells were prepared by Gabriela Müller. 50 μL aliquots of *E. coli* *DH5a* cells were thawed on ice for 15 min and then mixed with 1-5 μL of plasmid DNA. After 15 to 30 min of incubation on ice (omitted for re-transformations), the cells were heat-shocked at $40\text{ }^{\circ}\text{C}$ for 40 seconds. Afterwards, the cells were immediately put on ice and 500 μL SOC medium (Table 3.5.1) was added. The cells were recovered for 15 to 30 min at $37\text{ }^{\circ}\text{C}$ and 600 rpm prior to plating out 100 μL . The plates or the LB-medium were supplemented with 100 $\mu\text{g}/\text{ml}$ ampicillin and incubated overnight at $37\text{ }^{\circ}\text{C}$.

2.1.4 Cultivation of *N. crassa*

Neurospora was cultivated, depending on the needs either in liquid culture or on solid medium.

For cultivation in liquid medium, cultures were first pre-cultured in petri dishes with 25 mL of N- medium (1x Vogel's, 2% [w/v] glucose, and 0.5% [w/v] arginine). When confluence was reached after two to three days, the culture was divided by punching out mycelial discs with a sterile 15 mL falcon tube and transferring them to an Erlenmeyer flask with fresh N-medium. 30 mL of N-medium was used per disc. *Neurospora* strains were incubated at $25\text{ }^{\circ}\text{C}$ prior to harvest and shaken at 110 rpm and kept in either light or

dark, depending on the strain. Mycelia were harvested at the indicated time points by removing samples with forceps, squeezing out the remaining N-medium, transferring the samples to 2 mL safe-lock tubes and lastly freezing the sample in liquid nitrogen. The harvested mycelium were either stored at -80°C or directly used for protein extraction.

Slant-medium (Table 3.6.6) in an Erlenmeyer flask or slant was inoculated with a few drops of conidia harvested in 1M sorbitol. *N. crassa* was incubated at 30°C for two days and then allowed to grow at room temperature. After 5 to 14 days, conidia were harvested by adding ice-cold 1 M sorbitol.

2.1.5 Transformation of *N. crassa*

Conidia from solid grown *N. crassa* cultures were harvested after 5 to 14 days with 50 mL ice-cold 1 M sorbitol and filtered through a compress in an autoclaved funnel. After filtration the suspension was centrifuged (2000 g, 4°C , 10 min). The resulting conidia pellet was washed three times with 50 mL of ice-cold sorbitol. Then, the pellet was finally dissolved in the residual volume of sorbitol from the last washing step. For transformation via electroporation, 50 μL freshly harvested conidia spores and 500 to 1000 ng DNA (linearized plasmid DNA) was mixed in a 2 mm gap electroporation cuvette on ice. After electroporation (Biorad Gene pulser, settings: 1500 V/cm voltage, 25 μF capacitance and 600 Ω resistance) the cells were immediately diluted with 1 mL of 1 M ice-cold sorbitol and then transferred into 5 mL N-medium in a 15 mL falcon tube. The conidia were recovered by rotating slowly at RT for a minimum of 1 and up to 3 h. For a histidine prototrophy selection, 1 mL of the conidia suspension was added to 10 ml molten top agar and plated on bottom agar. After 3 - 7 days of growth at 30°C , colonies were picked onto slants filled with solid selection medium. After transformation of luciferase reporters plates were recorded by a camera and luminescent transformant colonies were picked only. Selected strains were further analyzed by Western blot analysis (section 2.4.3).

2.2 Molecular biological methods

2.2.1 Determination of DNA and protein concentrations

For the measurement of DNA concentrations an Implen nanophotometer (NP 80 mobile) was used with default settings for double stranded DNA (dsDNA). The Implen nanophotometer was also used to measure protein concentrations using the specific settings for determination of protein concentrations at OD1.

2.2.2 Extraction of plasmid DNA from *E. coli*

Plasmid DNA from *E. coli* was extracted using the GeneJET Plasmid Miniprep Kit (Thermo Fisher Scientific CAT#K0502) with 5 mL of liquid ON culture. After pelleting the culture, plasmid DNA was extracted according to the manufacturer's instructions. DNA was eluted from the spin column with 70°C 50 µL ddH₂O and incubated at 70°C for 5 min. A comprehensive list of all plasmids used in this thesis can be found in table 3.1.1 and 3.1.2.

2.2.3 Native protein extraction from *N. crassa*

Formerly harvested mycelium was grinded using pestle and mortar. All utensils were cooled using liquid nitrogen to prevent thawing of the probe. Mycelia powder was either stored at -80°C or directly used for protein extraction.

A total of 500 µL of frozen mycelial powder was suspended in 700 µL of ice-cold protein extraction buffer (PEX) (Table 3.4.2; supplemented freshly with protease inhibitors: 5 µg/ml leupeptin, 5 µg/ml pepstatin A, 1 mM PMSF and phosphatase inhibitors: 1 x PhosStop™ :Roche Diagnostics, CAT#4906845001). The suspension was incubated on ice and vortexed every 5 min for 30 min. After incubation, the sample was centrifuged for 30 min at 4°C and 20000 g to clear the protein extract. The supernatant was carefully transferred into a fresh tube and the protein concentration was subsequently determined as described in 2.2.1. The native protein extracts were stored at -80 °C. To prepare samples for gel electrophoresis, the protein extracts were diluted in a 3:1 ratio with 4 x Laemmli buffer (Table 3.4.5) or in a 1:1 ratio with 2 x Laemmli buffer and boiled at 95 °C for 5 min.

2.2.4 Polymerase chain reaction (Q5)

The polymerase chain reaction (PCR) employs the ability of DNA polymerase to synthesize a new DNA strand using an existing complementary strand as a template. This method enables the amplification of genes through the use of primers, dNTPs, buffer, water and thermally stable DNA polymerase. The success of DNA amplification is contingent upon three key steps: denaturation, annealing and elongation.

The DNA fragments were amplified by polymerase chain reaction (PCR) using the Q5 polymerase, which is capable of proofreading. All components of the PCR reaction

mixture (Table 2.2.4a) were prepared and the polymerase was added as the final step. The optimal primer design for standard PCR was found to consist of a length of 18 to 30 bp, a GC content of 40 to 60 %, the absence of hairpins or primer dimers, a G or a C as the final base, and a similar annealing temperature to the primer to pair with. However, primers used for cloning could reach up to 120 bp. Conditions for PCR are listed in table 2.2.4b.

Table 2.2.4a: PCR reaction mix

component	volume (μL)	final concentration
5x Q5 reaction buffer	10	1x
5x Q5 high GC enhancer	10	1x (only for Plasmid template)
10 mM dNTPs	1	200 μM
10 μM forward primer	1	200 nM
10 μM reverse primer	1	200 nM
template DNA	variable	10 ng of plasmid DNA/ 150 ng gDNA
2 U/ μL Q5 DNA polymerase	0,5	0.02 U/ μL (1 U)
ddH ₂ O	Ad to 50 μL	

Table 2.2.4b: PCR cycling conditions for Q5 polymerase

step	temperature	time	number of cycles
initial denaturation	98 °C	30 sec	
denaturation	98 °C	10 sec	28 – 42 x
annealing	* °C	30 sec	
elongation	72 °C	**	
final elongation	72 °C	5-10 min	
cooling	4 °C	2 min	
hold	8 °C	∞	

*annealing temperature was chosen as recommended by NEBTm Calculator

**depends on kb of PCR product (32 seconds/ kb)

2.2.5 Site-directed mutagenesis

For the introduction of mutations, site-directed mutagenesis PCR was employed. The system of QuikChange II XL Site-Directed Mutagenesis Kit was developed by Agilent (CAT# 200521). The kit was mostly used according to the manufacturer's instructions. The conditions for the PCR can be found in table 2.2.5a and 2.2.5b.

Table 2.2.5a: Pfu ultra PCR reaction mix

component	volume (μL)	final concentration
reaction buffer	5	1x
Quick solution	3	
10 mM dNTPs	1	200 μM
10 μM forward primer	1	125 ng/ μL
10 μM reverse primer	1	125 ng/ μL
template DNA	variable	50 to 200 ng
Pfu ultra DNA polymerase	1	0.02 U/ μL (1 U)
ddH ₂ O	Ad to 50 μL	

Table 2.2.5b: PCR cycling conditions for Pfu ultra mutagenesis

step	temperature	time	number of cycles
initial denaturation	95 °C	1 min	
denaturation	95 °C	1 min	18 x
annealing	* °C	30 sec	
elongation	68 °C	**	
final elongation	68 °C	7 min	
cooling	4 °C	2 min	
hold	12 °C	∞	

*annealing temperature was chosen as recommended by NEBTm Calculator (usually between 60-65 °C)

**depends on kb of PCR product (2 min/ kb)

After confirmation via agarose gel electrophoresis (section 2.4.1) that the PCR was successful, the PCR product was treated with DpnI for 90 min at 37 °C. Subsequently, a sodium acetate precipitation was conducted. This involved combining the PCR product with a 1:10 ratio of 3 M sodium acetate (pH 5) and a 2.5:1 ratio of 100% ethanol, followed by incubation at -80 °C for 30 min. Following a 30-min centrifugation at 4 °C at 14,000 rpm, the pellet was washed with 70 °C ice-cold ethanol (centrifugation: 4 °C, 10 min at 14,000 rpm). Once the pellet had been allowed to dry, it was resuspended in 10 µL of ddH₂O. 8 µL of the purified product were employed for the transformation of chemocompetent *E. coli* (section 2.1.3).

2.2.6 Purification of PCR products

PCR products were purified using the NucleoSpin Gel and PCR Clean-up kit (Macherey-Nagel CAT#740609.250) according to the manufacturer's instructions. DNA was eluted from the spin column with 70 °C 50 µL ddH₂O and incubated at 70°C for 5 min for a more efficient elution.

2.2.7 Restriction enzyme free cloning (cloning with overlapping regions)

Dr. Daniela Marzoll introduced restriction enzyme-free cloning in the Brunner lab. She adapted it mainly from Aslanidis and Colleagues (Aslanidis et al. 1994, Li and Elledge 2007, Liu and Naismith 2008, Jacobus and Gross 2015, Fuzik et al. 2016). In short, the method describes how a sequence overlap of two double-stranded DNA fragments can be joined *in vivo* by *E. coli*. The first step was to design primers with an overlap of 20 to 40 bp containing the desired DNA modification. PCR amplification of the DNA strands with the homologous sequences at the overlapping sites was performed using Q5 polymerase (Table 2.2.7). To increase the probability of success, the PCR products were split at the ampicillin resistance cassette so that colonies would only grow on a plate with ampicillin if both constructs were correctly combined.

Table 2.2.7: 2-step Q5 PCR program

step	temperature	time	number of cycles
initial denaturation	98 °C	30 sec	
denaturation	98 °C	10 sec	7x
annealing/ elongation	72 °C	32 sec/kb	
denaturation	98 °C	10 seconds	28x
annealing/ elongation	68 °C	39 sec/kb	
final elongation	72 °C	5 – 10 min	
step	temperature	time	number of cycles
cooling	2 °C	2 min	
hold	8 °C	∞	

To remove reagents from the PCR, such as unincorporated dNTPs, which could interfere with subsequent reactions, the PCR products were purified as described in 2.2.6. To further remove template DNA from the reaction mix, DpnI digestion was performed at 37°C for 90 min. DpnI only cleaves methylated DNA, therefore only template DNA is removed. The reaction was performed in NEBuffer 2.1 or cutsmart buffer (NEB). The enzyme was then heat-inactivated at 80 °C for 20 min. If three or more fragments were combined, the fragments were also treated with T4 DNA polymerase for 10 min at RT, which increases the efficiency of the transformation through its 3'→5' exonuclease activity. After inactivation of T4 DNA polymerase by incubation at 75°C for 20 min, the fragments were premixed in a volume of 5 µL for transformation into chemocompetent *E. coli* as described in section 2.1.3. NEB Tm Calculator was used to calculate the vector to insert ratio. For fragments of similar size, a 1:1 ratio was preferred. For shorter inserts, an insert: vector ratio of 3:1 or higher was used.

2.2.8 Cloning with restriction enzymes

Cloning with restriction enzymes is the more classical approach to cloning, requiring restriction sites on the target DNA and enzymes that cleave at these restriction sites. All enzymes used were purchased from NEB. After pipetting according to Table 2.2.8, the restriction mixture was incubated at 37 °C for 2 h. The enzyme was then heat-inactivated for 20 min at the specific inactivation temperature required for the enzyme. After the enzymatic digest was complete, the backbone of the vector had to be dephosphorylated to prevent re-ligation with itself. Approximately 5 to 10 µg of vector DNA was

dephosphorylated with calf intestinal alkaline phosphatase (CIP; NEB) at 37°C for 30 min according to the manufacturer's instructions. The mixture was incubated at 50°C for another 30 min and then allowed to cool at RT for 10 min. Before ligation the CIPed vector was purified from an agarose gel after electrophoresis using the NucleoSpin Gel and PCR Clean-up kit (Macherey-Nagel). For the ligation, T4 DNA ligase (NEB, CAT#M0202) was used mostly according to the manufacturer's instructions. After incubation at RT for 10 min 0.5 µL 10 mM ATP (in 20 mM HEPES pH 7.5) was added and the mix was incubated for another 15 min at RT. The ligation mix was then heat-inactivated at 65 °C for 20 min and transformed into chemocompetent *E. coli* as described in section 2.1.3.

Table 2.2.8: Restriction digestion for cloning with restriction enzymes

component		final concentration
DNA*	X µL	5 to 10 µg DNA
10x CutSmart	10 µL	1x
enzyme 1	1 µL	20 u
enzyme 2	1 µL	20 u
ddH2O		ad 100 µL

* plasmid DNA in the case of vector, purified PCR product in the case of an insert

2.3. Mammalian cell culture and sample preparation

2.3.1. Cell culture maintenance

U2OS T-Rex (U2OSTx; Life Technologies) cells were maintained in Dulbecco's Modified Eagle Medium (DMEM; Thermo Fisher Scientific CAT#) supplemented with 10% Fetal Bovine Serum (FBS; Thermo Fisher Scientific CAT#) and 1x Penicillin-Streptomycin (Thermo Fisher Scientific CAT#). DMEM and its supplements are then referred to as D10. The cells were grown and maintained at 37 °C in a humidified incubator containing 5% CO².

2.3.2. Transient transfection with plasmids

U2OSTx cells were transfected using Xfect™ Transfection Reagent (Xfect; Takara Bio, CAT# 631318) according to the manufacturer's instructions. U2OSTx cells were grown on multi well plates to approximately 60-80 % confluence. Two 1.5 mL tubes were prepared: the DNA mix tube contained the plasmid DNA and half the amount of Xfect

Reaction Buffer required for the reaction (4 μ L for 96 well plates). In the second 1.5 mL tube, the Xfect Mix, the Xfect Polymer was suspended in the other half of the Xfect Reaction Buffer. In the next step, Xfect Mix and DNA Mix were combined, vortexed and then incubated at RT for 20 min to allow the Xfect Polymer to complex with the DNA. D10 medium was used to dilute the reaction mix and fill the volume of the plate. The plate was afterwards incubated overnight at 37°C. The T-Rex promoter was then induced by the addition of 10 ng/mL doxycycline (DOX; Thermo Fisher Scientific CAT# 631311).

Table 2.3.2: Volumes for Xfect transfection

Vessel	DNA (μ g)	Xfect polymer	Total Volume in Xfect Reaction Buffer (μ L)	Final Volume (μ L, D10 added)
96 well plate	0.15-0.2		8	50 (42)
24 well plate	0.5-1	0.3 μ L of Xfect Polymer / 1 μ g of DNA	25	125 (100)
12 well plate	1-2.5		50	200 (150)
10 cm	15		600	4000 (3400)

2.3.3. Protein extraction from mammalian tissue culture

U2OSx cells were seeded in a 12-well plate and grown to approximately 60-80 % confluence. Cells were transiently transfected with Xfect as described in 2.3.2. At 4 and 14 h after induction, cells were scraped from the plate with 180 μ L of 2x Laemmli buffer and boiled at 95 °C for 5 min. 20 to 30 μ L of hot extract was loaded onto a 12 % SDS gel for Western blot analysis.

2.3.4 Incucyte Zoom analysis

Prior to transfection, 100 μ L of U2OSx cells were seeded into a 96-well plate. Transient transfection was then performed as described in section 2.3.2. After induction with DOX, the plate was placed in either the Incucyte ZOOM® or Incucyte® SX1 system (Sartorius). The Incucyte is a live cell imaging and analysis platform that allows quantification of cell or protein behavior over time by automatically acquiring and analyzing images around the clock. Images were acquired at 1-hour intervals for 48 h and then analyzed using the Incucyte® 2023A GUI (Sartorius) or Incucyte® 2016B GUI (Sartorius) software. In each experiment, 20 to 30 cells were quantified. Cells with fluorescence levels which were too low or excessively high were excluded from the analysis. The cytoplasmic and nuclear

distributions of mNG- and mK2-tagged proteins were examined, along with their co-localization and the number of foci as specified in each respective experiment. Data were visualized using BioRender Graph (Created in <https://BioRender.com>).

2.3.5 Leptomycin B treatment

To inhibit nuclear export, Leptomycin B (Merck; CAT# L2913-.5UG) was added to the cells 1 h after DOX induction at a final concentration of 20 nM (molar mass = 540.73 g/mol). The measurement was then continued using Incucyte analysis (section 2.3.4). An equal volume of methanol was added to one well as a negative control.

2.4 Biochemical and analytical methods

2.4.1 Agarose gel electrophoresis

For the detection of PCR products or digestion products from restriction enzymes, 3-5 μ L of DNA sample was mixed with 6x purple loading dye (NEB) and loaded onto an agarose gel. For size comparison, 6 μ L of the 1 kb plus DNA ladder (Thermo Fisher Scientific; CAT# SM1331) was loaded. Depending on the product size, the agarose gel was prepared with 0.7 - 2 % agarose in 1x TAE and a drop of ethidium bromide added (dropper bottle with 0.07 % ethidium bromide). The gels were run at 110 to 130 V for 15 to 30 min (power supply: EPS 301 from Amersham pharmacia biotech). The DNA fragments were visualized using UV light (Intas transilluminator 312 nm).

2.4.2 SDS-PAGE

Sodium dodecyl sulfate-polyacrylamide gel electrophoresis (SDS-PAGE) is a method of separating proteins based on their molecular mass. Laemmli buffer contains SDS molecules that disrupt the secondary structure of the protein and unfold the protein. When an electric field is applied, the protein-SDS complex migrates toward the positive electrode because the SDS-induced unfolding imparts a negative charge to the protein (Winogradoff et al. 2020).

Prior to loading, protein extracts and cells directly treated with Laemmli buffer (Table 3.4.5) were boiled at 95 °C for 5 min. For *Neurospora*, 300 to 600 μ g of native protein extracts were loaded per lane. The gel (Table 3.4.6) run was initiated by allowing the samples to run into the 5% acrylamide stacking gel (2 cm x 15 cm x 0.8 mm) for 30 min at 80 V. Subsequently, the samples were separated in the 12% resolving gel (8 cm x 15

cm x 0.8 mm). This gel was then either run overnight at 4-6 mA constant current or for a period of two h at 200 V.

2.4.3 Western blotting

Once the SDS-PAGE was complete, the resolving gel was transferred to a nitrocellulose membrane (GE Healthcare Protran™; CAT# 10402096) using semi-dry Western blotting (Towbin et al. 1979). Three layers of Whatman paper soaked in methanol-free blotting buffer (Pierce™; Thermo Fisher Scientific; CAT# 35045) were placed at the bottom of the blotting chamber. On top of that came the nitrocellulose membrane, the gel, and then another three layers of buffer-soaked Whatman paper. The gel was blotted onto the membrane at 250 mA for 2 h and 22 min. Subsequently, the transfer of the gel was verified by incubating the membrane for a period of 2 to 5 min in Ponceau S staining solution (Table 3.4.8), followed by a thorough washing with water. Once an even run had been verified, the Ponceau solution was removed from the membrane by washing it in 1x TBS (Table 3.4.9) buffer. Before the decoration with antibodies, unspecific binding to the membrane was blocked by incubating the membrane in 5 % skim milk in TBS for 20 min. Next, the primary antibody (in 5% skim milk) was incubated for either 2 h at RT or ON at 4 °C. The membrane was then washed three times for 10 min with 1x TBS buffer before the secondary antibody in 5% skim milk was added. The membrane was incubated with the secondary antibody overnight at 4°C. Again, the membrane was washed three times for 10 min with 1X TBS buffer. For signal detection, the membrane was placed in a film cassette and 1 mL of luminol mixture (Table 3.4.10) was added for approximately 10 seconds. X-ray films (Fujifilm) were placed on the membrane for different lengths of time and then developed in a developing machine (Konica Minolta SRX-101A Medical Film Processor).

2.4.4 Luciferase reporter assay (*in vivo*)

Rhythmic circadian oscillation of *N. crassa* can be investigated *in vivo* by the implementation of an *frq-luc* PEST reporter. In short, a luciferase reporter is cloned downstream of the *frq* promoter and then fused to a C-terminal PEST signal, which creates a short lived luciferase signal that acts as a faithful reporter of promoter activity (Gooch et al. 2008, Cesbron et al. 2013).

96-well plates were prepared with 150 μ L Luciferase Plate Medium (Table 3.6.7) and after solidification, 5 μ L conidial suspension ($OD_{420} = 2.2$) of the respective strains were pipetted into each well in four to six technical replicates. The plate was sealed tightly with PCR foil (Axon, CAT# 26979). Conidia were left to grow at RT for 3-5 d, before incubation at 25 $^{\circ}$ C overnight in the dark when the surface was covered with mycelium. Bioluminescence measurements were performed after synchronization by 12 h light:dark:light cycles and then released into constant darkness. Bioluminescence was recorded for 144 h (EnSpire; PerkinElmer) at 25 $^{\circ}$ C (incubator: E41L1C8 from CLF Plant Climatics).

2.5 Protein biochemical methods

2.5.1 Immunoprecipitation

For immunoprecipitation and co-immunoprecipitation, 60 μ L slurry of ANTI-FLAG[®] M2 beads (Merck; CAT# A2220) were transferred into a 1.5 mL low binding tube per sample and washed three times with 1 mL PBS supplied with protease inhibitors (Table 3.4.1). For each step, samples were centrifuged at 4 $^{\circ}$ C and 500 g and beads were left to settle for 1 min. 5-6 mg of native *Neurospora* protein extract in PEX buffer (section 3.4.2) was added to the beads. PBS supplied with protease inhibitors was added to a final volume of 500 μ L. The protein extract was incubated with the beads for 3 h at 4 $^{\circ}$ C on a rotating wheel. The supernatant was transferred into a fresh 1.5 mL tube and the beads were washed 2-3 times with 1 mL cold PBS supplied with protease inhibitors. The immunoprecipitated proteins were removed from the beads by incubation with 50-100 μ L 2x Laemmli (Table 3.4.5) for 2 min and boiled at 95 $^{\circ}$ C for 5 min. After a short spin down, the Laemmli supernatant was transferred into a fresh 1.5 mL tube. An equivalent of 400 μ g from load and supernatant and an equivalent of 1x IP (400 μ g) and 10x IP (4 mg) elution were loaded on an SDS-gel. After SDS-PAGE (section 2.4.2) and blotting, the Western blot (section 2.4.3) was decorated with the respective antibodies to detect co-immunoprecipitation.

2.5.2 Gel filtration (Size exclusion chromatography)

Protein complexes were analyzed via gel filtration chromatography. The system was equilibrated using a gel filtration buffer (Table 3.4.11). After priming, 8-10 mg of native *Neurospora* protein extracts were loaded onto a 200 μ L loop. Chromatography was

performed at 4°C with a flow rate of 0.5 mL/min using the Äkta Pure system (GE Life Sciences/Cytiva). Fractions of 490 µL were collected, and protein was precipitated by adding 122.5 µL of 50% TCA (w/v). The samples were incubated on ice for 10 min and then centrifuged (4°C, 14,000 g, 10 min). Pellets were washed with 1 mL acetone (4°C, 14,000 g, 10 min), air-dried for 3 min at room temperature, and resuspended in 90 µL of 2x Laemmli buffer. Samples were heated at 95°C for 5 min. From the resulting solution, 45 µL was loaded for SDS-PAGE (section 2.4.2), followed by Western blotting (section 2.4.3) for analysis.

2.5.3 In vitro phosphorylation

For *in vitro* phosphorylation of FRQ, *Neurospora* whole cell lysate was incubated ON at 4 °C with 2 µg purified recombinant CK1a previously prepared by Dr. Daniela Marzoll (Marzoll et al. 2022b) per mg of lysate in a buffer containing a final concentration of 50 mM Hepes/KOH pH 7.4, 120 mM NaCl, 11.3 mM MgCl₂, 12.5 mM ATP, 1xPhosStop (Roche), 1 mM PMSF, 1 µg/ml leupeptin, 1 µg/ml pepstatin.

3. Materials

3.1 Plasmids

3.1.1 Cell culture plasmids

Table 3.1.1: Plasmids used for expression in U2OStx cells

Plasmid	Backbone	Source
pcDNA4/TO-mk2-FRQ	pcDNA ^{TM4} /TO	Alexander Rau
pcDNA4/TO-FRQ-mNG	pcDNA ^{TM4} /TO	Alexander Rau
pcDNA4/TO-mk2-FRH	pcDNA ^{TM4} /TO	Alexander Rau
pcDNA4/TO-FRH-mNG	pcDNA ^{TM4} /TO	Alexander Rau
pcDNA4/TO-FRQ	pcDNA ^{TM4} /TO	This thesis
pcDNA4/TO-FRH	pcDNA ^{TM4} /TO	This thesis
pcDNA4/TO-FRH ^{R806H}	pcDNA ^{TM4} /TO	This thesis
pcDNA4/TO-mk2-WC-2	pcDNA ^{TM4} /TO	This thesis
pcDNA4/TO-WC-2-mNG	pcDNA ^{TM4} /TO	This thesis
pcDNA4/TO-WC-2	pcDNA ^{TM4} /TO	This thesis
pcDNA4/TO-WC-1-mNG	pcDNA ^{TM4} /TO	This thesis
pcDNA4/TO-WC-1	pcDNA ^{TM4} /TO	This thesis
pcDNA4/TO-mk2-FRQ ⁹	pcDNA ^{TM4} /TO	This thesis
pcDNA4/TO-mk2-FRQ ^{C-term}	pcDNA ^{TM4} /TO	This thesis
pcDNA4/TO-mk2-FRQ ^{6B2}	pcDNA ^{TM4} /TO	This thesis
pcDNA4/TO-mk2-FRQ ^{NLS1}	pcDNA ^{TM4} /TO	This thesis
pcDNA4/TO-mk2-FRQ ^{NLS2}	pcDNA ^{TM4} /TO	This thesis
pcDNA4/TO-mk2-FRQm ^{NLS123}	pcDNA ^{TM4} /TO	This thesis
pcDNA4/TO-mk2-FRQ ^{C-term-NLS}	pcDNA ^{TM4} /TO	This thesis

3.1.2 *Neurospora* plasmids

Table 3.1.2: Plasmids used for transformation of *N. crassa*

Plasmid	Backbone	Source
pBM60-wt	pBM60	Gorl et al., 2001
pBM60frqmNLS2	pBM60-wt	This work
pBM60frqmNLS3	pBM60-wt	This work
pBM60frqmNLS2/3	pBM60-wt	This work
pBM60pccg-1::frh2xFLAG	pBM60	Lauinger et al., 2014

3.2 Oligonucleotides

3.2.1 Oligonucleotides for mammalian vectors

Table 3.2.1: Oligonucleotides for mammalian vectors

Primer name	Primer sequence	Plasmid created
FRQ _bb_mKate2_F (66 °C)	AGGACGTCTCATCCTCGTGAGGATCCC CGGGTTAAG	pcDNA4/TO-6x His- mK2-FRQ
FRQ _bb_mKate2_R (65 °C)	TTATCCCCACTATCCGCCATACCAGAA CCACCACC	pcDNA4/TO-6x His- mK2-FRQ
bb_mKate2_FR Q_F (66 °C)	GTTCTGGTGGTGGTTCTGGTATGGCGG ATAGTGGGGAT	pcDNA4/TO-6x His- mK2-FRQ
bb_mKate2_FR Q_R (66 °C)	AATTCTTAACCCGGGGATCCTCACGAG GATGAGACGTCC	pcDNA4/TO-6x His- mK2-FRQ
FRQ _bb_mNeonGre en_F (66 °C)	TGGAGGACGTCTCATCCTCGGGTGGTT CTGGTGG	pcDNA4/TO- FLAGFRQ-mNG
FRQ _bb_mNeonGre en_R (66 °C)	TTATCCCCACTATCCGCCATCTTGTCGT CATCGTCTTGTAGTC	pcDNA4/TO- FLAGFRQ-mNG
bb_mNeonGree n_FRQ_F (66 °C)	ACAAAGACGATGACGACAAGATGGCG GATAGTGGGGATAAATC	pcDNA4/TO- FLAGFRQ-mNG
bb_mNeonGree n_FRQ_R (67 °C)	GAACCACCACCAGAACCACCCGAGGA TGAGACGTCCTCC	pcDNA4/TO- FLAGFRQ-mNG
HisFRQ_delmut AscI_F61	TTTTGGCGCGCCGGGTATGGCGGATAG TGG	pcDNA4/TO-6His - FRQ
HisFRQ_delmut AscI_R61	TTTTGGCGCGCCGTGATGGTGATGGTG ATG	pcDNA4/TO-6His - FRQ
FRQ_start_OL_ F Tm65	CTTGCGCGAGATACTAGCAG	pcDNA4/TO-6His – mK2-FRQmNLS123
FRQ_start_OL_ R Tm65	AGTAACTCTGCTGCTAGTATCTCG	pcDNA4/TO-6His – mK2-FRQmNLS123
FRQ_end_OL_ F Tm66	GCAAATCCTCATTCTCGGACAAC	pcDNA4/TO-6His – mK2-FRQmNLS123
FRQ_end_OL_ R Tm66	CGTGTTGTTGTCCGAGAAATGAG	pcDNA4/TO-6His – mK2-FRQmNLS123

Table 3.2.1 continued: Oligonucleotides for mammalian vectors

Primer name	Primer sequence	Plasmid created
mK2-FRQ(720-end)_F	GTTCTGGTTTCGACCCCGGAAACCCG	pcDNA4/TO-6His-mk2-FRQ C-term-NLS
mK2-FRQ(720-end)_R	GTTTCCGGGGTTCGAAACCAGAACCACCAC	pcDNA4/TO-6His-mk2-FRQ C-term-NLS
4TO-FRQ(D630)_F	GTTCTGGTGATTTTACGGATCGGGGACAAC	pcDNA4/TO-6His-mk2-FRQ C-term
4TO-FRQ(D630)_R	TCCGCTAAAATCACCAGAACCACCACCAGAAC	pcDNA4/TO-6His-mk2-FRQ C-term
FRQd413-989_NLS1_fwd	CTGGAAGCGGAGATGGAAGTTGAGGATCCCCGGGTAAAG	pcDNA4/TO-6His-mK2-FRQNLS1
FRQd413-989_NLS1_rev	GATATCTGCAGAATTCTTAACCCGGGGATCCTCAACTTCC	pcDNA4/TO-6His-mK2-FRQNLS1
CS_FRQ412-Tobb_fwd	GAAGCGGAGATGGAAGTTGAGGATCCCGGGTTAAGAATTCTG	pcDNA4/TO-6His-mK2-FRQNLS1
CS_FRQ412-Tobb_rev	GATTTATCCCCACTATCCGCCATACCA GAACCACCAC	pcDNA4/TO-6His-mK2-FRQNLS1
FRQ_NLS2_fwd	GTTCTGGTGATTTTACGGAGGCTCGGATAAGAATGGTCG	pcDNA4/TO-6His-mK2-FRQNLS2
FRQ_NLS2_rev	TAACCCGGGGATCCTCATTGCGTTGTC C	pcDNA4/TO-6His-mK2-FRQNLS2
NLS2-4/Tobb_fwd	GGACAACGCAATGAGGATCCCCGGGT TAAG	pcDNA4/TO-6His-mK2-FRQNLS2
NLS2-4/Tobb_rev	AGCCTCCGCTAAAATCACCAGAACCAC CACCAG	pcDNA4/TO-6His-mK2-FRQNLS2
FRQdNLS1_fwd	GGTACATGGCTTAGAGTTGGAGGCAACGC	pcDNA4/TO-6His-mK2-FRQΔNLS1
FRQdNLS1_rev	GCGTTGCCTCCA ACTCTAAGCCATGTACC	pcDNA4/TO-6His-mK2-FRQΔNLS1
FRQ 6B2 AAA	GTACTTCCTGACGCCGCTGCTGTGATGCTCGTC	pcDNA4/TO-6His-mK2-FRQ6B2
FRQ 6B2 AAA	GACGAGCATCACAGCAGCGGCGTCAG GAAGTAC	pcDNA4/TO-6His-mK2-FRQ6B2
XL_frqdeltaCC mut F62	GATGACTACCGCAGTGTCTTTGGTTCC GACGTGATG	pcDNA4/TO-6His-mK2-FRQΔCC
XL_frqdeltaCC mut RC 62	CATCACGTCGGAACCAAAGACACTGC GGTAGTCATC	pcDNA4/TO-6His-mK2-FRQΔCC
FRQ ⁹ F	GCACCGATCTTTCATGAGACCCTGGCG ATAT	pcDNA4/TO-6His-mK2-FRQ9

Table 3.2.1 continued: Oligonucleotides for mammalian vectors

Primer name	Primer sequence	Plasmid created
FRQ ⁹ rev	ATATCGCCAGGGTCTCATGAAAGATCG GTGC	pcDNA4/TO-6His- mK2-FRQ9
FRH_bb_mKate 2_F (66 °C)	TCAACAGTCTGTATCTGTAAGGATCCC CGGGTTAAGAATTC	pcDNA4/TO-6x His- mK2-FRH
FRH_bb_mKate 2_R (65 °C)	ACCTCAAAGAGGTCGTCCATAACCAGA ACCACCACC	pcDNA4/TO-6x His- mK2-FRH
bb_mKate2_FR H_F (64 °C)	GTTCTGGTGGTGGTTCTGGTATGGACG ACCTCTTTGAGG	pcDNA4/TO-6x His- mK2-FRH
bb_mKate2_FR H_R (64 °C)	AATTCTTAACCCGGGGATCCTTACAGA TACAGACTGTTGAAAGAAAC	pcDNA4/TO-6x His- mK2-FRH
FRH _bb_mNeonGre en_F (66 °C)	CTTTCAACAGTCTGTATCTGGGTGGTT CTGGTGGTG	pcDNA4/TO-FLAG- FRH-mNG
FRH _bb_mNeonGre en_R (66 °C)	ACCTCAAAGAGGTCGTCCATCTTGTCG TCATCGTCTTTGTAGTC	pcDNA4/TO-FLAG- FRH-mNG
bb_mNeonGree n_FRH_F (64 °C)	ACAAAGACGATGACGACAAGATGGAC GACCTCTTTGAGG	pcDNA4/TO-FLAG- FRH-mNG
bb_mNeonGree n_FRH_R (64 °C)	GAACCACCACCAGAACCACCCAGATA CAGACTGTTGAAAGAAACAATG	pcDNA4/TO-FLAG- FRH-mNG
FRH_delmutAs cI_F72	TTTTGGCGCGCCGTAAGGATCCCC	pcDNA4/TO-FLAG- FRH
FRH_delmutAs cI_R72	TTTTGGCGCGCCAGAACCACCTCACAG ATACAGACTG	pcDNA4/TO-FLAG- FRH
FRH(R608H)_F	CTTGGCCAGCTGCATGTTTTCTTGCC	pcDNA4/TO-FLAG- FRH R806H
FRH(R608H)_R	GGCAAGAAAACATGCAGCTGGCCAAG	pcDNA4/TO-FLAG- FRH R806H
WC-1 F	AGCACAGTGGCGGCCGCTCGAGACC ATGAACAACAACACTACTACGGTTCCC	pcDNA4/TO-WC-1- mNG;
WC1-R	CACCAGAACCACCACCAGAACCACC TACTTAAAGCCCTGTTGATGTTCG	pcDNA4/TO-WC-1- mNG;
		pcDNA4/TO-WC-1

Table 3.2.1 continued: Oligonucleotides for mammalian vectors

Primer name	Primer sequence	Plasmid created
4TO-mNG-R	GGGAACCGTAGTAGTTGTTGTTTCAT GGTCTCGAGCGGCCGCCACTGTGCT	pcDNA4/TO-WC-1- mNG
4TO-mNG-F	CGAACATCAACAGGGCTTAAGTGTA GGTGGTTCTGGTGGTGGTTCTGGTGCA TGCTCATCAGGC	pcDNA4/TO-WC-1- mNG
WC1-notag-R	CGAGGATATCTGCAGAATTCTTAACCC GGGGATCCCTATACTTAAGCCCTGT TGATGTTCG	pcDNA4/TO-WC-1
WC2-F	GTGGCGGCCGCTCGAGACC ATGTCTCACGGACAGCCTCC	pcDNA4/TO-WC-2
WC2-R	TCTGCAGAATTCTTAACCCGGGGATCC CTATCCCATATGATCGCCCATGGG	pcDNA4/TO-WC-2
mKate2-WC2-F	GAGGTGGTTCTGGTGGTGGTTCTGGTA TGTCTCACGGACAGCCTCC	pcDNA4/TO-mk2- WC-2
4TO-WC2-F	CCATGGGCGATCATATGGGATAGGGA TCCCCGGGTAAAGAATTCTGCAGATAT CCTCGAGTCTAG	pcDNA4/TO-mk2- WC-2; pcDNA4/TO- WC-2
4TO-mkate2- WC2-R	GGAGGCTGTCCGTGAGACATAACCAGA ACCACCACCAGAACCACCTCTG	pcDNA4/TO-mk2- WC-2
4TO- WC2notag-R	GGAGGCTGTCCGTGAGACAT GGTCTCGAGCGGCCGCCAC	pcDNA4/TO-WC-2
CS_WC-2- mnG_Fwd	CATGGGCGATCATATGGGAGGTGGTTC TGGTGGTGGTTCTG	pcDNA4/TO-FLAG- WC-2-mNG
CS_mNG_Rev	GGGGATCCTTACTTGTACAATTCGTCC ATACCATAACGTCAGTGAAAG	pcDNA4/TO-FLAG- WC-2-mNG
mNG- 4/TO_Fwd	GACGAATTGTACAAGTAAGGATCCCC GGGTAAAGAATTCTGC	pcDNA4/TO-FLAG- WC-2-mNG
WC2-OH- mNG_Rev	GAACCACCACCAGAACCACCTCCATA TGATCGCCCAT	pcDNA4/TO-FLAG- WC-2-mNG

3.2.2 Oligonucleotides for *Neurospora* vectorsTable 3.2.2: Oligonucleotides for *Neurospora* vectors

Primer name	Primer sequence	Plasmid created
XL_frqmNLS2 F	CTCGGATAAGAATGGTCGTGGccAGGA	pBM60frqmNLS2
	GCGGAAAACGCAGCAGG	pBM60frqmNLS23
		pBM60frqmNLS123
XL_frqmNLS2 R	CCTGCTGCGTTTTCCGCTcCTGGCCACG	pBM60frqmNLS2
	ACCATTCTTATCCGAG	pBM60frqmNLS23
		pBM60frqmNLS123
XL_frqmNLS3 F	ACAACGCAACAACGGGGGcAGgGTCGA	pBM60frqmNLS3
	TACGATGGCG	pBM60frqmNLS23
		pBM60frqmNLS123
XL_frqmNLS3 R	CGCCATCGTATCGACcCTgCCCCCGTTG	pBM60frqmNLS3
	TTGCGTTGT	pBM60frqmNLS23
		pBM60frqmNLS123

3.3 Antibodies

Table 3.3: Antibodies applied in Western blotting and Co-IP

Antibody	Origin	Dilution	Incubation conditions	Secondary
α -FLAG	Monoclonal ANTI-FLAG M2 antibody produced in mouse from Sigma-Aldrich(CAT# F3165)	1:5000	overnight at 4 °C or 2 h at RT	α -mouse
α -FRQ	Generated from cell culture supernatant in the Brunner laboratory N-term aa65-100, 11/2019, mouse monoclonal	1:10	overnight at 4 °C or 2h at RT	α -mouse
α -mouse	goat anti-mouse IgG (H+L)-HRP conjugate from Bio-Rad(CAT# 170-6516)	1:10 000		2 h at RT or overnight at 4 °C
α -rabbit	goat anti-rabbit IgG (H+L)-HRP conjugate from Bio-Rad(CAT# 172-1019)	1:10 000		2 h at RT or overnight at 4 °C

for Western blots, all antibodies were diluted in 5% skim milk in TBS

*antibodies from serums (Pineda Antikörper-Service) were affinity purified by Thomas Pils

3.4 Solutions and buffers for biochemical methods

Table 3.4.1: Phosphate buffered saline (PBS) pH 7.4

Components	10x	1x
NaCl	1370 mM	137 mM
KCl	27 mM	2.7 mM
Na ₂ HPO ₄	100 mM	10 mM
KH ₂ PO ₄	18 mM	1.8 mM

Table 3.4.2: Solutions for native *Neurospora* protein extraction (PEX)

Component	1x
HEPES/KOH pH 7.4	30 mM
NaCl	137 mM
Glycerol	10 %
EDTA/ NaOH pH 8.0	5 mM
Leupeptin 1 mg/mL*	5 µg/mL
Pepstatin A 1 mg/mL*	5 µg/mL
PMSF 24 mg/mL*	17 µg/mL
PhosSTOP*	1 tabl. / 10 mL buffer
* added freshly before use	

Table 3.4.3: Solutions for native *Neurospora* protein extraction with NP40 (PEX +NP40)

Component	1x
HEPES/KOH pH 7.4	50 mM
NaCl	137 mM
Glycerol	10 %
NP-40	0.4 %
PhosSTOP cOmplete mini (EDTA free)*	1 tabl. / 10 mL buffer
* added freshly before use	

Table 3.4.4: TAE (Tris-Acetic acid-EDTA)

Components	50x	1x
Tris	2 M	40 mM
Acetic acid	5.71% (w/v)	0.1142% (w/v)
EDTA 4 H ₂ 4 Na ₂	110 mM	2.21 mM

Table 3.4.5: Laemmli sample buffer (Laemmli 1970)

Component	4x	2x
Tris-HCl pH 6.8	250 mM	125 mM
Glycerol	40% (w/v)	20% (w/v)
SDS	8% (w/v)	4% (w/v)
Bromphenol blue	0.04% (w/v)	0.02% (w/v)
β-mercaptoethanol*	20% (v/v) (2.868 M)	10% (v/v) (717 mM)
*added freshly		

Table 3.4.6: SDS gel mix

Component	Stacking gel 5%	Resolving gel (12 %)
TrisHCl	60 mM (pH 6.8)	375 mM (pH 8.8)
Acrylamide: bisacrylamide	5% (29.5:0.5)	12 % (29.8:0.2)
SDS	0.1% (w/v)	0.1 % (w/v)
APS (10%)	0.05 % (v/v)	0.06 % (v/v)
TEMED*	0.1% (v/v)	0.1 % (v/v)
*APS and TEMED are added freshly as TEMED starts the polymerization reaction		

Table 3.4.7: SDS running buffer for SDS-PAGE

Components	1x
Tris	50 mM
Glycine	373 mM
SDS	0.1% (w/v)

Table 3.4.8: Ponceau S staining solution

Components	1x
Trichloroacetic acid (TCA)	0.2% (v/v)
Ponceau S	3.0% (w/v)

Table 3.4.9: Tris buffered saline (TBS) pH 7.4

Components	20x	1x
Tris	200 mM	10 mM
NaCl	3 M	150 mM
HCl	ad pH 7.4	ad pH 7.4

* for IP's protease inhibitors were freshly added: 5 ng/ μ L leupeptin, 5 ng/ μ L pepstatin A, 17 ng/ μ L (= 1mM) PMSF

Table 3.4.10: Luminol mix

Components	
TrisHCl (pH 8.5)	100 mM
Luminol	2.2×10^{-2} % (w/v)
Coumaric acid	3.3×10^{-3} % (w/v)
H ₂ O ₂	9.0×10^{-3} % (v/v)

prepare luminol mix freshly before use

Table 3.4.11: Gelfiltration buffer

Components	
HEPES/ KOH (pH 7.4)	25 mM
NaCl	140 mM
EDTA (pH 8.0)	1 mM
Glycerol	1% (w/v)
Triton X-100	0.05% (v/v)

prepare luminol mix freshly before use

3.5 Media and solutions for the handling of *E. coli*

Table 3.5.1: Super optimal broth (SOB)/ SOB with catabolite repression (SOC)*

Components	
Tryptone	2% (w/v)
Yeast extract	0.5% (w/v)
NaCl	10 mM
KCl	2.5 mM
MgCl ₂ x 6 H ₂ O	10 mM
MgSO ₄ x 6 H ₂ O	10 mM

* in case of SOC 20 mM glucose is added to SB for catabolite repression
autoclave (120 °C, 1 bar, 20 min) without magnesium (or glucose) components
sterile filter (0.45 µm) medium after mixing nutrient and magnesium (and glucose) solution

Table 3.5.2: LB Medium and LB Agar plates

Components for 1 L	
tryptone	10 g
yeast extract	5 g
NaCl	10 g
ddH ₂ O	Add to 1 L

LB agar plates with 2% agar and supplemented with ampicillin were prepared by Selene Cordeiro

3.6 Media and solutions for the growth and transformation of *N. crassa*

Table 3.6: Supplements

Component	Stock concentration	Final concentration
Histidine	25 mg/mL	0,5 mg/mL autoclaved
Hygromycin B	100 mg/mL	250 µg/mL
D(+)-Biotin	100 µg/mL	15 ng/mL in Vogel's solution 50 ng/mL in solid medium 100 ng/mL in luciferase medium
Luciferin	25 mM	150 µM for top agar 50 µM for Luciferase plate

Table 3.6.2: Vogel's solution* (Vogel 1956)

Components	50x	1x
Na ₃ citrate x 2 H ₂ O	12.5% (w/v)	0.25% (w/v)
KH ₂ PO ₄	25.0% (w/v)	0.50% (w/v)
NH ₄ NO ₃	10.0% (w/v)	0.20% (w/v)
MgSO ₄ x 7 H ₂ O	1.0% (w/v)	0.02% (w/v)
CaCl ₂ x2 H ₂ O	0.5% (w/v)	0.01 % (w/v)
D(+)-Biotin	2.5 x 10 ⁻⁵ % (w/v)	5 x 10 ⁻⁷ % (w/v)
Trace elements	0.05% (v/v)	0.01% (v/v)

prepared by Sabine Schultz, 2 mL chloroform added for preservation

Table 3.6.3: FGS (fructose-glucose-sorbose) solution

Components	10x	1x
Fructose	0.5% (w/v)	0.05%
Glucose	0.5% (w/v)	0.05%
Sorbose	10% (w/v)	1%

autoclave (120 °C, 1 bar, 20 min)

Add after autoclavation:

10x FGS	1x
Histidine	100 µg/mL
Hygromycin B	250 µg/mL

cast plates with 25 mL bottom agar per petri dish

Table 3.6.4: Top agar

Components	1x
50x Vogel's solution	1x
Yeast extract	2% (w/v)
Sorbitol	18.2% (w/v)
Agar	1% (w/v)

autoclave (120 °C, 1 bar, 20 min)

leave to cool down to 60 °C and add

10x FGS	1x
Histidine	100 µg/mL

pour 6 mL top agar into a 15mL tube and store at 60 °C

Table 3.6.5: Bottom agar

Components	1x
50x Vogel's solution	1x
Yeast extract	2% (w/v)
Agar	1% (w/v)
autoclave (120 °C, 1 bar, 20 min)	
after autoclaving add	
10x FGS	1x
Histidine	100 µg/mL
Hygromycin B	250 µg/mL
cast plates with 25 mL bottom agar per petri dish	

Table 3.6.6: Slant and flask medium*/**

Components	1x
50x Vogel's solution	1x
Sucrose	2% (w/v)
Agar	2% (w/v)
autoclave (120 °C, 1 bar, 20 min)	
leave to cool down to 60 °C and then add:	
Histidine	100 µg/mL
Hygromycin B	200 µg/mL
*for slants: pour 2-3 mL medium into a glass slant, keep tilted at an almost 90° angle until solidified	
**for flasks: pour 100 mL into a 500mL flask (20 mL into a 100mL flask), rotate at an angle on ice until solidified	

Table 3.6.7: Composition of Luciferase plate medium

Medium A	
Component	1 x
Agarose	4 % (w/v)
D(+)-Biotin	100 ng/µL
3x Vogel's solution	33,3 % (v/v)

Table 3.6.7 continued: Composition of Luciferase plate medium

ddH ₂ O	ad 25 mL
Medium B	
Component	1 x
D(-)-Fructose	0,1 % (w/v)
D(+)-Glucose monohydrate	0,1 % (w/v)
L(-)-Sorbitose	4 % (w/v)
ddH ₂ O	ad 25 mL
Autoclave separately, then mix medium A and medium B, each 50 % (v/v)	
Luciferin 50 µM added after autoclaving and then 150 µL /well is plated out (96 well plate).	

Table 3.6.8: Trace elements

Components	Stock solution
Citric acid x 1 H ₂ O	5 % (w/v)
ZnSO ₄ x 7 H ₂ O	5 % (w/v)
(NH ₄) ₂ Fe(SO ₄) ₂ x 6 H ₂ O	1 % (w/v)
CuSO ₄ x 5 H ₂ O	0,25 % (w/v)
MnSO ₄ x 1 H ₂ O	0,05 % (w/v)
H ₃ BO ₃	0,05 % (w/v)
Na ₂ MoO ₄ x 2 H ₂ O	0,05 % (w/v)
prepared by Sabine Schultz	

3.7 Enzymes, chemicals, disposals and kits

Table 3.7.1: Enzymes

Enzyme	Supplier
CIP	New England Biolabs
Pfu ultra polymerase (CAT# 600384)	Agilent
Q5 DNA polymerase	New England Biolabs
Restriction enzymes (various)	New England Biolabs
T4 DNA ligase	New England Biolabs
T4 DNA polymerase	New England Biolabs

Table 3.7.2: Chemicals, beads and ladders

Chemical	Supplier
Acetic acid (CAT# 64-19-7)	Merck
Acetone	
Acrylamid 30 % Rotiphorese Gel A (CAT# 3037.1)	Carl-Roth
Acrylamid/Bis-Lösung 30 (29:1) (CAT# A124.2)	Carl-Roth
Agar (CAT# 9002-18-0)	Zentrallager (various)
Agarose (CAT# 9012-36-6)	Zentrallager (various)
Ammonium sulphate (CAS 7783-20-2)	Merck
Ampicillin (sodium salt) (CAS 69-52-3)	Merck
APS (CAT# 7727-54-0)	Merck
Arginine (hydrochloride) (CAT# 1119-34-2)	AppliChem
ATP (disodium salt hydrate) (CAT# 1068)	Gerbu
BCS (CAT# B1125)	Merck
D(+)-Biotin (CAT# 58-85-5)	AppliChem
Bromphenol blue (CAT# 115-39-9)	Waldeck
BSA (albumin Fraction V) (CAT# 9048-46-8)	AppliChem
butane/ propane gas CV470 PLUS (campingaz)	Apragaz
CaCl ₂ x 2 H ₂ O (CAT# 10035-04-8)	Merck
Chloroform (CAT# 67-66-3)	Merck
Citric acid x 1 H ₂ O	Fisher Scientific
cOmplete ULTRA Tablets, EDTA-free (CAT# 04693159001)	Roche Diagnostics
<i>p</i> -Coumaric acid (CAT# 501-98-4)	Merck
CutSmart buffer (CAT# B7204)	New England Biolabs
CuSO ₄ x 5 H ₂ O (CAT# 7758-99-8)	AppliChem
DMEM (CAT# 10569010)	Thermo Scientific
DMSO (CAT# 67-68-5)	Merck
DNA ladder 1 kb plus (CAT# 10787026)	Thermo Scientific
dNTPs (CAT#31802)	Axon
Doxycycline (CAT# 631311)	Thermo Scientific
DPBS (CAT# 14190169)	Thermo Scientific
DTT (CAT# 3483-12-3)	Gerbu Biotechnik
EDTA disodium salt dihydrate (CAT# 6381-92-6)	AppliChem
Ethanol (CAT# 64-17-5)	VWR

Table 3.7.2 continued: Chemicals, beads and ladders

Chemical	Supplier
Ethanol, 1% petrol ether	Zentrallager (various)
Ethidium bromide (CAT# HP46.2)	Carl-Roth
Fetal Bovine Serum (FBS) (CAT# 10270106)	Thermo Scientific
Fructose (CAT# 57-48-7)	Carl Roth
Glucose (CAT# 50-99-7)	Merck
Glycerol (CAT# 56-81-5)	Merck
Glycine (CAT# 56-40-6)	Labchem international
HCl (CAT# 7647-01-0)	Honeywell (Fluka)
HEPES (CAT# 7365-45-9)	Carl Roth
H ₃ BO ₃ (CAT#10043-35-3)	AppliChem
H ₂ O ₂ (CAT# 107209)	Merck
Hygromycin B gold solution (CAT# ant-hg-5)	Invivogen
Imidazole (CAT# 288-32-4)	Merck
Kanamycin sulphate (CAT# 70560-51-9)	AppliChem
K ₂ HPO ₄ x 3 H ₂ O (CAT# 16788-57-1)	Merck
KH ₂ PO ₄ (CAT# 7778-77-0)	Chemsolute
KNO ₃ (CAT# 7757-79-1)	Merck
LB medium (CAT# X968.2)	Carl Roth
Leptomycin B (CAT# L2913-.5UG)	Merck
Leupeptin (CAT# 103476-89-7)	AppliChem
Loading dye for agarose gels, purple 6x (CAT# B7024)	New England Biolabs
Luciferin (CAT# 2591-17-5)	p.j.k.
Luminol (CAT# 521-31-3)	AppliChem
β-mercaptoethanol (CAT# 60-24-2)	Merck
Methanol (CAT# 67-56-1)	VWR
MgCl ₂ x 6 H ₂ O (CAT# 7791-18-6)	AppliChem
MgSO ₄ x 7 H ₂ O (CAT# 10034-99-8)	AppliChem
MnSO ₄ x H ₂ O (CAT# 10034-96-5)	AppliChem
Milk powder (CAT# T145.1)	Carl Roth
Na ₃ citrate (CAT# 6132-04-3)	Fisher Scientific
NaCl (CAT# 7647-14-5)	Bernd Kraft
Na ₂ MoO ₄ x 2 H ₂ O (CAT# 10102-40-6)	AppliChem
NaOH (CAT# 1310-73-2)	Zentrallager (various)

Table 3.7.2 continued: Chemicals, beads and ladders

Chemical	Supplier
(NH ₄) ₂ Fe(SO ₄) ₂ x 6 H ₂ O (CAT# 7783-85-9)	AppliChem
NH ₄ NO ₃ (CAT# 6484-52-2)	Bernd Kraft
NH ₄ Oac (CAT# 631-61-8)	Riedel-de Haën
NP40 (CAT# 9016-45-9)	AppliChem
Penicillin-Streptomycin (CAT#15140122)	Thermo Scientific
Pepstatin A (CAT# 26305-03-3)	AppliChem
<i>ortho</i> -phosphoric acid (CAT# 7664-38-2), 85%	Merck
PhosSTOP (CAT# 56-25-7)	Roche Diagnostics
PIERCE Western blot transfer buffer (CAT# 35040)	Thermo Scientific
PIPES (CAT# 5625-37-6)	AppliChem
PMSF (CAT# 329-98-6)	AppliChem
Ponceau S (CAT# 6226-79-5)	AppliChem
Proline (CAT# 147-85-3)	AppliChem
D(-)-Quinic acid (CAT# 138622)	Merck
SDS (CAT# 151-21-3)	SERVA
Sorbitol (CAT# 50-70-4)	Merck
Sorbose (CAT# 87-79-6)	Carl Roth
Sucrose (CAT# 57-50-1)	AppliChem
TCA (CAT# 76-03-9)	Merck
TEMED (CAT# 110-18-9)	Carl Roth
Tris (CAT# 77-86-1)	Carl Roth
Triton X-100 (CAT# 9002-93-1)	Merck
Trypsin-EDTA (0.05%), phenol red (CAT# 25300096)	Thermo Scientific
Tryptone (CAT# 91079-40-2)	BD
ZnSO ₄ x 7 H ₂ O (CAT# 7446-20-0)	AppliChem

Table 3.7.3: Disposals

Disposals	Supplier
12- well plate (CAT# CC7682-7524)	CytoOne
24- well plate (CAT# CC7682-7512)	CytoOne
96-well plate, white flat bottom (CAT# 3917)	Costar

Table 3.7.3 continued: Disposals

Disposals	Supplier
96 well plate (CAT# 3598)	Corning
Beads, Protein A sepharose (CAT# CL-4B)	Cytiva
Beads, Anti-FLAG M2 Affinity Gel (CAT# A2220)	Merck
Beads, Protein G Sepharose (CAT# 17-0618-01)	Cytiva
Cryotubes, CRYO.S PP	greiner bio-one
Cuvette, for OD measurements (CAT# 67.742)	Sarstedt
Cuvette, for electroporation (Cat# 75-EP-202)	biolabs products
Filter pipette tips, volumes 10, 200, 1000 μ L (CAT# S1120-3710-C/ S1120-1710-C/ S1122-1730-C)	Starlab
Filter pipette tips 200 μ L (CAT# LC2867)	Biozym
Glass pipettes (Pasteur pipettes)	Zentrallager (various)
Gloves, nitrile (CAT# SG-C)	Starlab
HisTrap HP purification columns (CAT# 17524701)	Cytiva
Nitrocellulose blotting membrane, Amersham Protran supported 0.45 μ m NC	Cytiva
Paper towel, WypAll	Kimberly-Clark Prof.
Parafilm M, laboratory film	Bemis
Petri dishes, 9 cm	Sarstedt
Petri dishes (TC treated, 100x 20 mm) (CAT# CC7682-3394)	CytoOne
Pipette tips, volumes 10 and 200 μ L	Greiner bio-one
Pipette tips, volumes 1000 μ L	Sarstedt
Pipette tips, volumes 200 μ L, gel loading	VWR
Pipette (serological), volumes 5, 10, and 25 mL	Sarstedt
Reagent reservoir (CAT# E2310-1025)	Starlab
Sterile filter, Steritop 0.22 μ m 500 mL	Millipore
Superose® 6 Increase 10/300 GL (CAT# 29-0915-96)	Cytiva
Tubes, for PCR	Zentrallager (various)
Tubes, 1.5 and 2 mL volumes	Zentrallager (various)
Tubes, 1.5 and 2 mL volumes, low-binding	Sarstedt
Tubes, 15 and 50 mL volumes	Sarstedt
Whatman paper, 3 mm CHR	Cytiva
X-ray films, Super RX-N, medical X-ray film 13x18	FUJIFILM

Table 3.7.4: Kits

Kit	Supplier
QuikChange II XL Site-Directed Mutagenesis Kit (CAT# 200521)	Agilent
GeneJET Plasmid Miniprep Kit (CAT# K0503)	Thermo Scientific
NucleoSpin Gel and PCR Clean-up (CAT# 740609.250)	Macherey-Nagel
Xfect™ Transfection Reagent (CAT# 631318)	Takara Bio

3.8 Machines, devices and reusables

Table 3.8: Devices, machines and reusables

Device	Model	Manufacturer
Autoclave	SANOclav	Wolf
Äkta	Äkta pure™	Cytiva
Bottles, 50 mL – 2L	Schott flask	Duran/ SIMAX
Blotting chamber		peqlab
Boxes, plastic 500 mL, 1 L, 2 L		Carl-Roth
Cell spreader	drigalski, glass 145x50	Carl-Roth
Centrifuge , table	5424	Eppendorf
Centrifuge , table, cold	5417R	Eppendorf
Centrifuge, table (2 – 50 mL volumes)	multifuge 1L-R Kendro	Heraeus Instruments
Developer machine	SRX-101 A	Konica Minolta
Electroporation device, for <i>Neurospora</i>	GenePulser Xcell	Bio-Rad
Film cassette for Western blot detection	24 x 30 cm	Advansta; Other manufacturers
Flasks 25 mL – 2 L	KIMAX	Kimble
Fridge, 4° C		Liebherr
Freezer -20 °C		Liebherr
Freezer -80 °C	VIP Series -86°C	Sanyo
Incucyte	ZOOM and SX1	Sartorius
Incubator, 30 °C	WTC	Binder
Incubator, 60 °C	Heraeus Function line	Heraeus Instruments
Incubator/shaker, 18 to 37 °C	Multitron	Infors
Incubator/shaker, 37 °C		Binder

Table 3.8 continued: Devices, machines and reusables

Device	Model	Manufacturer
Incubator for plate reader	E41L1C8	CLF Plant Climatics
Incubator for Incucyte ZOOM	ICH260	Memmert
Incubator for Incucyte SX1	STERI-CYCLE i160	Thermo Scientific
Magnetic stirrer	yellow line	neolab
Nanophotometer	NP 80 mobile	Implen
PCR cycler with and without gradient	lab cycler	SensoQuest
Photometer	6300	Jenway
Pipettes	pipetman	Gilson
Pipette, multichannel		
Pipette, automated	Pipetboy acu	Integra Biosciences
Plate reader	EnSpire	PerkinElmer
Power supply, SDS-PAGE and WB	peqPOWER 300	peqlab
Power supply Agarose gels	EPS 301	Amersham pharm. Biotech
Power supply SDS-PAGE and WB	EPS 601	Amersham pharm Biotech
Rotating wheel	Rotator 2-1175	neolab
Scanner and printer	IMC3000	Ricoh
Shaker, RT		Neolab
Shaker, cold room (4 °C)	3013	GFL
Test tubes, glass		neolab
Thermal block	Thermomixer compact	Eppendorf
Thermal block, with cooling	Thermomixer comfort	Eppendorf
Tubes, centrifugal, 50 mL volume		Beckmann
Unichromat incubator (Äkta)	1500	UniEquip
Vacuboy		Integra Biosciences
Vortexer	Vortex genie 2	Scientific Industries

3.9 Service providers, web services and software

Table 3.9: Websites, providers and software

Web tool/ web service	Use
benchling	Editing of plasmid maps; check sequencing, etc.
BioRender	Graph production; creation of images
ChimeraX (1.4)	Protein structure analysis
deepL	Text procession, translations
EndNote	Reference manager
Eurofins	Sanger and whole plasmid sequencing
FungiDB	<i>Neurospora crassa</i> genome search
ImageJ	Incucyte Image analysis and procession
Incucyte 2023A / 2016B	Incucyte image analysis, program to use machine
Multalin	Alignment of DNA and protein sequences
NEBioCalculator	Calculation of insert and vector ratios
NEB Tm Calculator PCR	Annealing temperature calculation
NLStradamus	NLS prediction tool showing all options
Npsa prabi coiled-coil prediction	Prediction of coiled-coil using standard settings
Office (Microsoft)	Excel, PowerPoint, Word
OligoEvaluator (Merck)	Calculation of DNA features such as secondary structures of DNA primers
OpenAI's GPT-4 language model	Suggestions for titles; improvement of the clarity and phrasing of some text passages
SnapGene Viewer	View Plasmid maps

4. Results

With this dissertation, I present the following findings: I successfully reconstructed parts of the *Neurospora* circadian clock in mammalian cells. This was achieved by fusing the core clock proteins FRQ, FRH, CK1a, and WCC to the fluorophore reporter proteins mKate2 (mK2) or mNeonGreen (mNG) and monitoring their expression and subcellular dynamics using non-invasive live-cell imaging platforms, namely Incucyte® ZOOM and Incucyte® SX1 (sections 2.3.4 and 4.1). This approach enabled the identification of novel indicators of interaction interfaces within the FFC complex and uncovered a previously unknown role for FRH in the circadian clock. Additionally, the use of this cellular system facilitated the rapid analysis of clock mutants, which would have been challenging or even impossible to investigate in *Neurospora* (sections 4.2–4.3). Whenever appropriate, mutants were used for further investigation in *N. crassa* (sections 4.2.3, 4.4.2, and 4.5.2). Finally, I explored how phosphorylation of FRQ by CK1a remodels the subunit composition of the FFC complex in ways that were unexpected and not previously anticipated (section 4.5).

4.1 The overexpression of FRQ, WCC and FRH in U2OS T-REx cells allows for the screening of the clock proteins without the influence of other factors

Prior to undertaking an analysis of the interactions of the subunits of the FFC complex, I examined each *N. crassa* clock protein individually in order to identify their expression phenotype and subcellular localization in U2OS T-REx cells (U2OStx). Therefore, I transiently overexpressed mK2-FRQ, FRH-mNG, WC-1-mNG and mK2-WC-2 in U2OStx cells by induction with doxycycline (DOX; section 2.3.2). Fluorescence levels and expression patterns were then measured using live cell imaging using the Incucyte® ZOOM or Incucyte® SX1 (section 2.3.4). The transient transfection of U2OStx cells had the advantage of allowing for the titration of plasmid dosages, which consequently allowed for the titration of protein levels.

By transiently overexpressing fluorescently tagged FRQ, I found that FRQ can form phase-separated foci in the nucleus. The formation of foci was dependent on the concentration of plasmid used for transfection. At medium plasmid concentrations (50 ng), the formation of foci was observed in 73% of cells (Figure 4.1, second image from the left; Figure S2 B). However, at high plasmid levels (75-100 ng), the foci fused and

the signal quickly spread throughout the nucleus, making individual foci unrecognizable. Furthermore, low plasmid levels (25 ng) did not lead to foci-formation. Instead, only a weak signal from FRQ was recognizable in the cell nucleus. Recently, recombinant FRQ has been recently reported to phase-separate *in vitro*, and focal assemblies of FRQ have been described in *Neurospora* (Tariq et al., 2024). It will be interesting to further analyze FRQ in this system to observe whether its potential to self-interact has functional significance.

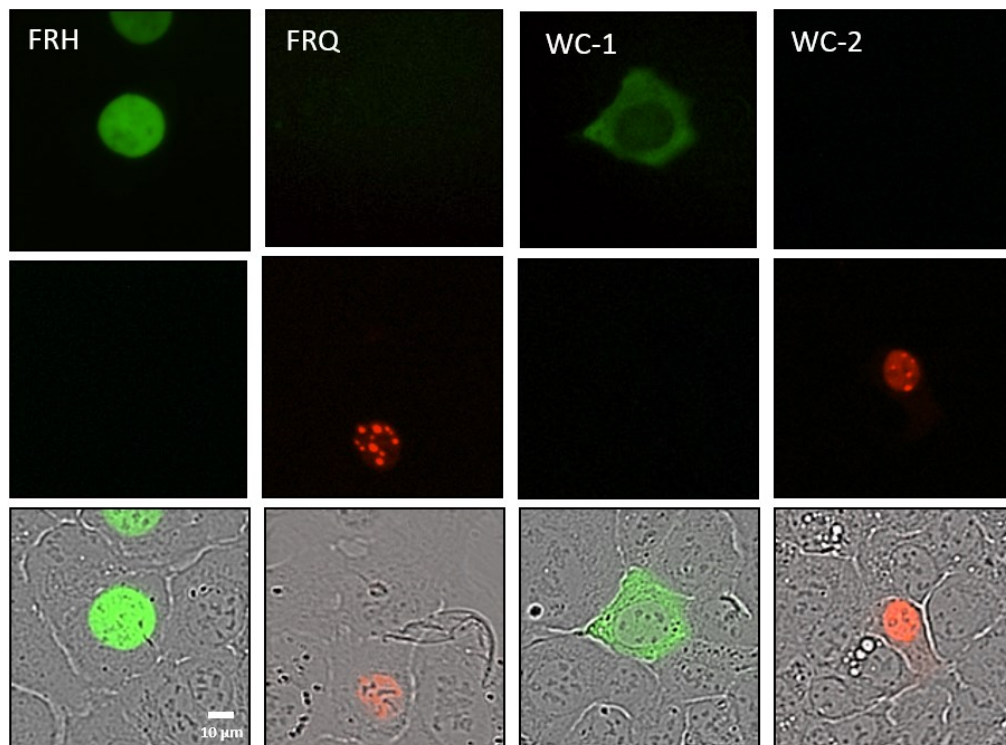


Figure 4.1: Transient expression and localization of fluorescently tagged *N. crassa* clock proteins in U2OSTx cells.

Incucyte® live cell analysis of cellular localization of transient FRH, FRQ, WC-1 and WC-2: FRH-mNG (50 ng) is uniformly distributed in the nucleus. MK2- FRQ (50 ng) forms droplets in the nucleus. WC-1-mNG (50 ng) localizes to the cytosol. MK2- WC-2 (50 ng) forms nuclear droplets in addition to homogenously expressed WC-2 in the nucleus. 20x objective, scale bar 10 µm.

It is noteworthy that the FRQ signal remained stable even without co-transfection of FRH, suggesting that FRQ is more stable when expressed in U2OSTx cell lines than in *N. crassa*, where FRQ is quickly degraded by the proteasome when its interaction with FRH is compromised (Cheng et al. 2005, He and Liu 2005).

The fluorescently tagged FRH generated a strong nuclear signal. Even though no NLS has been shown in the crystal structure of FRH (Figure 1.6), NLS prediction tools identify an NLS for FRH between aa405-418 (Figure S2 D). No foci were observed at different plasmid concentrations or using a different fluorescence tag (Figure 4.1; Figure S2 B).

When I transiently expressed WC-1-mNG, I observed that it was mostly homogeneously distributed in the cytoplasm. Occasionally WC-1 also formed phase-separated foci around the nucleus or was present in cytosol and nucleus (25 %). My observation was that the appearance of WC-1 foci correlated with increasing concentrations of plasmid used for transient transfection. However, the phenotype of WC-1 expressed homogeneously in the cytosol was more common (75 %, 50 ng) and therefore relevant for my study than the rarer phenotype that showed foci-formation (Figure 4.1; second image from the right).

Overexpressed mK2-WC-2 exhibited both foci-formation and a slightly homogeneous distribution within the nucleus (Figure 4.1). Notably, the balance between mK2-WC-2 foci and its dissolved form varied depending on the level of WC-2 expression within individual cells (an image with higher amounts of dissolved mK2-WC-2 can be seen in Figure S2 C). Additionally, over time the foci fused and the signal quickly spread throughout the nucleus, making individual foci unrecognizable. The fusion of foci was accelerated by the use of higher amounts of plasmid for transient transfection.

4.2 FRQ-FRH and WCC co-localization: validation in U2OStx cells

The objective was to analyze protein interactions in U2OStx that are known to interact, based on studies in *N. crassa*, and to demonstrate that this approach could be employed to investigate the interactions and localizations of *Neurospora* clock proteins in mammalian cells. For this purpose, pairs of *N. crassa* clock proteins were expressed in U2OStx cell lines. FRQ forms a complex with FRH, which protects FRQ from premature degradation in *N. crassa*. After the validation of interaction between FRQ and FRH (section 4.2.1), I studied FRQ9, FRQ6B2 as well as the FRQNLS mutants in cell culture as well as *Neurospora* (section 4.2.2 and 4.2.2). WC-1 and WC-2 are the subunits of WCC, and thus, as expected, I was able to validate that they co-localize in U2OStx cells (section 4.2.4).

4.2.1 FRH prevents the accumulation of FRQ in nuclear foci

The phenotype that I observed when FRH-mNG was co-expressed with mK2-FRQ in U2OS_{tx} cells was dependent on the ratio and amounts of transfected vectors. At a transfection ratio of mK2-FRQ to FRH-mNG of 1:1 (50 ng: 50 ng), co-expression of both plasmids at the same concentration resulted in the two proteins being evenly distributed in the cell nucleus (Figure 4.2.1b B). At low concentrations of FRH (FRQ: FRH; 50 ng: 16.5 ng or 12.5 ng), FRH migrated into mK2-FRQ foci (Figure 4.2.1b A). In all observed cases, FRQ and FRH were either co-localized in nuclear foci or homogeneously distributed throughout the nucleus. My data clearly shows that FRH-mNG impairs the formation of mK2-FRQ foci in the nucleus. Therefore, I defined an interaction between FRQ and FRH either when FRH dissolved FRQ foci or when FRH migrated to FRQ foci, depending on the protein concentrations used during transient transfection.

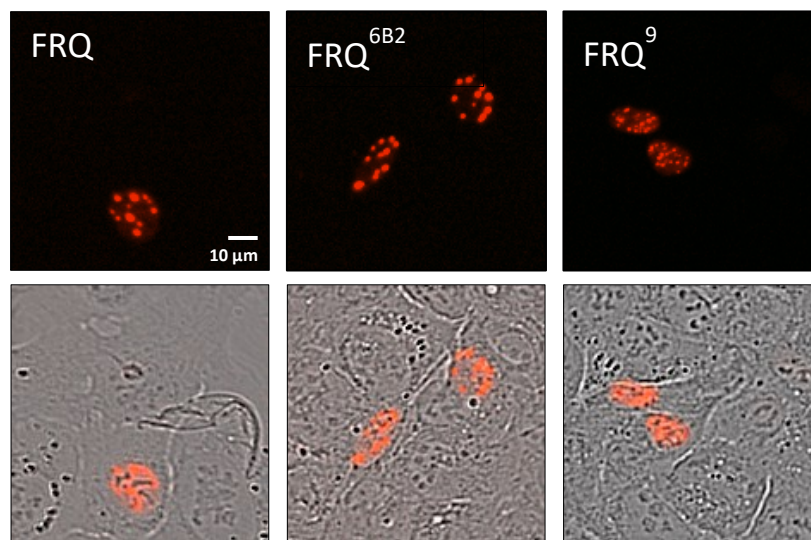


Figure 4.2.1a: **The C-terminus of FRQ is not essential for foci-formation**

Transient expression in U2OS_{tx} cells of mK2-tagged FRQ. The FRQ^{6B2} mutant carries an alanine substitution of residues 774-776, DHF to AAA (Guo et al, 2010). FRQ⁹ (Loros et al, 1986) disturbs clock function and contains a stop codon at aa623. 50 ng of vector was used for transfection, respectively. FRQ, FRQ^{6B2} and FRQ⁹ all form nuclear foci, indicating that the C-terminus of FRQ is not needed for foci-formation. Scale bar = 10 μm.

FRQ^{6B2} contains a triple alanine substitution of amino acids 774–776 in FRQ, which has been shown to abolish FRH binding (Guo et al. 2010). When I transiently expressed mK2-FRQ^{6B2} with and without FRH-mNG (Figure 4.2.1a and 4.2.1b C), I observed no effect of FRH-mNG on the accumulation of nuclear foci of mK2-FRQ^{6B2}. Though, I found that FRH was partially recruited to FRQ's nuclear foci, suggesting that FRQ^{6B2} and FRH share a weak interaction. These findings are consistent with previous results, further confirming that the 6B2 region is a critical interaction site for FRH.

There are reports which state that FRQ⁹ has a disrupted clock function and is known to not bind to FRH (Loros et al. 1986, Aronson et al. 1994). To investigate this in U2OSx cells, I transiently co-transfected mK2-FRQ⁹, which is truncated at the C-terminus by the insertion of a stop codon at aa623, with FRH-mNG. MK2-FRQ⁹ formed nuclear foci that were not resolved by FRH-mNG, and no co-localization with FRH was observed, in contrast to FRQ or FRQ^{6B2} (Figure 4.2.1a and Figure 4.2.1b A-D). Based on these findings, along with previous research, my data confirm that the C-terminus of FRQ contains the interaction site for FRH (Cheng et al. 2005, Guo et al. 2010).

To further verify this data, I generated a construct which contains only the C-terminal part of FRQ (mK2-FRQ^{C-term}; aa630-989). To my surprise, FRQ^{C-term} did not form nuclear foci, while still mainly localizing to the nucleus. Upon co-transfection of mK2-FRQ^{C-term} with FRH, I observed a more distinct confinement of the signal within the nucleus, which suggested that the C-terminus of FRQ indeed interacts with FRH (Figure 4.2.1b E and 4.2.2 A).

My data suggests that the tight anchoring of FRH to its binding site in the C-terminal 6B2 region of FRQ prevents the accumulation of FRQ in foci within the nucleus. Foci-formation seems to be a process requiring regions of FRQ outside the FRH anchoring site, which has previously been suggested by our group (Marzoll et al. 2022a, Marzoll et al. 2022b). In the case of a mutated 6B2 anchor, I observed no co-localization between FRH and FRQ indicating a loss of interaction (Figure 4.2.1b C). Therefore, FRQ^{6B2} was able to form foci even in the presence of FRH.

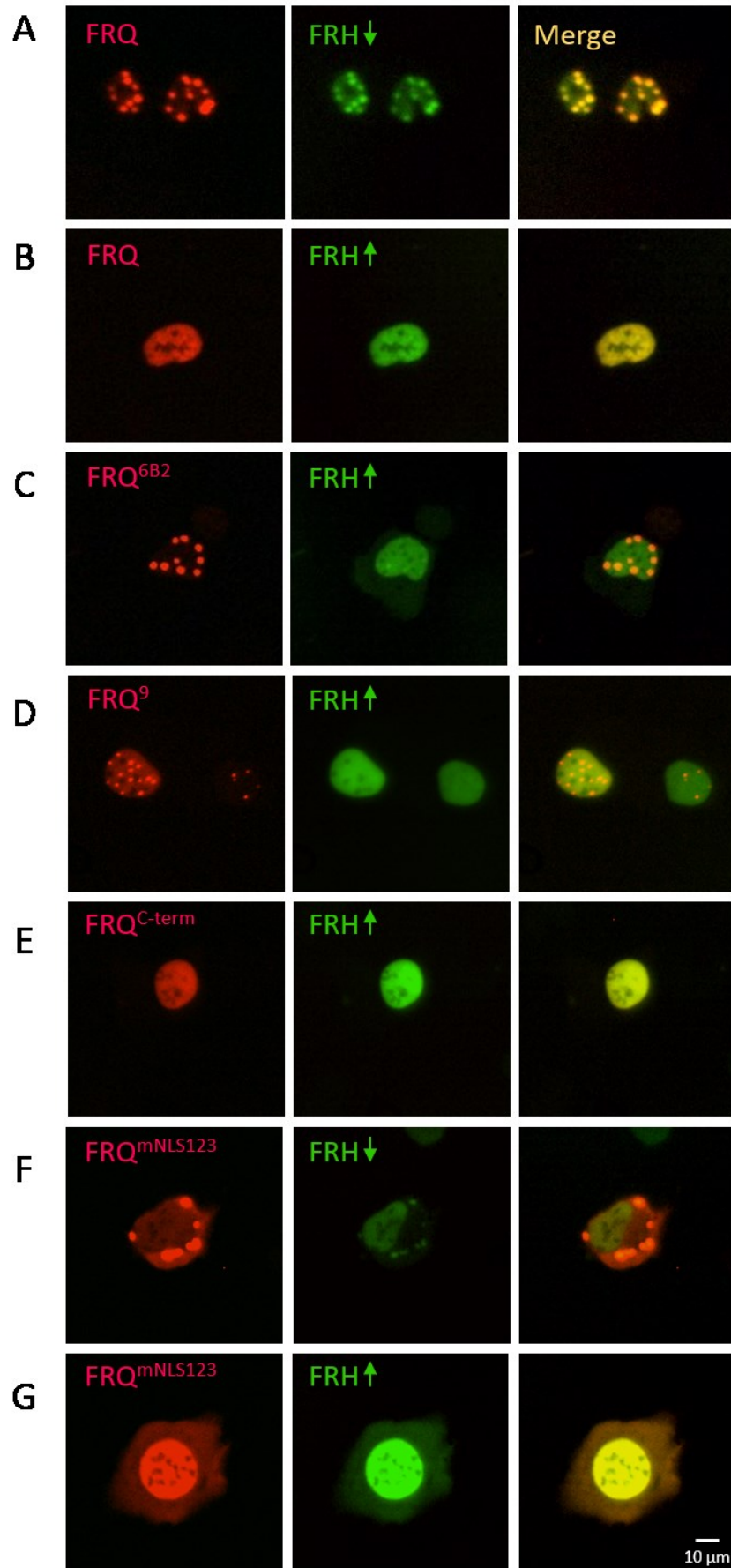


Figure legend on next page

Figure 4.2.1b: Saturating amounts of FRH binding to FRQ prevent FRQ nuclear foci-formation in U2OSStx cells

The indicated mK2-tagged FRQ variants were co-expressed with FRH-mNG. (A) Co-expression of mK2-FRQ (50 ng DNA) with non-saturating amounts of FRH-mNG (16.5 ng) leads to co-localization of FRQ and FRH in nuclear foci. (B) Co-expression of mK2-FRQ (50 ng) with saturating FRH-mNG (50 ng) results in nuclear dispersion of both proteins. (C) and (D) Co-expression of mK2-FRQ^{6B2} or FRQ⁹ (50 ng each) with FRH-mNG (50 ng) shows nuclear dispersion of FRH-mNG while mK2-FRQ^{6B2} and FRQ⁹ forms nuclear foci. (E) Co-expression of mK2-FRQ^{C-term} (50 ng) with FRH-mNG (50 ng). Both proteins are dispersed in the nucleus. (F) and (G) Co-expression of mK2-FRQ^{mNLS123} (50 ng) with FRH (50 ng). Cytosolic FRQ foci recruit non-saturating amounts of FRH. Saturating amounts of FRH dissolve cytosolic FRQ foci and recruit FRQ in the nucleus.

4.2.2 FRQ has three functional NLS sequences

NLS sequences are specific regions within a protein that are essential for the regulated nuclear import of that protein. In the case of FRQ NLS prediction tools, such as NLStradamus (Nguyen Ba et al. 2009), predicted two NLS at the following locations: aa194-199 and aa562-568. A third NLS-like sequence is predicted at aa639-645, albeit with a lower score (Figure 4.2.2 B, upper panel). FRQ^{C-term} (aa630-989) is predominantly localized in the nucleus (Figure 4.2.2 A). In contrast, the FRQ C-terminal domain, lacking the NLS-like sequence (aa720-989), did not undergo nuclear relocation (Figure 4.2.2 A).

To further analyze the other putative NLS sequences, I proceeded to divide FRQ into sequences comprising solely one of the predicted sequences. The following FRQ NLS sequences were analyzed: FRQ^{NLS1} (aa1-412), FRQ^{NLS2} (aa556-637) and FRQ^{C-term}, which contained the third NLS-like sequence. All of the FRQ fragments were observed to localize to the nucleus, although no stable nuclear foci were formed for either of the short fragments (Figure 4.2.2 A). This indicates that the accumulation of FRQ in nuclear foci seems to require longer regions and that the entire FRQ molecule might contribute to foci-formation, presumably through self-interaction. In conclusion, my data on the NLS mutants suggest that all three sequences predicted to be NLS are capable of transporting FRQ into the nucleus in U2OSStx cells.

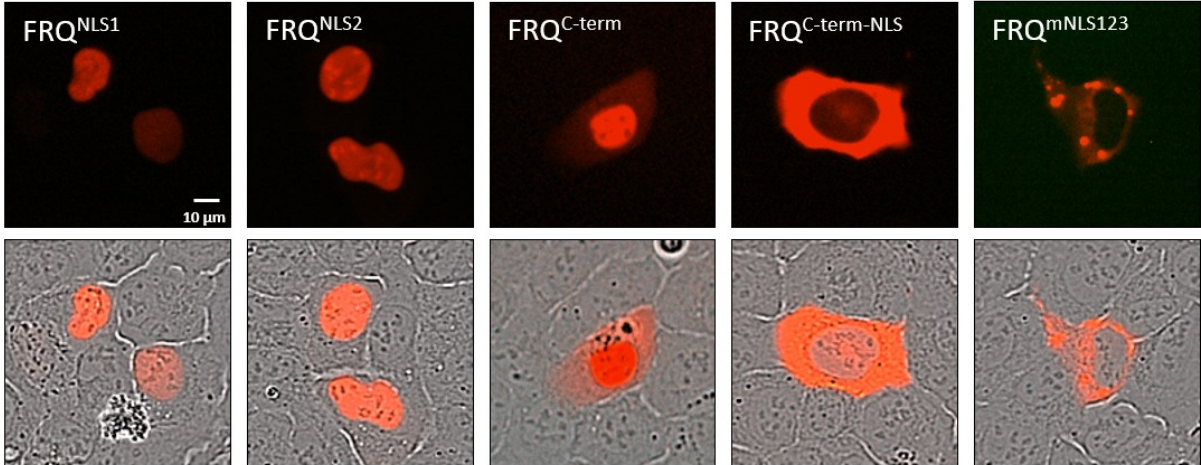
My part-time technician Bianca Ruppert introduced mutations into all three putative NLSs of FRQ within the pcDNA4/TO vector containing mK2. The NLS1 sequence, RRKKR, was replaced with RQKKQ. For NLS2, the amino acid sequence RRKKRK was modified to RGQERK. In FRQ^{mNLS3}, the RRKRR sequence was substituted with RGQG. Analysis of the expressed protein through overexpression in the cellular system revealed that it no longer retained its nuclear localization and instead formed cytoplasmic foci (Figure 4.2.2 A). These findings indicate that the mutation of all three NLSs leads to the exclusion of FRQ from the nucleus, providing further evidence that FRQ contains three distinct NLSs. Interestingly, when I co-transfected mK2-FRQ^{mNLS123} with high levels of FRH-mNG, this resulted in the relocalization of FRQ^{mNLS123} to the nucleus. This suggests that FRQ can be transported to the nucleus through its interaction with FRH. However, when lower amounts of FRH were used, FRH was partially retained in the cytosol (Figure 4.2.1b F and G).

The mutated amino acids in NLS1, NLS2, and NLS3 were specifically chosen to avoid altering the charge of FRQ in order to preserve its structural organization. To confirm that the NLS function was eliminated by these mutations, I tried to find NLS sequences using NLStradamus for the sequences of FRQ^{mNLS23} and FRQ^{mNLS123} and compared them with the previous prediction of wild-type (WT) FRQ. No NLS could be predicted for these sequences (Figure 4.2.2 B), suggesting that the NLSs were effectively removed by the mutations.

Figure 4.2.2: FRQ contains three NLSs

(A) Transient expression in U2OSTx cells of nuclear localization signal mutants of mK2-tagged FRQ (50 ng). FRQ^{NLS1} (aa1-412), FRQ^{NLS2} (aa556-637) and FRQ^{C-term} (aa630-989) localize in the nucleus. FRQ^{C-term-NLS} (aa720-989) and FRQ^{mNLS123} (functional mutations of all three NLS) do not localize in the nucleus. (B) Prediction of the FRQ NLS in FRQ, FRQ^{mNLS23} and FRQ^{mNLS123} by NLStradamus (Nguyen et al., 2009). The first NLS (aa194-199), which has been reported by Luo and colleagues in 1998 and the second predicted NLS (aa562-568) are marked in green. Putative NLS3 (aa639-645), which has a much lower peak than NLS1 and 2 is marked in blue. The predictions for FRQ^{mNLS23} and FRQ^{mNLS123} shows that the functional mutations introduced into the sequence of FRQ removed the predictions of an NLS at the respective sites.

A



B

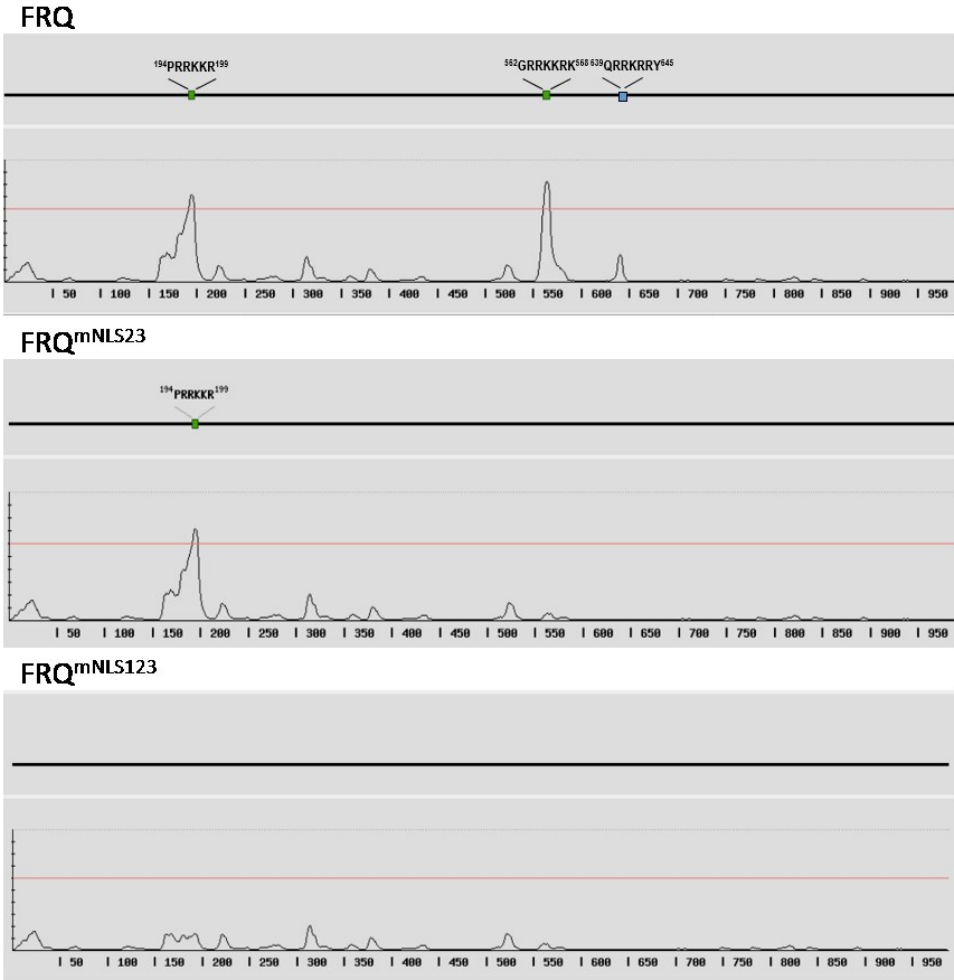


Figure legend on previous page

4.2.3 FRQ has three functional NLS in *N. crassa* of which one is essential for clock function

Sabine Schultz, together with Dr. Axel Diernfellner, conducted experiments to assess the effects of NLS mutations in *N. crassa*. Schultz first generated *Neurospora* strains expressing mutated versions of FRQ (section 2.1.5), each with altered putative NLSs, under the control of the native *frq* promoter. She also created a control strain expressing WT FRQ. Additionally, these strains carried a *frq-lucP* reporter, enabling *in vivo* circadian rhythm analysis through bioluminescence recordings (section 2.4.4). To mutate NLS2, the amino acid sequence of each NLS was altered as described in section 4.2.2. A double-mutant strain with both NLS2 and NLS3 mutations had these sequences modified accordingly, as did a strain where all three NLSs were modified.

In our luciferase reporter assay (section 2.4.4), the strains were cultured in 96-well plates and subjected to a light/dark cycle. Specifically, they were exposed to 12 hours of light, followed by 12 hours of darkness, another 12 hours of light, and were then finally transitioned to constant darkness. Dr. Diernfellner observed that the control strain expressing WT FRQ exhibited a strong and stable bioluminescence rhythm in constant darkness (Figure 4.2.3 A). Previous research (Luo et al. 1998) had shown that a strain lacking NLS1 (FRQ Δ NLS1) was arrhythmic. Therefore we were interested in observing similar phenotypes by mutating NLS1, NLS2 and NLS3.

The strains expressing FRQ with mutated NLS2 (FRQ^{mNLS2}) and NLS3 (FRQ^{mNLS3}) showed altered circadian periods: FRQ^{mNLS2} exhibited a longer period with $\tau=25.57 \pm 0.93$ h and an early circadian phase (Figure 4.2.3 B). Meanwhile, clones with FRQ^{mNLS3} displayed a shorter rhythm at $\tau=18.38 \pm 0.88$ h (Figure 4.2.3 C). The double mutant (FRQ^{mNLS23}) displayed a damped rhythm but maintained a period length similar to that of WT ($\tau=22.73 \pm 0.89$ h) (Figure 4.2.3 D). These findings suggest that while NLS2 and NLS3 seem to influence the robustness and periodicity of the circadian rhythm, they are not essential for clock function.

With these results, we closely examined NLS1. After mutation, FRQ^{mNLS1} displayed a rhythm comparable to WT at $\tau = 22.60 \pm 0.55$ h. The rhythm dampened after several days in darkness, a behavior we also observed in the other NLS mutants. The triple mutant, FRQ^{mNLS123}, exhibited an altered rhythm of $\tau = 24.00 \pm 0.91$ h (Figure 4.2.3 F). We hypothesize that NLS1 plays an important role, likely due to its proximity to the coiled-coil domain, suggesting its involvement in FRQ dimerization. Its localization within the

protein could make its functional removal impossible due to charge (Cheng et al. 2001, Lauinger et al. 2014).

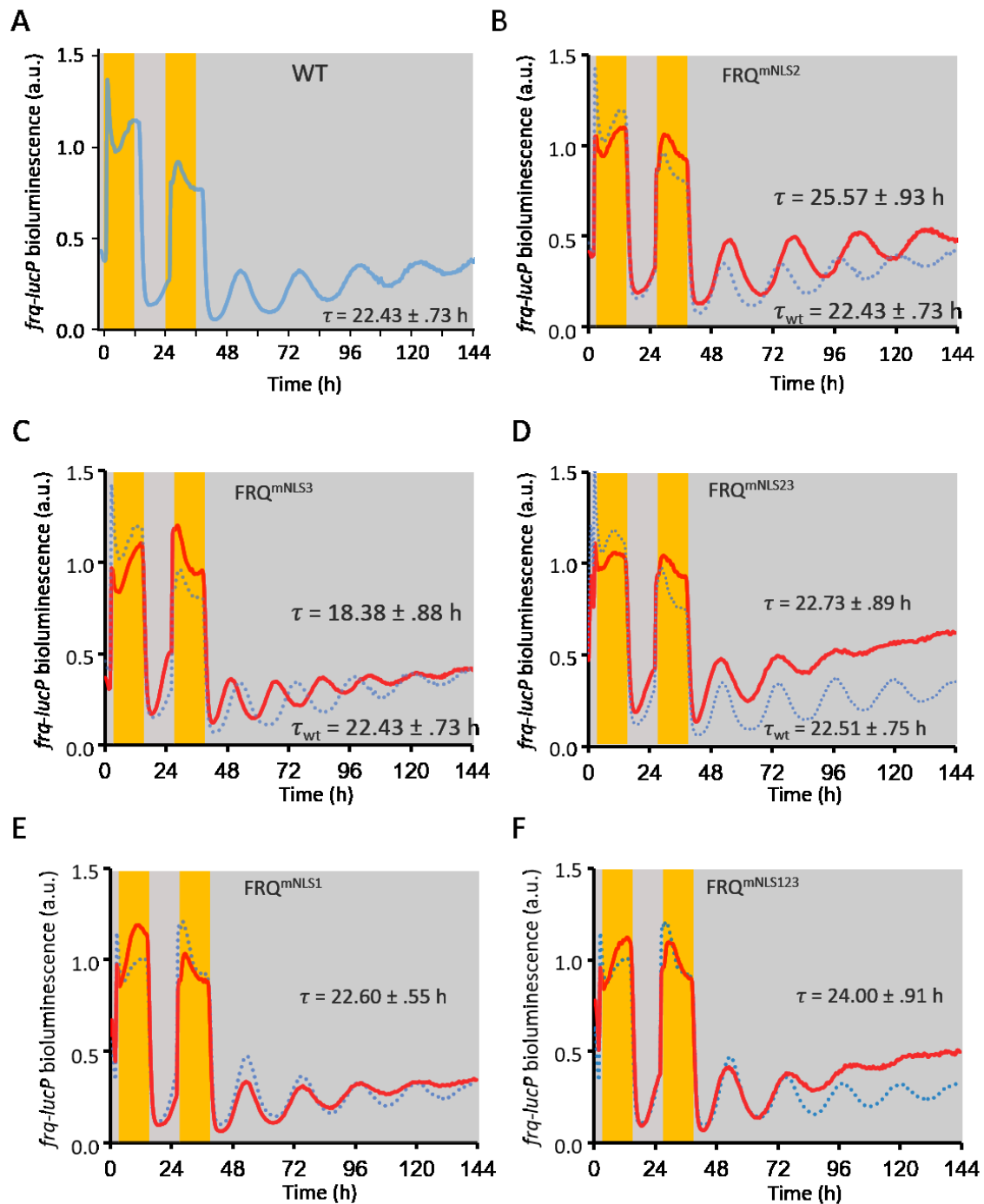


Figure 4.2.3: NLS1, NLS2 and NLS3 of FRQ affect circadian phase and period length

Bioluminescence recordings of *Neurospora frq-lucP* reporter strains expressing the indicated *frq* genes. (A) WT *frq*. The trajectory represents the average of 12 replicates from two independent clones. (B) *frq^{mNLS2}*. 12 replicates, 3 clones. (C) *frq^{mNLS3}*. 12 replicates, 3 clones. (D) *frq^{mNLS23}*. 15 replicates, 5 clones. (E) *frq^{mNLS1}*. 16 replicates, 4 clones. (F) *frq^{mNLS123}*. 8 replicates, 2 clones.

However, the phenotypes of the NLS mutants are not completely arrhythmic, indicating the presence of additional mechanisms that at least partially seem to compensate for the loss of normal NLS functionality.

4.2.4 WC-2 supports nuclear accumulation of WC-1

In *N. crassa*, WC-1 and WC-2 form the transcription factor WCC. In the absence of its stabilizing partner WC-2, WC-1 is rapidly degraded. My objective was to determine whether the interaction of WC-1 and WC-2 could be observed by co-localization in U2OSx cells. Upon co-expression in the transient cellular system, WC-1-mNG was observed to migrate from its previous cytosolic localization to the nuclear foci of mK2-WC-2, as anticipated, indicating an interaction between the two WCC subunits.

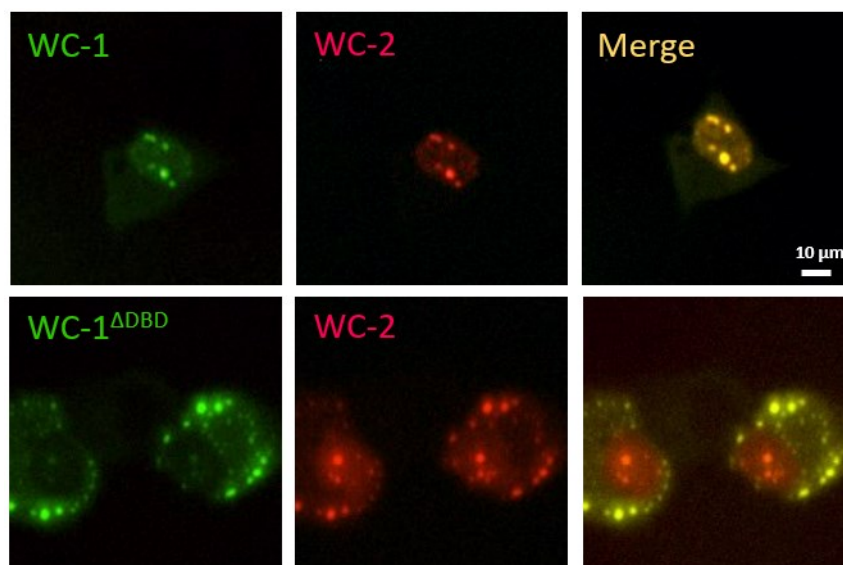


Figure 4.2.4: **WC-2 recruits WC-1 to the nucleus**

Transient expression in U2OSx cells of mK2-tagged WC-2 and mNG tagged WC-1 and WC-1^{ΔDBD} (Wang et al., 2016). Upon co-expression of WC-1-mNG (50 ng) and mK2-WC-2 (25 ng) both proteins accumulate in nuclear foci. Co-expressed WC-1^{ΔDBD} (50 ng) –mNG and mK2-WC-2 (25 ng) accumulate in nuclear and cytosolic foci. Scale bar= 10 μm.

Furthermore, I investigated the effects of a mutation in a basic region of WC-1, proximal to the DNA-binding ZnF domain, referred to as defective in binding DNA (DBD). Several functions have been attributed to this region: initially, it was thought to mediate nuclear localization, while subsequent findings suggest it plays a role in DNA binding and facilitating interactions with the FFC (Wang et al. 2015b). When I co-transfected the WCC, consisting of WC-1^{ΔDBD}-mNG and mK2-WC-2, it was predominantly localized

in the cytosol. This observation suggests that the deleted region may indeed be essential for DNA-binding and nuclear localization of the WCC, as initially proposed.

Consequently, the data I obtained from the co-localization experiments of fluorescently tagged WCC and FRQ-FRH (section 4.2.1) demonstrate that the approach of transiently expressing *Neurospora* clock proteins in a heterologous system not only circumvents the instability of FRQ and WC-1 when expressed without WC-2 and FRH, respectively, but also reliably reflects their interactions. Therefore, we concluded that this method can be employed to investigate further interactions and localizations of *Neurospora* clock proteins.

4.3 Dissecting the FFC-WCC interaction in circadian regulation: impact of FRH

The interaction between the FFC complex and the circadian transcription factor WCC has been observed to be relatively weak and dynamic. This interaction results in the inactivation of WCC through phosphorylation by CK1a (Schafmeier et al. 2005). Previous publications have indicated that FRH plays a pivotal role in mediating the interaction between FRQ and WCC (Shi et al. 2010). This section provides further analysis of the interaction between WCC and FRQ through co-expression in U2OStx cells with fluorescently tagged proteins and further analyzes the role of FRH. Furthermore, I investigated whether FRQ also co-localized with either WC-1-mNG (section 4.3.3) or WC-2 (section 4.3.4).

4.3.1 Investigating the role of FRH in FRQ and WCC co-localization and interaction

Former studies suggested that FRH is needed for FFC–WCC interaction (Shi et al. 2010). To further investigate this idea, I co-overexpressed mK2- FRQ, WC-1-mNG and unlabeled WC-2 in U2OStx cell lines and titrated different concentrations of unlabeled FRH. I defined interaction between FRQ, FRH and WCC as either co-localization within the same nuclear foci or homogeneous nuclear co-localization, as opposed to segregation into separate foci.

When I co-expressed mK2-FRQ, WC-1-mNG, WC-2, and sub-saturating levels of FRH (12.5 ng of FRH to 50 ng of each mK2-FRQ and WC-1-mNG, and 25 ng of WC-2), I observed partially co-localized yellow foci alongside distinct green foci. This suggests that FRQ and FRH may partially interact with WCC. However, not all of FRQ and FRH were recruited into the foci with WCC, with some forming separate green WCC foci in the nucleus (Figure 4.3.1A).

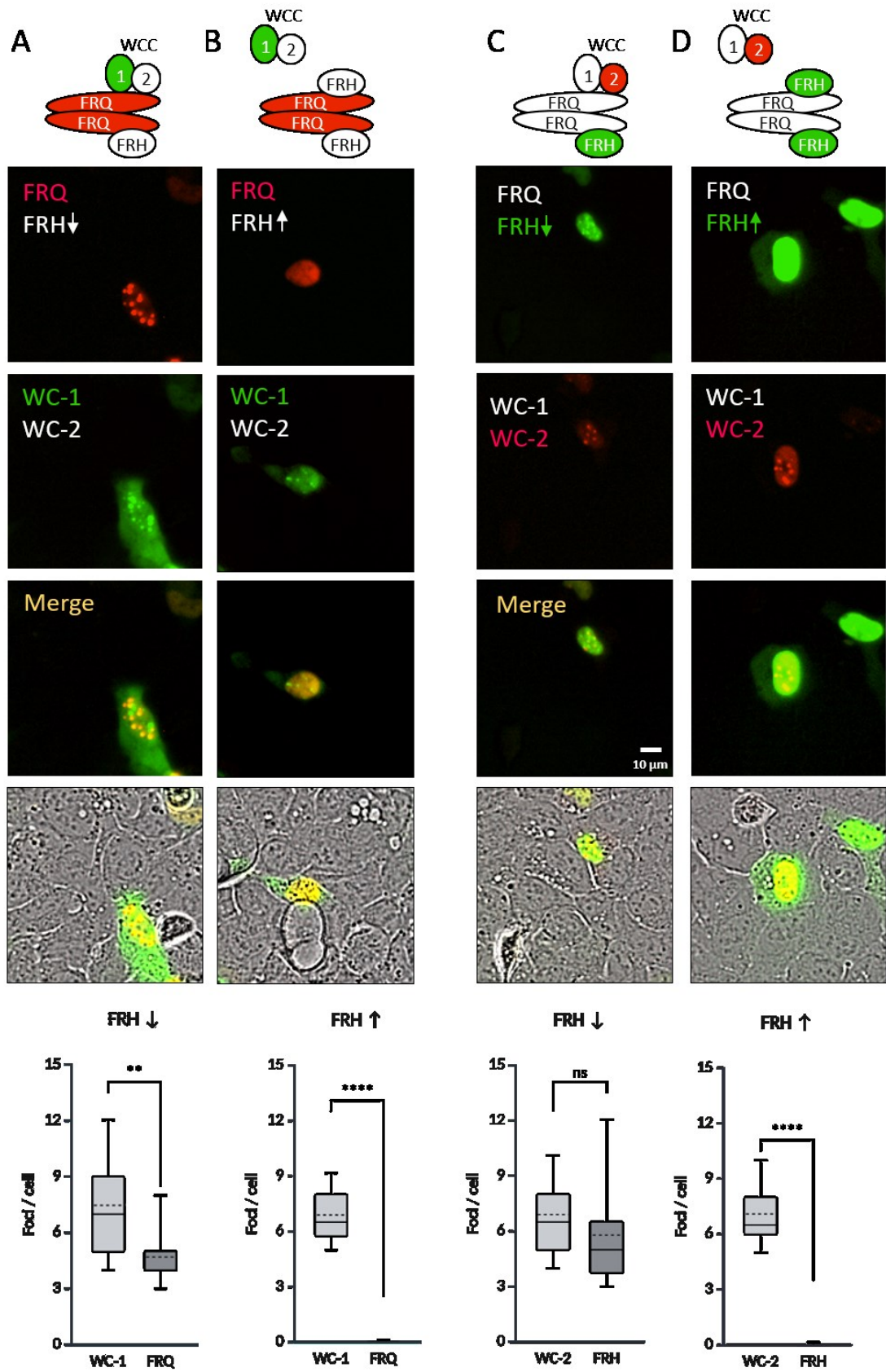


Figure legend on next page

Figure 4.3.1: Saturating amounts of FRH interfere with binding of FRQ to WCC

Top: Schematics illustrate the interactions of fluorescently tagged (green and red) and untagged (white) proteins. (A) Co-expression of mK2-FRQ (50 ng) and sub-saturating amounts of untagged FRH (12.5 ng) with WC-1-mNG (50 ng) and untagged WC-2 (25 ng). MK2-FRQ and WC-1-mNG co-localize in nuclear foci. (B) Co-expression of mK2-FRQ (40 ng) and saturating amounts of untagged FRH (80 ng) with WC-1-mNG (50 ng) and untagged WC-2 (25 ng). MK2-FRQ is dispersed throughout the nucleus, indicating expression of saturating amounts of FRH. WC-1-mNG (WCC) accumulates in nuclear foci, which do not contain mK2-FRQ. (C) Co-expression of untagged FRQ (50 ng) and sub-saturating amounts of FRH-mNG (12.5 ng) with untagged WC-1 (50 ng) and mK2-WC-2 (25 ng). FRH-mNG and mK2-WC-2 co-localize in nuclear foci. (D) Co-expression of mK2-FRQ (40 ng) and saturating amounts of untagged FRH (80 ng) with WC-1-mNG (50 ng) and untagged WC-2 (25 ng). FRH-mNG is dispersed in the nucleus, while mK2-WC-2 accumulates in nuclear foci.

Quantification (lower panels): (A and B): Nuclear foci of WC-1-mNG and mK2-FRQ in 30 cells. (C and D): Nuclear foci of FRH-mNG and mK2-WC-2. Statistical analysis: Unpaired t-test, **: $P \leq 0.01$, ****: $P \leq 0.001$, ns: $P > 0.05$. Black lines indicate median, dashed lines indicate mean. Scale bar = 10 μm .

In contrast, when I added higher levels of unlabeled FRH (80 ng) while FRQ foci were dissolved by FRH (as described in section 4.2.1), WCC foci remained stable (Figure 4.3.1 B). Neither FRQ nor FRH were recruited into these nuclear WCC foci (Figure 4.3.1 B). I made similar observations when I swapped fluorescent tags, co-transfecting unlabeled FRQ and WC-1 with mK2-WC-2 and saturating or sub-saturating amounts of FRH-mNG (Figure 4.3.1, C and D). Similarly, co-transfecting mK2-FRH with WC-1-mNG alongside unlabeled FRQ and WC-2 (Figure S3) confirmed these findings as well. My data suggests that FRH may not be necessary for the FRQ-WCC co-localization.

4.3.2 FRQ and WCC exhibit co-localization in nuclear foci independently of FRH

In order to further characterize the interaction of WCC with FRQ without FRH, I co-expressed mK2-FRQ with WC-1-mNG and unlabeled WC-2.

As previously shown in section 4.2.4, recruitment of WC-1-mNG in nuclear foci indicates that it interacts with unlabeled WC-2, forming the WCC (Figure 4.2.4, upper panels). FRQ forms nuclear foci. I found that mK2-FRQ also exhibited the formation of nuclear foci when co-expressed with WCC (Figure 4.3.2 A and B). It was unexpected, though,

that FRQ and WCC foci mostly overlapped leaving only few separate foci (Figure 4.3.2 A and B) similar to when only few amounts of FRH were present. Therefore, my data not only suggests that FRH may not be necessary for the FRQ-WCC co-localization but also that saturating amounts of FRH may even interfere with co-localization between FRQ and WCC.

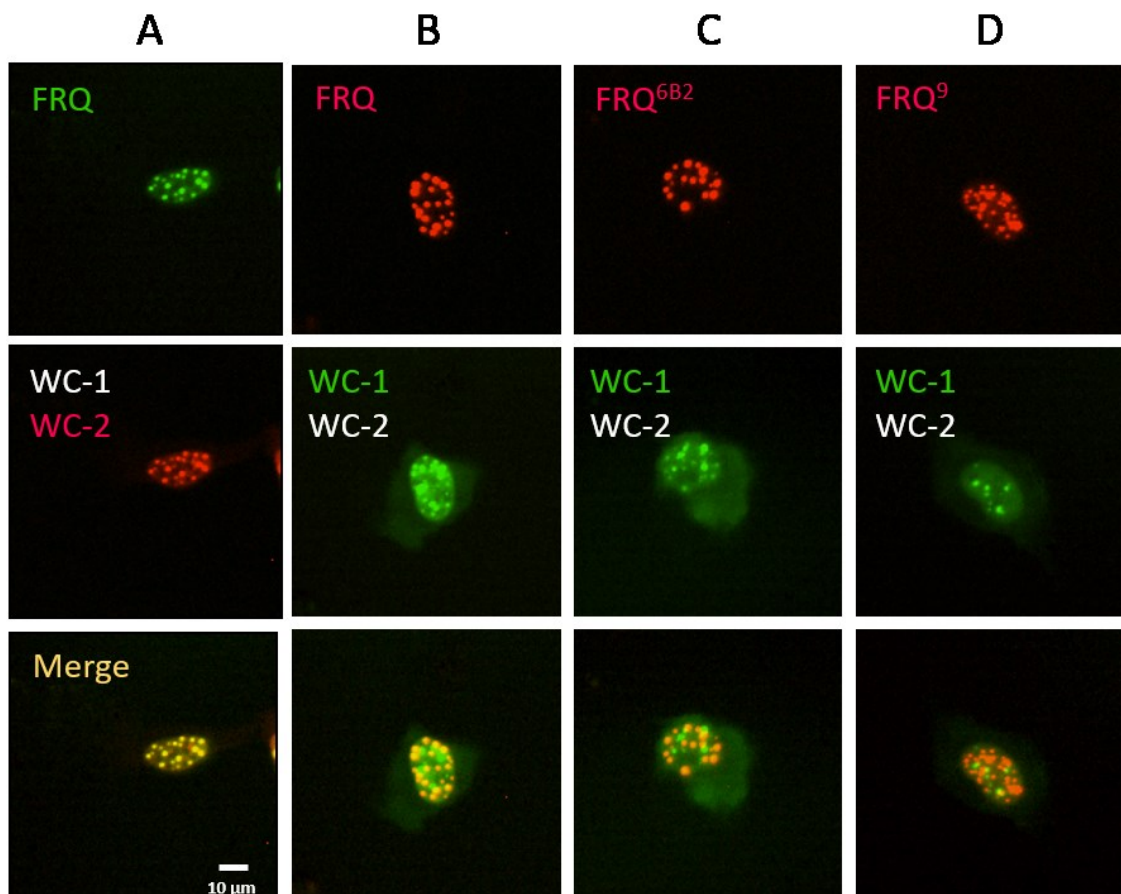


Figure 4.3.2: **FRQ interacts with WCC in the absence of FRH**

(A) Co-expression of FRQ-mNG with untagged WC-1 and mK2-WC-2. FRQ-mNG and mK2-WC-2 co-localize in nuclear foci. (B) Co-expression of mK2-FRQ (50 ng) with WC-1-mNG (50 ng) and untagged WC-2 (25 ng). MK2-FRQ and WC-1-mNG co-localize in nuclear foci. (C) Expression of mK2-FRQ^{6B2} (50 ng) with WC-1-mNG (50 ng) and untagged WC-2 (25 ng). MK2-FRQ^{6B2} and WC-1-mNG co-localize in nuclear foci. (D) Expression of mK2-FRQ⁹ (50 ng) with WC-1-mNG (50 ng) and untagged WC-2 (25 ng). FRQ⁹-mNG and mK2-WC-2 accumulate in distinct, non-overlapping nuclear foci. Scale bar=10 μm.

Since FRH does seem to influence the interaction between FRQ and WCC, I investigated next whether the 6B2 region exerts a comparable influence on the FRQ-WCC interaction

as it has on FRH. As seen in figure 4.2.1b C, a mutation in the 6B2 region of FRQ nearly completely abolishes interaction with FRH. Therefore, I co-transfected WCC with FRQ^{6B2} (Figure 4.3.2 C). As with wild-type FRQ, nuclear foci were also formed in mK2-FRQ^{6B2}. Similar to WT FRQ, the WCC (WC-1-mNG and unlabeled WC-2) foci mostly overlapped with FRQ^{6B2}. This indicates that the 6B2 region is not needed for FRQ-WCC interaction. It is noteworthy that when mK2-FRQ⁹ and WCC (WC-1-mNG and unlabeled WC-2) were co-transfected, no contact or overlap between the foci was observed indicating that WCC does not interact with FRQ⁹ (Figure 4.3.2 D).

4.3.3 The C-terminus of FRQ interacts with WC-1

As mentioned before, the accumulation of WCC in nuclear foci is dependent on WC-2 (section 4.2.4). Consequently, the interaction between mK2-FRQ and WC-1-mNG was easy to examine since an interaction would require the recruitment of either WC-1 to the nucleus or FRQ to the cytosol. When co-expressed, WC-1-mNG, which is cytosolic by itself (section 4.1), was observed to completely localize to the nuclear foci of mK2-FRQ (Figure 4.3.3 A).

Previously, the interaction between WCC and FRQ was partially assigned to the C-terminal region of FRQ (Wang and Dunlap 2023). I was able to confirm that WC-1 interacts with the C-terminus of FRQ and not the N-terminal part of FRQ by co-expression of WC-1-mNG with mK2-FRQ^{C-term} (Figure 4.3.3 D). The results indicated that the C-terminus of FRQ is sufficient for interaction with WC-1, as evidenced by the enrichment of WC-1-mNG in the nucleus. This finding was further supported by the co-expression between WC-1-mNG and mK2-FRQ⁹ (Figure 4.3.3 C), which demonstrated that WC-1-mNG was not recruited to the nuclear foci of FRQ⁹. Furthermore, I co-transfected WC-1-mNG and mK2-FRQ^{6B2}. In contrast to FRQ^{6B2} and FRH, WC-1 was still co-localizing with FRQ^{6B2} (Figure 4.3.3 B).

Despite these findings, I was unable to identify a specific FRQ interaction site within WC-1.

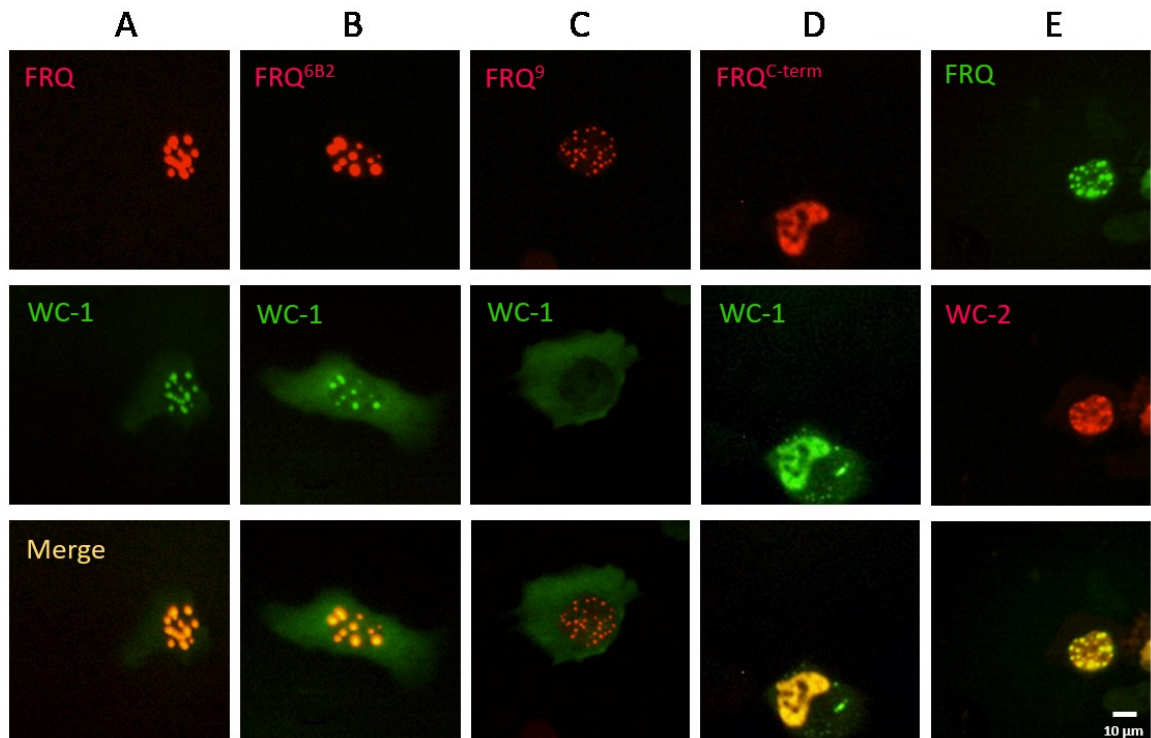


Figure 4.3.3: **FRQ can interact with WC-1 and WC-2 individually**

(A) mK2-FRQ and WC-1-mNG co-localize in nuclear foci. (B) mK2-FRQ^{6B2} (50 ng) and WC-1-mNG (50 ng) co-localize in nuclear foci. (C) FRQ⁹ (50 ng) forms nuclear foci while co-expressed WC-1-mNG (50 ng) remains in the cytosol. (D) mK2-FRQ^{C-term} (50 ng) is homogeneously dispersed in the nucleus and recruits WC-1-mNG (50 ng) from the cytosol to the nucleus. (E) FRQ-mNG (25 ng) (together with unlabeled FRQ; 50 ng) co-localizes with mK2-WC-2 (50 ng) in nuclear foci. Scale bar = 10 μ m.

4.3.4 FRQ and WC-2 co-localize in nuclear foci

I conducted a series of experiments to determine whether FRQ can also co-localize and potentially interact with WC-2. Following the individual transient transfection of both proteins, the foci were observed to fuse after a short period of time. Initially, this phenomenon was also observed when both proteins were co-transfected and therefore co-localization was difficult to analyze. Upon co-transfection of FRQ-mNG with unlabeled FRQ, I observed that FRQ's foci appeared to be more stable, with discernible individual foci (Figure 4.3.3 E).

To further analyze whether WC-2 could interact with FRQ, mK2-WC-2 was co-expressed with FRQ-mNG and unlabeled FRQ (Figure 4.3.3 E). MK2-WC-2 localized in the nuclear foci together with FRQ. Similar to before, I found that WC-2-mNG foci merged with

mK2-FRQ foci completely. This evidence supports my conclusion that FRQ interacts with WC-2 as well as WC-1.

4.3.5 FRH does not interact with WCC in absence of FRQ

To further investigate the potential co-localization and interaction of FRH with the WCC, I conducted co-transfection experiments combining FRH with WCC.

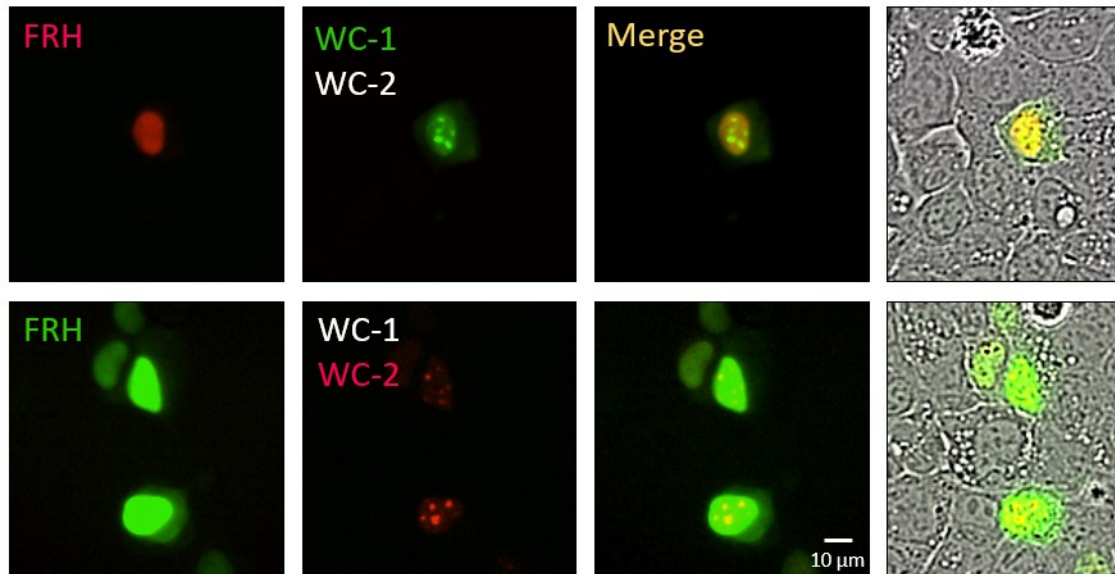


Figure 4.3.5: **FRH does not interact with WCC**

In U2OSx cells, transiently expressed mK2- or mNG-tagged FRH did not co-localize with WCC.

Upper panel: mK2-FRH (50 ng) was uniformly distributed in the nucleus. WCC forms nuclear foci (WC-1-mNG (50 ng) and unlabeled WC-2 (25 ng))

Lower panel: FRH-mNG (50 ng) did not co-localize with WCC (unlabeled WC-1 (50 ng) and mK2-WC-2 (25 ng)). Scale bar = 10 µm.

First, mK2-FRH was co-transfected with WC-1-mNG and unlabeled WC-2. WCC formed green nuclear foci; however, mK2-FRH was not recruited into these foci and instead remained distributed homogeneously throughout the nucleus (Figure 4.3.5, upper panel).

Then, I swapped the fluorescent labels by co-transfecting mK2-WC-2 with FRH-mNG and unlabeled WC-1. The results mirrored those of the previous experiment: FRH remained homogeneously distributed in the nucleus and was not recruited into the WCC foci (Figure 4.3.5, lower panel).

Based on these findings, I concluded that there is no evidence that FRH is able to interact with either WC-1 or WC-2 in the absence of FRQ.

4.4 FRH disrupts FRQ interaction with WC-1 and WC-2

My results from section 4.3.1 and 4.3.2 indicated a putative interference of FRH with the FRQ-WCC interaction. To verify and further research these findings, I conducted experiments and co-expressed either WC-1-mNG with mK2-FRQ or mK2-WC-2 with FRQ-mNG together with unlabeled FRH. This was possible due to the fact that WC-1 and WC-2 were able to co-localize both, alone and together with FRQ (section 4.3.2 - 4.3.4). In the following I will further demonstrate that the interaction of FRQ with FRH disrupts the interaction of FRQ with WC-1 and WC-2 (section 4.4.1 and 4.4.2). A more detailed analysis of WC-1 interaction with FRQ and FRH offered the advantage of enhanced interpretability, as WC-1-mNG is localized in the cytosol, unlike WC-2 and WCC (section 4.4.1). Although, in both cases I observed when FRQ and FRH were co-transfected with either WC-2 (section 4.4.2) or WCC (section 4.3.1) that FRQ and FRH were homogenously distributed in the nucleus, while WC-2 or WCC formed separate foci, which did not contain either FRQ or FRH.

4.4.1 FRH and WC-1 binding to FRQ: mutually exclusive interactions in the C-terminal region

To analyze how FRH affects the interaction of WC-1 with FRQ and to further analyze FRH's role, I transiently co-overexpressed mK2-FRQ and WC-1-mNG with and without untagged FRH in U2OSTx cells. In absence of FRH, WC-1-mNG was recruited into the foci of mK2-FRQ, as described in section 4.3.3. The co-expression of FRH interfered with the formation of FRQ nuclear foci, as shown above (section 4.2.1). Surprisingly, however, I found that when I co-expressed mK2-FRQ, WC-1-mNG and high levels of FRH, WC-1-mNG was predominantly cytoplasmic, suggesting that FRH prevents WC-1 binding to FRQ (n=3; 20 cells each; Figure S4 A). Both FRH and WC-1 seem to interact with the C-terminal portion of FRQ though not at the same site (Figure 4.3.3 B and D; Figure 4.2.1b C and E).

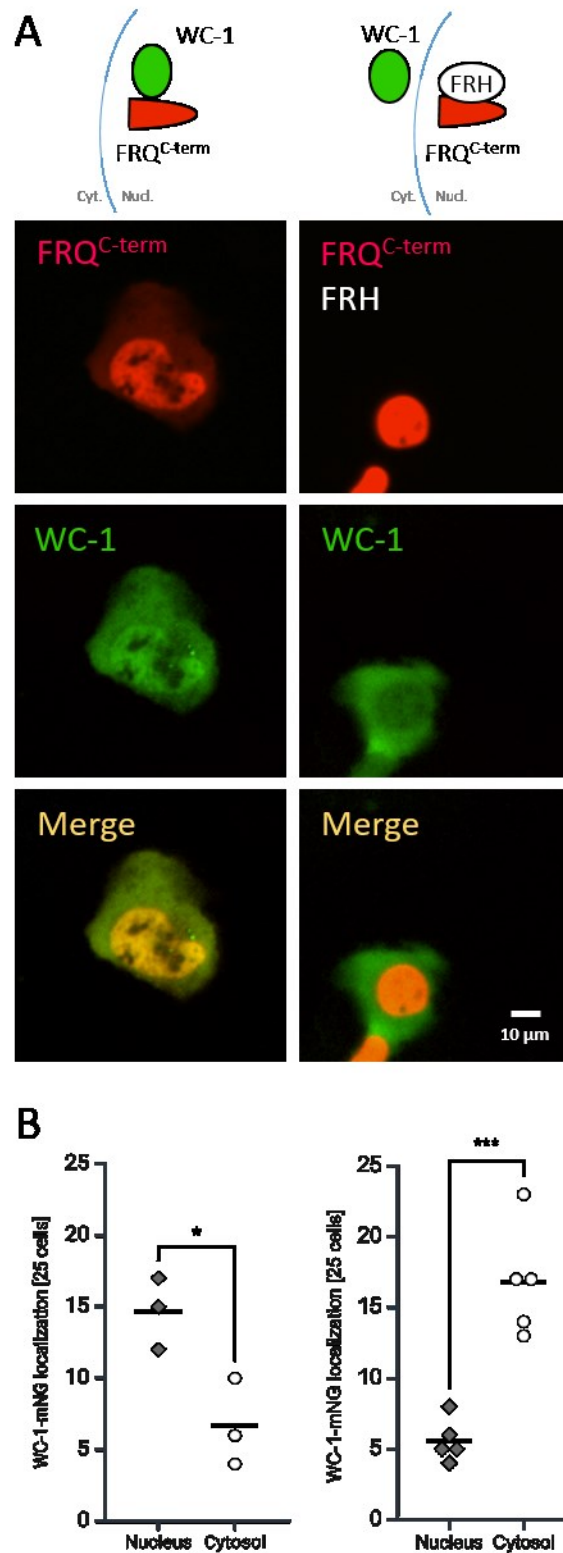


Figure 4.4.1: **FRH interferes with binding of FRQ^{C-term} to WC-1**

Top: Schematics depict the interactions of fluorescently tagged (green and red) and untagged (white) proteins. Co-expression of mK2-FRQ^{C-term} (50 ng) and WC-1-mNG (50 ng) without FRH (left) and with saturating amounts of FRH (80 ng, right). (B) FRH prevents the recruitment of

WC-1-mNG into the nucleus. - FRH: n=3 x 25 cells, + FRH: n= 5 x 25 cells. Unpaired T-test, *: $P \leq 0.05$; ***: $P \leq 0.001$.

To determine whether FRH prevents WC-1 from binding to the C-terminal part of FRQ or whether this effect is due to the dissolving of FRQs nuclear foci, I co-expressed mK2-FRQ^{C-term}, WC-1-mNG and high levels of FRH. In case of an interaction between FRQ^{C-term} and WC-1-mNG, WC-1 would be recruited to the nucleus. This was the case in the absence of FRH. However, when FRH was co-expressed in a saturating concentration, WC-1-mNG was predominantly cytoplasmic, confirming my previous results with WT FRQ (n=3; 25 cells each; Figure 4.4.1).

As stated before, when the 6B2 region is mutated, FRH does not interact with FRQ (Guo et al. 2010). When I co-expressed WC-1-mNG with mK2-FRQ^{6B2}, both proteins co-localized in nuclear foci (Figure 4.3.3 B).

My data support the idea that FRH blocks the binding of WC-1 to FRQ and suggests that WC-1 and FRH bind to the C-terminal part of FRQ in a mutually exclusive manner. The finding was surprising and unexpected because it had been suggested before that FRH is necessary for the interaction of WCC with FFC. This suggestion was based on data showing convincingly that WCC did not interact with FFC containing an FRH mutant with an R806H substitution.

In order to take a closer look at the effects of FRH^{R806H}, I co-expressed mK2-FRQ with WC-1-mNG and saturating amounts of unlabeled FRH^{R806H} which I then compared to the effects of WT FRH. Both FRH and FRH^{R806H} competed with the nuclear recruitment of WC-1-mNG by mK2-FRQ. However, FRH^{R806H} was a stronger competitor than FRH, supporting the idea that R806H is a dominant negative mutation that more effectively disrupts WC-1 binding to FRQ (n=3, 25 cells each; Figure S4 C).

4.4.2 FRH prevents the interaction of FRQ with WC-2

Given that FRQ is also capable of independent interaction with WC-2 (section 4.3.5), I co-expressed FRQ-mNG, unlabeled FRQ, and mK2-WC-2 with or without high amounts of FRH (Figure 4.4.2). When I co-transfected sub-saturating amounts of FRH, FRQ-mNG and mK2-WC-2 foci fused. However, when higher concentrations of FRH were present, FRQ foci were dissociated and mK2-WC-2 foci remained. This suggests that FRH may interfere with the interaction between FRQ and WC-2. In summary, the data that I

presented in this dissertation suggest that FRH is not required for the interaction between FRQ and WC-2 and may, in fact, inhibit this interaction.

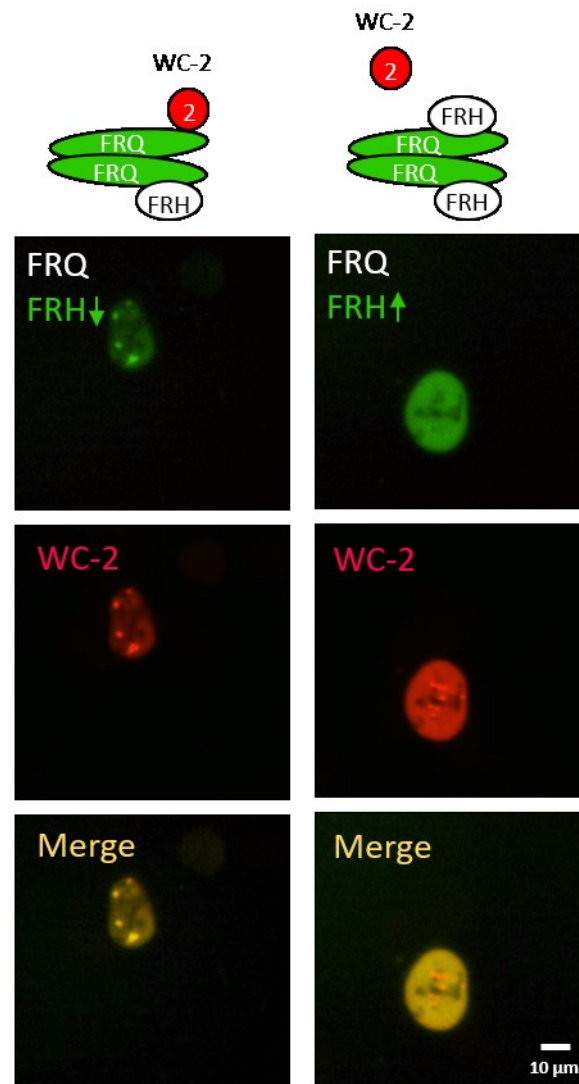


Figure 4.4.2: **FRH interferes with binding of FRQ to WC-2**

Top: Schematics depict the interactions of fluorescently tagged (green and red) and untagged (white) proteins. Lower left: Co-expression of FRQ-mNG (25 ng), unlabeled FRQ (50 ng) and WC-2-mNG (25 ng) with sub-saturating amounts of unlabeled FRH (12.5 ng). FRQ-mNG forms stable nuclear foci with mK2-WC-2.

Lower right: Co-expression of FRQ-mNG (25 ng), unlabeled FRQ (50 ng) and WC-2-mNG (25 ng) with saturating amounts of unlabeled FRH (80 ng). FRQ foci are dissolved by FRH. The nuclear foci of mK2-WC-2 remain. Higher expression of mK2-WC-2 in the cell lead to additional homogenously expressed WC-2 (compare to Figure S2 C). Scale bar= 10 µm

4.5 Phosphorylation-driven regulation of FRQ-FRH interaction may have an impact on WCC binding

The interaction between FRQ and FRH is quite stable and does not allow for interaction with WCC (Figure 4.3.1). It was found before that one FRQ dimer binds 1.5 FRH (Lauinger et al. 2014). I discovered a fine tuning mechanism which allows interaction between FRQ and FRH to loosen up. Through phosphorylation of FRQ by CK1a, the interaction of FRQ with FRH is first loosened and then terminated and FRQ is exported into the cytosol (section 4.5.1). Furthermore, we were able to observe this in *Neurospora*, confirming this finding (section 4.5.2).

4.5.1 Phosphorylation of FRQ by CK1a induces its dissociation from FRH and nuclear export

In *Neurospora*, CK1a gradually hyperphosphorylates FRQ, which inactivates FRQ and ultimately results in its degradation (He and Liu 2005, Marzoll et al. 2022a). To further analyze the impact of CK1a on FRQ and FFC complex formation, I conducted a co-expression experiment in U2OStx cells, wherein unlabeled CK1a was co-expressed with FRH-mNG and either mK2-FRQ, mK2-FRQ^{6B2}, or mK2-FRQ⁹. All three versions of the FRQ protein were hyperphosphorylated in a CK1a-dependent fashion, whereas FRH was not (Figure 4.5.1a; Figure S6). Endogenous kinases, such as CK1 δ or CK1 ϵ , which play a role in the mammalian circadian clock, did not appear to efficiently phosphorylate the overexpressed FRQ protein, as observed in the control where CK1a was absent. Only when CK1a was co-expressed, FRQ was hyperphosphorylated.

Interestingly, phosphorylated FRQ assembled in the cytosol after several hours of co-expression with CK1a, while FRH remained in the nucleus (Figure 4.5.1b). These data demonstrate that phosphorylated mK2-FRQ dissociates from FRH-mNG and is exported from the nucleus into the cytosol (Figure 4.5.1b A; S6A). Additionally, a mutant that is unable to interact with FRH, such as mK2-FRQ^{6B2}, was also exported from the nucleus, albeit at a substantially faster rate than mK2-FRQ (Figure 4.5.1b B; S6 B). In contrast, mK2-FRQ⁹ was not exported from the nucleus when co-expressed with CK1a and FRH-mNG (Figure 4.5.1b C, S6 C). Leptomycin B is an antifungal antibiotic derived from the *Streptomyces species*. It has been shown to act as a specific inhibitor of nuclear export. Its cellular target is chromosomal region maintenance 1 protein (CRM1), also known as exportin 1 or Xpo1. CRM1 is the primary receptor for the nuclear export of proteins and

RNA containing a nuclear export signal (NES) (Liu et al. 2008, Benko et al. 2010, Sun et al. 2021). When I inhibited CRM-1-dependent nuclear export using leptomycin B as described in section 2.3.5, mK2-FRQ and mK2-FRQ^{6B2} remained in the nucleus (Figure 4.5.1b B, S6B), indicating that the C-terminus of FRQ contains an NES. However, the NES appears to be relatively weak, as FRQ^{C-term}, which would include the NES and only one predicted NLS (Figure 4.2.2 B, S1), shows mainly nuclear localization with only some cytoplasmic localization (Figure 4.2.2 A). Full length FRQ contains three putative NLSs and is therefore strongly enriched in the nucleus.

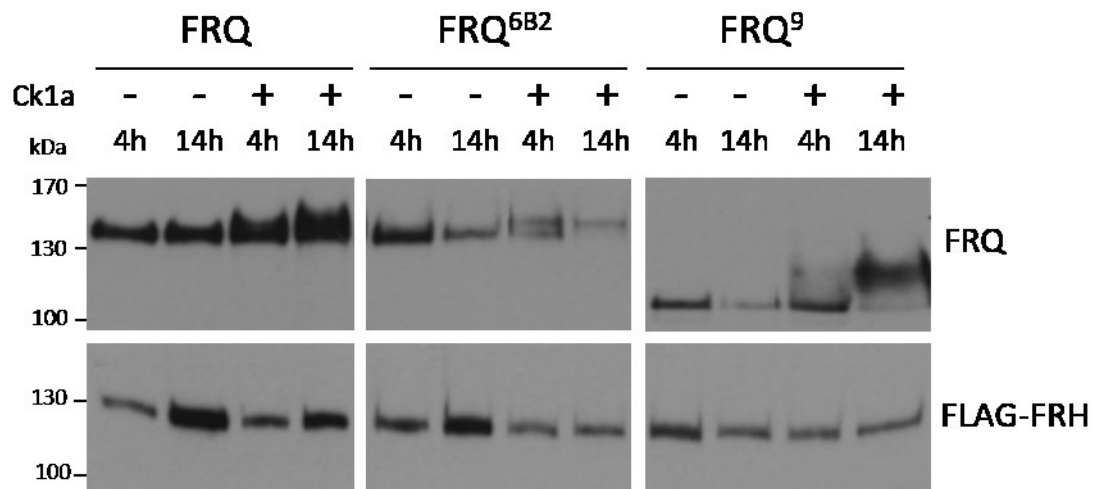


Figure 4.5.1a: **CK1a phosphorylates FRQ, FRQ^{6B2} and FRQ⁹ in U2OStx cells over the course of time**

Western blot analysis of mK2-FRQ, mK2-FRQ^{6B2} and mK2-FRQ⁹ co-expressed with and without CK1a in U2OStx cells after 4h and 14h post induction with DOX. In all cases FRQ is phosphorylated over time by CK1a indicated by the gel shift. Meanwhile, FRH is not phosphorylated. n=3, representative Western blot result is shown, repeats are shown in Figure S6.

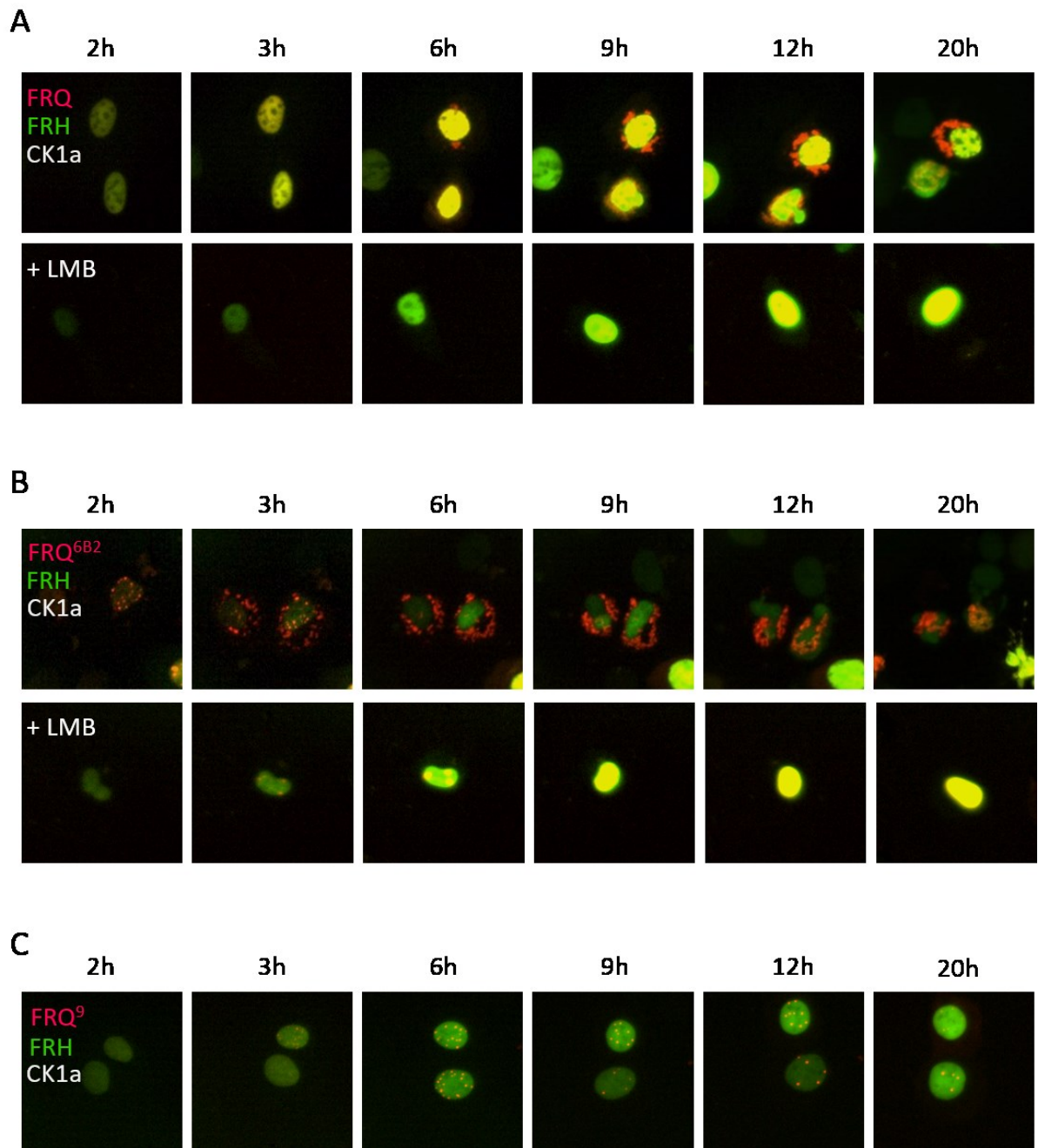


Figure 4.5.1b: Phosphorylation of FRQ by CK1a triggers its dissociation from FRH and nuclear export

(A, B, C) Incubate time courses from 2 h to 20 h post DOX induction of transfected U2OSTx cells upon co-expression of FRH-mNG (50 ng) and untagged CK1a (50 ng) with (A) mK2-FRQ (50 ng), (B) mK2-FRQ^{6B2} (50 ng), and (C) mK2-FRQ⁹ (50 ng). Phosphorylated mK2-FRQ and mK2-FRQ^{6B2} are exported after 6 h and 2 to 3 h post induction respectively. Phosphorylated FRQ⁹ is not exported from the nucleus. Nuclear export inhibitor leptomycin B (LMB) was added when indicated. Here phosphorylation induced export is inhibited and FRQ is enriched in the nucleus.

4.5.2 Native FFC dissociates upon phosphorylation of FRQ by CK1a

In *Neurospora*, all of the detectable FRQ exists in a complex with FRH, which protects FRQ from degradation (Hurley et al. 2013, Lauinger et al. 2014). FRQ with mutations in the C-terminus that encompass the 6B2 region, such as FRQ^{6B2} and FRQ⁹, are unable to interact with FRH and are therefore rapidly degraded. As a result, these mutants accumulate only at very low levels, despite being synthesized in excessive amounts due to a defective negative feedback loop. Since free FRQ does not accumulate to significant levels in *Neurospora*, it is difficult to study whether its gradual hyperphosphorylation leads to dissociation from FRH.

To prevent the degradation of unbound FRQ, Sabine Schultz prepared native *Neurospora* cell extracts of a strain carrying FLAG-FRH under the control of the *cgc-1* promoter. Hyperphosphorylation of FRQ was induced *in vitro* by adding recombinant CK1a and ATP (Figure 4.5.2a A; section 2.5.3). An untreated cell extract was used as a control. Both extracts were then subjected to immunoprecipitation as described in section 2.5.1. In the control sample, hypophosphorylated FRQ was co-immunoprecipitated with FRH (Figure 4.5.2a B, left panels, S7). In contrast, after treatment with CK1a and ATP, hyperphosphorylated FRQ could no longer be co-immunoprecipitated with FRH (Figure 4.5.2a B, right panels; S7).

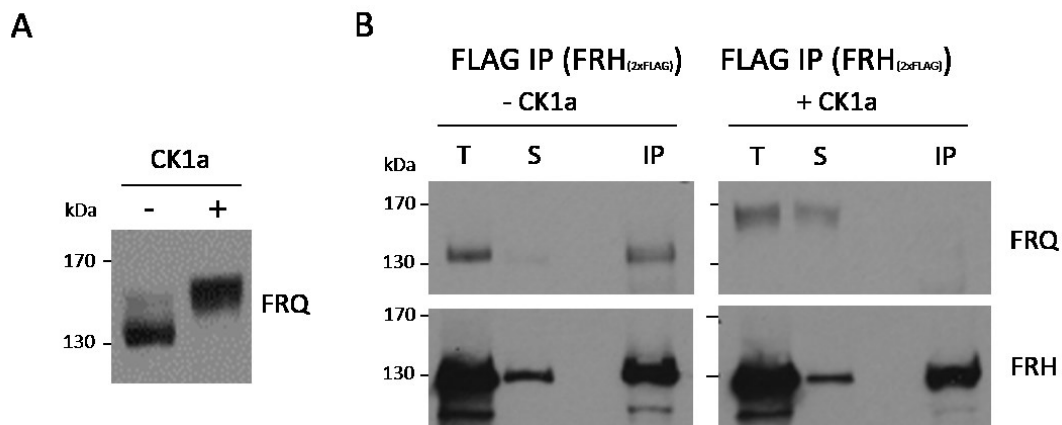


Figure 4.5.2a: **Hyperphosphorylated FRQ does not interact with FRH in *Neurospora***

(A) To accumulate high levels of hypophosphorylated FRQ, *Neurospora* expressing a FLAG-tagged FRH was grown in the dark for 10 h, followed by a 3-h exposure to light. Whole cell lysate (WCL) was prepared and incubated overnight at 4°C with recombinant CK1a and ATP, or left untreated. (B) FLAG immunoprecipitation of 2xFLAG-tagged FRH. Total (T), supernatant (S), and immunoprecipitate (IP) were analyzed by Western blot with antibodies against FRQ (upper panels) and 2xFLAG-FRH (lower panels). n = 3, representative IP is shown.

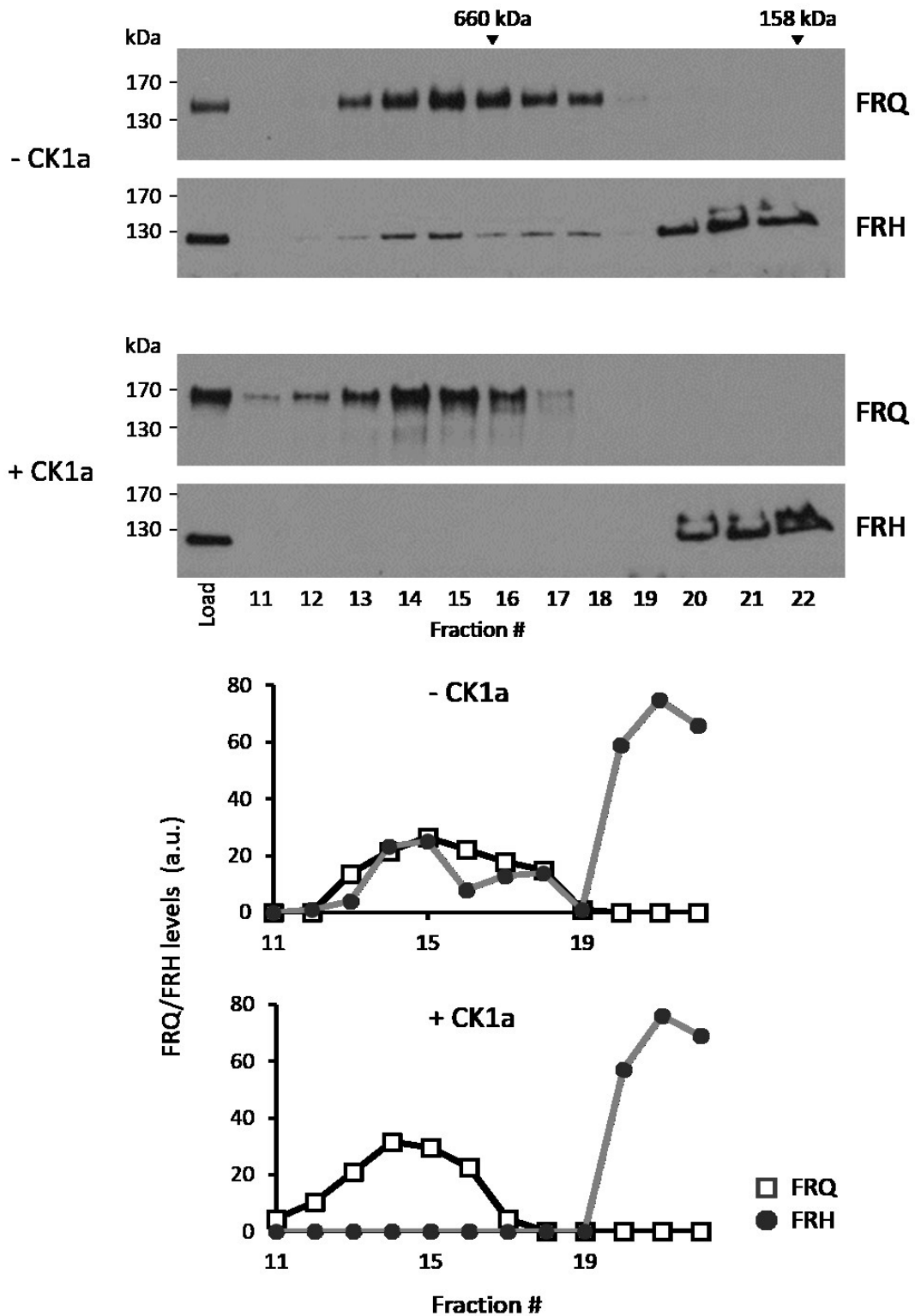


Figure 4.5.2b: Phosphorylation of FRQ by CK1a triggers its dissociation from FRH

(A) A *Neurospora* strain expressing FRQ under the control of the quinic acid (QA)-inducible *qa-2* promoter was induced for 4 h. Whole cell lysate (WCL) was prepared and treated with or without CK1a, as described in figure 4.5.2a. The samples were then analyzed by size exclusion

chromatography using a Superose 6 Increase 10/300 GL column. FRQ and FRH were detected by Western blot and quantified using ImageJ.

(B) Densitometric signals were plotted against the fraction number.

Additionally, Schultz performed size exclusion chromatography (SEC) on an untreated native *Neurospora* extract, which showed that FRH co-eluted with FRQ in a high molecular mass fraction, confirming their interaction (Figure 4.5.2b). These findings are consistent with previous observations from our laboratory, where elution profiles of FRQ and FRH were analyzed. In those studies, FRQ eluted at a higher molecular mass, a result attributed to its intrinsically disordered conformation and its status as a homodimer (Lauinger et al. 2014). Moreover, our SEC analysis of the CK1a-treated extract revealed that FRH no longer co-eluted with FRQ in the high molecular mass fraction (Figure 4.5.2b). These results strongly suggest that phosphorylation of native FRQ by CK1a leads to its dissociation from FRH.

5. Discussion

The kinetics of phosphorylation of the FRQ plays a crucial role in circadian timekeeping in *Neurospora*. The progressive hyperphosphorylation of FRQ by CK1a occurs slowly and gradually over several hours and is temperature-compensated. In this thesis, I provide evidence that FRH, whose reported role in the circadian clock is the stabilization of its intrinsically disordered binding partner FRQ, can detect the time-dependent phosphorylation state of FRQ. This ability constitutes the basis of a sophisticated time-keeping mechanism that enables the circadian clock to transition between different states. I show that the slow phosphorylation of FRQ, triggers subunit remodeling of the FFC complex by modulating the FRQ-FRH interaction in two distinct steps: first, the stabilization of inactive FRQ dimers by binding of two FRH molecules, then the activation of FRQ by the release of one FRH, exposing a WCC binding site and initiating negative feedback, and ultimately, inactivation and degradation of FRQ by the release of the second FRH. My data reveal that this mechanism is facilitated by previously unknown competitive interactions between FRH and WCC.

5.1 Studying the FFC complex: a technical question

Despite extensive research since the discovery of the circadian clock in the late 20th century and the substantial knowledge accumulated about its core components and the negative feedback loop, the precise molecular mechanisms by which these components measure time still remain elusive.

One reason for this persistent challenge is the complexity of analyzing the FFC complex and deciphering the mechanism and timing of its interaction with the WCC. The inherent properties of the core clock components pose significant challenges to the analysis. For example, investigating how FRH protects FRQ from degradation, and why this protection requires a separate protein, is difficult because FRQ, which cannot interact with FRH, is rapidly degraded. Additionally, FRH is an essential protein involved in other pathways beyond the circadian clock, making its deletion or inactivation impossible. Similarly, CK1a plays essential roles beyond the circadian clock, making its deletion unfeasible. Moreover, similar challenges are encountered when studying the WCC. WC-1 cannot be studied in isolation, as it is rapidly degraded in absence of WC-2, complicating biochemical analyzes of the WCC.

Despite the availability of various cell biology and biochemical tools for studying the circadian clock of *N. crassa*, working with this filamentous fungus presents severe challenges. One significant drawback is the extended time required to generate specific mutants. Additionally, performing microscopy is challenging due to *Neurospora*'s dense hyphal network, which contains numerous highly motile nuclei that are rapidly transported along the hyphae (Suelmann et al. 1997, Ramos-Garcia et al. 2009). Furthermore, it may not be feasible to study the interaction and subcellular dynamics of a protein with a blue light photoreceptor like WC-1 *in vivo* using a microscope. To overcome these challenges and address the open questions mentioned above, I transiently transfected mammalian cells with the core clock proteins of *Neurospora*, tagged with a fluorescent marker. I then analyzed their interactions and subcellular dynamics using live-cell imaging. Using this unique approach to visualize the clock proteins using Incucyte ZOOM and SX1, I was able to fully visualize all of the proteins (Figure 4.1). Even when expressed alone, FRQ and WC-1 were stable in the mammalian system and could therefore be studied without their respective stabilization partners FRH and WC-2.

I observed that overexpressed FRQ formed nuclear foci in U2OSx cells (Figure 4.1, 2nd image from left to right). In a physiological context, FRQ might form phase-separated condensates (droplets), although to a lesser extent compared to the overexpression observed in this study, resulting in smaller hubs rather than distinct foci. Recent findings support the physiological relevance of my observations, demonstrating that FRQ indeed undergoes liquid-liquid phase separation (LLPS) both *in vitro* and *in vivo* in *Neurospora*, consistent with predictions based on its sequence properties and comparisons with its functional analogues, dPER and hPER1 (Tariq et al. 2024).

My straightforward live-cell assay allowed us to examine interactions and processes that are difficult, or even impossible, to study in *Neurospora*. In the light of these observations, we devised novel experimental approaches for validation in *Neurospora*, which would not have been designed without these insights.

5.2 FRH is anchored to the C-terminal part of FRQ and disrupts FRQ self-interaction

In 2005, it was demonstrated that all FRQ is associated with FRH, whose function in the circadian clock had previously been unknown (Cheng et al. 2005). It has since been

established that FRH plays a crucial role in maintaining the stability of FRQ. In the absence of the FRH interaction site, or when FRH levels are reduced, FRQ undergoes rapid hyperphosphorylation and is rapidly targeted for degradation via the proteasome. This is characteristic of intrinsically disordered proteins, which are more susceptible to such degradation (Tsvetkov et al. 2008, Hurley et al. 2013). Typically, FRQ degradation follows the ubiquitin-proteasome pathway, a process facilitated by the ubiquitin E3 ligase (SCF) FWD-1. The loss of FRH interaction appears to accelerate FRQ's phosphorylation and degradation, highlighting FRH's crucial role in stabilizing FRQ and regulating its turnover in the circadian clock system (He et al. 2003, He and Liu 2005).

It is well-established that FRH is anchored to the C-terminus of FRQ and interacts with this central clock protein via the FFD domain (aa 774-782), with the 6B2 (aa774-776) and 6B5 (aa776-782) regions identified as critical interaction sites (Guo et al. 2010). In addition, recent findings from Jankowski and colleagues indicate that the positive charge of RR783-784aa facilitates FRH binding to FRQ (Jankowski et al. 2024).

Interestingly, my assay revealed that low levels of FRH allowed FRQ to remain in foci, whereas higher concentrations of FRH, likely saturating FRQ, disrupted foci formation and reduced FRQ's propensity for self-interaction (Figure 4.2.1b A and B). These findings suggest that FRH modulates FRQ by promoting weak interactions between FRQ molecules associated with FRH over FRQ self-interactions. Notably, even saturating levels of FRH failed to dissolve the foci of FRQ⁹. Furthermore, FRQ with a mutation in the 6B2 region exhibited a significantly reduced interaction with FRH, as evidenced by the inability of FRH to dissolve FRQ^{6B2} foci. This confirms that FRH anchors to the C-terminal region of FRQ (Figure 4.2.1b C). These results highlight two key findings: first, FRQ foci formation does not depend on the C-terminus of FRQ; and second, anchoring FRH at the C-terminus is sufficient to disrupt FRQ self-interactions. Moreover, when I disrupted the anchor at the 6B2 region, weak co-localization of FRH with FRQ foci was still observed, suggesting the presence of thermodynamically weak interactions between FRQ and FRH in addition to the FFD domain (Figure 4.2.1b C). As mentioned above, it is well-established that FRH primarily interacts with FRQ at the FFD domain, which encompasses the 6B2 and 6B5 regions. Disruption of either region in co-immunoprecipitation experiments resulted in a loss of detectable interaction (Guo et al. 2010). This indicates that my assay is sensitive enough to visualize putative low-affinity

interactions, as evidenced by the co-localization of FRH with FRQ^{6B2} foci despite the disrupted anchor. Furthermore, recent peptide array studies have proposed that FRH interacts with multiple regions distributed across the entire FRQ protein (Jankowski et al. 2024). My results strongly support the idea of weak interactions between FRH and FRQ in addition to the strong association with the 6B2 region.

5.3 FRH dissociates from phosphorylated FRQ

Previously, FRQ was primarily found to be localized in the cytosol (Schafmeier et al. 2005). Later, our lab discovered that FRQ undergoes subcellular redistribution, a process regulated by CK1a-mediated phosphorylation that controls its rapid nuclear export and import (Diernfellner et al. 2009). In this study, I successfully replicated these findings using a heterologous cellular system. MK2-FRQ co-expressed with CK1a in U2OStx cells was rapidly exported from the nucleus to the cytosol (Figure 4.5.1b, Figure S6).

Phosphorylation plays critical roles in the circadian clock, particularly in modulating the function and regulation of FRQ. CK1a has been shown to bind FRQ early in the circadian cycle, regulating FRQ over time to ensure the proper functioning of the feedback loop through interactions with other clock components. Phosphorylation at specific sites within FRQ alters its function in distinct ways. For instance, phosphorylation at the PEST2 sequence in the C-terminal region of FRQ triggers its export from the nucleus, following its role in executing negative feedback, to initiate its role in positive feedback on the WCC (Schafmeier et al. 2006). In contrast, phosphorylation at the PEST1 region, located centrally in FRQ, promotes its turnover (Görl et al. 2001). However, not all phosphorylation sites in FRQ serve such discrete functions. FRQ is an intrinsically disordered protein with unevenly distributed charged residues. In its hypophosphorylated state, FRQ adopts a relatively condensed state probably initiated through long-range intramolecular interactions, allowing the positively charged N-terminus to interact with distant regions of the protein. This configuration appears to be critical for facilitating CK1a binding. As FRQ becomes progressively phosphorylated, it shifts toward an open conformation, deactivating the protein and then enabling the phosphorylation of the PEST1 sequence, which leads to its degradation (Liu et al. 2000, Görl et al. 2001, Querfurth et al. 2011, Lauinger et al. 2014). Importantly, the phosphorylation status of FRQ, independent of its turnover, has been shown to influence the length of the circadian period. This indicates that while deactivation and degradation of FRQ are sequential

processes, they occur independently of one another (Larrondo et al. 2015). This complex interplay between phosphorylation and the structural dynamics of FRQ is central to the timekeeping mechanisms of the circadian clock.

In *Neurospora*, FRQ that is not bound to FRH is highly unstable and rapidly degraded, which makes it challenging to study the influence of FRQ phosphorylation in the absence of FRH. Therefore, one of the most intriguing observations from my experiments in U2OSx cells was that CK1a-mediated phosphorylation of FRQ triggered the dissociation of the FRQ-FRH complex, resulting in the nuclear export of FRQ, while FRH remained within the nucleus of U2OSx cells.

Interestingly, in my assay, cells expressing FRQ^{6B2}, FRH, and CK1a exhibited faster nuclear export of FRQ^{6B2} compared to cells expressing WT FRQ with FRH and CK1a, where FRQ export was noticeably delayed (Figure 4.5.1b). Importantly, the phosphorylation levels of both FRQ variants were comparable (Figure 4.5.1a). This indicates that FRQ capable of binding FRH is temporarily retained in the nucleus due to this interaction. In contrast, FRQ that cannot bind FRH, such as FRQ^{6B2}, is exported more rapidly following phosphorylation and the resulting inactivation of its NLSs. These findings imply that FRH not only stabilizes phosphorylated FRQ but also delays its nuclear export, allowing FRQ to undergo phosphorylation over time. This delay may offer new insights into the regulatory dynamics between FRH and FRQ and their role in circadian rhythm regulation. Taking these results, I developed new strategies to explore the interaction between FRH and FRQ, and the role of CK1a-driven phosphorylation in regulating this interaction in *Neurospora*. The phosphorylation-dependent dissociation of the FRQ-FRH complex was further supported by co-immunoprecipitation (Figure 4.5.2a; Figure S7) and gel filtration chromatography experiments (Figure 4.5.2b) performed by analyzing native FRQ-FRH complexes from *Neurospora*. Accordingly, the data I collected in the cellular system align with those obtained in *Neurospora* and validate the reliability of my experimental approach (Figure 4.5.1 and Figure S6).

5.4 The subcellular localization of FRQ is regulated by three NLSs and one NES
Sequence analysis tools like NLStradamus (Nguyen Ba et al. 2009) predict two NLSs in FRQ. One of these NLS has experimentally been characterized (Luo et al. 1998). However, during my analysis, I also discovered smaller clusters of positively charged

residues that, while falling below the standard NLS threshold, warranted further investigation. Upon closer examination of the sequence, I identified a third NLS-like sequence between aa639-642, which displayed some similarities to the other known NLSs of FRQ. By generating a C-terminal fragment of FRQ containing only this NLS-like structure, I was able to confirm that this region was sufficient to localize FRQ predominantly to the nucleus, thus identifying a third functional NLS. Further transient transfection experiments, combined with co-expression of CK1a, revealed that phosphorylation appeared to all three NLS regions, preventing accumulation of FRQ in the nucleus and leading to CRM1-dependent nuclear export. This suggests that FRQ likely contains a nuclear export signal (NES). Because FRQ⁹ was not exported from the nucleus upon phosphorylation the NES is located in the C-terminal region of FRQ.

The NLSs in FRQ are functionally dominant over its NES, resulting in the nuclear accumulation of FRQ. This also applies to FRQ^{6B2}, which cannot bind FRH and is exported upon phosphorylation more rapidly than wild-type FRQ. Based on my findings, I propose the following model: FRH enhances nuclear retention of FRQ by masking an NES when bound, thereby delaying its nuclear export. Phosphorylation of FRQ by CK1a unmasks the NES through the dissociation of FRH, facilitating FRQ's export from the nucleus. The cytoplasmic accumulation of FRQ is likely facilitated by the phosphorylation-dependent inactivation of the otherwise dominant NLSs.

Previous studies on the deletion of the NLS between amino acids 194-199 demonstrated that FRQ is unable to enter the nucleus, leading to the disruption of the circadian clock rhythm (Luo et al. 1998). Given that NLS1 is situated near the coiled-coil region responsible for FRQ dimerization, its deletion likely disrupts this crucial process (Lauinger et al. 2014), resulting in a severe phenotype and impaired protein function (Luo et al. 1998, Cheng et al. 2001). Our findings demonstrate that the mutated NLS1, which has lost its nuclear localization function but retains its structure, supports an intact circadian rhythm (Figure 4.2.3). Our data is further supported by the coiled-coil domain predictions for FRQ, FRQ^{mutNLS123}, and FRQ^{ΔNLS1}. While a coiled-coil structure is predicted at NLS1 for both FRQ and FRQ^{mutNLS123}, no such structure is observed for FRQ^{ΔNLS1}. This observation further suggests that NLS1 seems to play a direct role in FRQ dimerization (Figure 5.4) Specifically, these findings suggest that NLS1 is crucial for

proper clock function by facilitating FRQ dimerization, rather than serving as a key element for nuclear import (Figures 4.2.2 and 5.4).

Our mutations in NLS2 and the newly identified NLS3 revealed that these alterations affect the rhythm phase of the clock, yet the clock remains functional. Therefore, while NLS2 and NLS3 contribute to the robustness of the circadian rhythm, they are not required for the clock's functionality. NLS1, however, is essential due to its role in dimerization. Additionally, our data suggest that FRQ can be imported independently of its own NLS when bound to FRH.

When Bianca Ruppert mutated all three NLS of FRQ and coexpressed the protein with FRH in U2OXTx cells, we found that saturating levels of FRH supported nuclear accumulation of FRQ and FRH, suggesting that bound FRH provides an import signal for FRQ^{mutNLS123} while masking FRQ's NES. In contrast, unsaturated levels of FRH were not sufficient to recruit FRQ^{mutNLS123} to the nucleus, but instead FRH was recruited to foci in the cytosol. In contrast, unsaturated levels of FRH were insufficient to recruit FRQ^{mutNLS123} into the nucleus and instead led to the recruitment of FRH into cytoplasmic foci. Under these conditions, the limited availability of FRH was inadequate for importing FRQ into the nucleus, resulting in FRH being incorporated into cytoplasmic foci alongside FRQ (Figure 4.2.1b F). These observations suggest two key points. First, they indicate the existence of a FRQ dimer species in which only a single FRH molecule is bound (FRQ₂:FRH₁). Given that FRQ phosphorylation occurs stochastically, NLS regions are deactivated, and FRH molecules dissociate randomly, leading to a heterogeneous pool of FRQ-FRH complexes. Second, the findings imply that FRH may mask the putative NES of FRQ. At subsaturating levels, this masking effect appears to be insufficient to counteract the dominant export signal of FRQ, thereby limiting the ability of FRH to import FRQ into the nucleus.

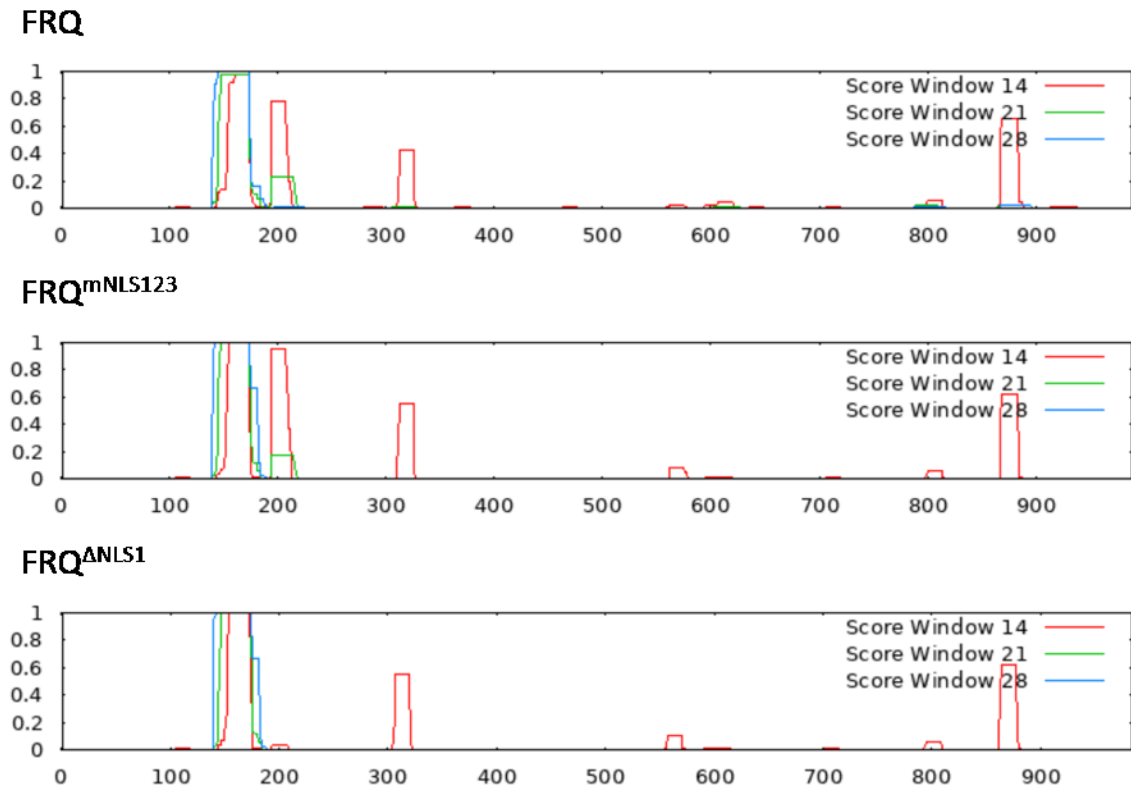


Figure 5.4: **Prediction of coiled-coil domains in FRQ using npsa-prabi** (Lupas et al. 1991)

The top image depicts the predicted profile for the coiled-coil domain of FRQ (aa155-175). Furthermore, the tool indicates the presence of a coiled-coil close to NLS1 (aa194-199), in addition to smaller peaks at aa320 and aa890. The middle panel illustrates the impact of NLS1, NLS2, and NLS3 mutations, as described in sections 4.2.2 and 4.2.3. Notably, the coiled-coil peak remains detectable in these mutants; however, in the NLS1-deleted sequence (FRQ Δ NLS1), the peak for the coiled-coil is significantly reduced.

Bianca Rupert's and my results are further supported by the findings of Sabine Schultz and Axel Diernfellner, , who demonstrated that, even with mutations in all three NLSs in FRQ, the circadian clock retained at least a residual, damped circadian rhythm. This suggests that FRQ may not require its NLS regions for nuclear import, as FRH partially substitutes by promoting FRQ's import into the nucleus. This observation aligns with a study by Cha and colleagues, which proposed that FRH regulates FRQ localization (Cha et al. 2011). Furthermore, this underscores the role of FRH in retaining FRQ in the nucleus following phosphorylation. A mutant with a defect in FRH interaction is exported much more rapidly than wild-type FRQ, indicating that FRH introduces a delay in FRQ's nuclear export, potentially by masking FRQ's NLS. This delay likely plays a key role in

the regulation of circadian rhythm by modulating the timing of FRQ's activity within the clock.

5.5 FRH masks the WCC binding-site

Aside from stabilizing FRQ, FRH plays several crucial roles in the *Neurospora* circadian clock. Amino acid residues 100–150 of FRH are required for binding to FRQ but not for other functions of FRH. Bound FRH acts as a "nanny" for FRQ by supporting a compact conformation that protects FRQ from degradation (Querfurth et al. 2011, Hurley et al. 2013), thereby directly influencing the negative feedback mechanism of the circadian clock. This hypothesis is supported by observations from Shi and colleagues (2010), who identified an FRH mutant that led to a disrupted feedback loop in *Neurospora* caused by a single substitution in R806H. In FRH^{R806H}, *frq* mRNA expression levels were upregulated and fluctuated randomly, while FRQ protein levels remained high with all phosphorylated isoforms present at all time points. Additionally, FRH^{R806H} failed to promote WCC phosphorylation and WCC binding to the FFC complex was completely abolished. This resulted in hypophosphorylated and hyperactive WCC, which is unstable (Schafmeier et al. 2006, Shi et al. 2010). This led to the suggestion that both FRH and FRQ are necessary for the negative feedback regulation of the circadian clock, ensuring proper phosphorylation and activity of WCC (Shi et al. 2010).

My data show that FRH regulates the interaction of FRQ with WCC in an unexpected way. Upon co-expression, I observed no co-localization of WC-1, WC-2, or WCC with FRH, unlike the clear co-localization seen between WCC and FRQ. Moreover, FRH prevented the co-localization of WCC with FRQ, which was surprising given the data from Shi and colleagues (2010). In contrast, my findings suggest that the association between FRQ, WCC, and FRH are mutually exclusive.

My data show an interaction of WCC with FRQ but not with FRQ⁹, which lacks the C-terminal part, suggesting that WCC binds to the C-terminal part of FRQ. The binding site overlaps with but is distinct from the FRH binding site. This conclusion is supported by the observation that the 6B2 substitution in FRQ abolished the interaction between FRH and FRQ but did not disrupt the interaction between FRQ and WCC (Figure 4.3.2 C).

Previous research (Wang et al. 2015b, Wang et al. 2019) has proposed that regions in the N-terminal and central part of FRQ are required for the interaction with WCC. These

observations can be explained by alternative mechanisms: The suggested WCC interaction region in the N-terminal part FRQ interfere with dimerization of FRQ and thereby indirectly affect WCC recruitment, because monomeric FRQ is rapidly degraded when FRH is released to expose a WCC binding site. Wang and Dunlap (2023) showed furthermore that a FRQ Δ 482-510 mutant is no longer capable of interacting with WCC. However, this deleted region includes the FCD2 domain (aa485-496), which is essential for interaction with CK1a (Querfurth et al. 2011, Wang and Dunlap 2023). These findings suggest that CK1a, and possibly the phosphorylation of FRQ, is required for its interaction with WCC. Additionally, my data show that without phosphorylation of FRQ by CK1a, FRH will not be released. As a result, the WCC binding site is constitutively blocked in the FRQ Δ 482-510 mutant, which accounts for the observed lack of interaction with WCC.

Furthermore, I demonstrated that the mutant FRH^{R806H} protein effectively blocked the WC-1 binding site more efficiently than WT FRH. This increased binding affinity of FRH^{R806H} may account for the observed lack of interaction between WCC and FRQ in a *Neurospora* strain expressing FRH^{R806H} (Shi et al. 2010). By masking the WCC binding site, FRH^{R806H} might lead to a phenotype characterized by a loss of negative feedback within the circadian clock.

My data indicate that tight anchoring of FRH to hypophosphorylated FRQ obstructs the WCC binding site, which only becomes accessible when at least one FRH molecule is released from initially formed tetrameric FRQ₂:FRH₂ complex following the phosphorylation of FRQ. This observation aligns with a model previously proposed by our group: in 2022, we suggested that FRQ binds to FRH not only via the FFD domain, but also through numerous low-affinity interactions. This supports a condensed conformation of FRQ around FRH (Marzoll et al. 2022b). This hypothesis of low-affinity interaction sites is further supported by peptide assay data published earlier this year (Jankowski et al. 2024). Our findings suggested that slow, progressive phosphorylation reduces these low-affinity interactions, causing FRQ to expand over time, transitioning from an inactive FRQ that can accumulate to an active negative complex (Marzoll et al. 2022b). My findings refine this model by explaining the details of the switch and how the delay is established. Slow, progressive phosphorylation leads to the gradual dissociation of FRQ from FRH, making room for interaction with WCC and subsequent repression.

This proposed mechanism would introduce the necessary delay for the clock to function properly. But Jonkowski and colleagues also further support my model with their findings for a FRQ^{RR/AA} mutant. Here, RR783-784 were substituted with two As. FRQ^{RR/AA} did not co-immunoprecipitate with FRH, but its expression remained stable in contrast to other mutants deficient in FRH binding. Additionally, WC-1 expression was stable, indicating that the negative feedback was intact. Indicating that FRH might not be needed for the interaction and phosphorylation of WCC (Jonkowski et al. 2024).

Based on the data presented, I propose novel roles for FRH, which has traditionally been recognized solely as a "nanny" protein protecting FRQ from degradation. My findings suggest that FRH's function extends beyond this role. The data indicate that the time-dependent phosphorylation state of the intrinsically disordered FRQ dimer is interpreted by its structured partner, FRH. Phosphorylation of FRQ affects its interaction with FRH, resulting in a stepwise remodeling of an initially nuclear heterotetrameric FFC complex with a FRQ₂:FRH₂ stoichiometry, which also includes bound CK1a. This complex is inactive because FRH prevents the binding and inactivation of WCC, allowing ongoing WCC-dependent transcription of *frq* and hence the accumulation of substantial levels of FRQ₂:FRH₂ complexes. The slowly progressing phosphorylation of FRQ by bound CK1a triggers with a delay the release of one FRH molecule, resulting in remodeling of the inactive FRQ₂:FRH₂ complex into a trimeric FRQ₂:FRH₁ complex. This complex is active because the release of one FRH molecule exposes a WCC binding site in one of the two FRQ molecules which is now able to interact with and inhibit WCC, initiating negative feedback and inhibiting further *frq* transcription. Because phosphorylation of FRQ is slow and stochastic, the two FRH molecules are not simultaneously released. Thus, ongoing phosphorylation will eventually also trigger the dissociation of the second FRH, resulting in a FRQ₂ complex. This complex is in principle active, as it exposes two WCC binding sites. However, phosphorylation has inactivated FRQ's NLSs and release of FRH, exposed the NESs, leading to relocalization of the complex into the cytosol where FRQ is rapidly degraded (see Figure 5.6).

In conclusion, the FFC complex undergoes two distinct molecular switches that facilitate two different functions within the circadian clock mechanism. Initially, the complex exists in an inactive state, which is crucial for creating a delay in the negative feedback loop of the circadian clock. During this phase, the first switch is triggered by the

phosphorylation of FRQ, resulting in the exposure of its WCC binding site. As phosphorylation continues to progress, it activates the “off switch,” leading to the inactivation and complete disassociation of the complex. This process subsequently relocates FRQ to the cytosol, where it is targeted for degradation.

My proposed model not only aligns with numerous previously published findings, but also offers potential explanations for unresolved questions. For instance, the monomeric FRQ variant, in which the coiled-coil domain (aa145-174) is mutated or deleted, results in the loss of clock function (Luo et al. 1998, Cheng et al. 2001, Lauinger et al. 2014). This suggests that FRQ dimerization is essential for the proper operation of the *Neurospora* circadian clock. Although monomeric FRQ has been shown to interact with FRH and CK1a, a monomeric FFC complex is unable to associate with WCC, thus preventing the initiation of negative feedback (Luo et al. 1998, Cheng et al. 2001, Lauinger et al. 2014). According to my model, monomeric FRQ remains tightly bound to FRH, hindering its association with WCC and blocking negative feedback. Upon phosphorylation and subsequent release of FRH, monomeric FRQ, unlike the FRQ dimer, is immediately exported to the cytosol, where it remains inactive and undergoes rapid degradation.

A recent study by Wang and Dunlap (2023) aimed at pinpointing the regions of FRQ responsible for binding to WCC, employing deletion analysis to identify key D/E clusters. They found that deletion of these clusters prevented co-immunoprecipitation of WCC. Notably, one cluster in the N-terminus of FRQ (aa149-187) overlaps with the coiled-coil domain required for FRQ dimerization, while another mutant that fails to bind WCC carries a mutation in the FCD2 domain, one of two CK1a binding sites (Querfurth et al. 2011, Wang and Dunlap 2023). Though deletions in the C-terminus of FRQ seem to directly affect the WCC binding site. As previously mentioned, FRQ mutants that remain monomeric are inactive, unable to participate in a negative feedback. My model provides a convincing explanation for why CK1a binding deficient mutants are similarly unable to interact with WCC: in these mutants, FRQ is trapped in the inactive FRQ₂:FRH₂ stoichiometry, as FRH cannot be released without phosphorylation of FRQ by CK1a.

My model also offers an explanation for findings that initially seemed puzzling in relation to other data sets. While regions 6B2 (aa774-776) and 6B5 (aa776-782) were identified as critical interaction sites between FRH and FRQ (Guo et al. 2010), other evidence

suggested that FRH may also interact with various positively charged regions throughout FRQ (Hurley et al. 2013). According to my model, FRH is anchored to these defined regions on FRQ, but phosphorylation of FRQ—and the subsequent alteration of its charge—likely disrupts these interactions (Marzoll et al. 2022b). This charge alteration could interfere with FRH binding, leading to the release of FRH. My model supports this idea and cements the concept that phosphorylation acts as a key regulator, facilitating the dynamic remodeling of the FRQ-FRH complex and enabling the progression of the circadian feedback loop.

It is evident that my model remains incomplete, and several questions remain unresolved. For instance, I have yet to determine the specific timing and phosphorylated states at which the respective molecular switches occur and we need to characterize in detail the specific properties of the FRQ₂:FRH₂, the FRQ₂:FRH₁ and the FRQ₂ complexes. However, I am committed to refining the model as new information becomes available. Drawing upon the data collected prior to and throughout this thesis, I believe we have formulated a comprehensive mechanistic concept for how a eukaryotic circadian clock measures time at a molecular level. I hope that this framework will inspire novel research approaches in this field.

5.6 Model

From my data the following model emerges (as seen in Figure 5.6). Newly synthesized, unphosphorylated FRQ forms a nuclear heterotetramer with an FRQ₂:FRH₂ stoichiometry. Its nuclear localization is mediated by three NLSs and further supported by its interaction with FRH, which either stabilizes FRQ in the nucleus by masking its NES or shifts the equilibrium to nuclear import. The binding of two FRH molecules also blocks the binding sites for the White Collar Complex (WCC), rendering FRQ₂:FRH₂ inactive and preventing negative feedback on WCC. Consequently, WCC remains active, promoting *frq* transcription and leading to the continued accumulation of inactive FRQ₂:FRH₂.

Over time, slow phosphorylation of FRQ by CK1a inactivates its NLSs and initiates the dissociation of FRH. Due to the stochastic progressive phosphorylation of FRQ, FRH dissociates asymmetrically, resulting in the transient formation of an FRQ₂:FRH₁ intermediate. The FRQ subunit that has lost its bound FRH becomes active and can

interact with WCC, leading to CK1a-mediated phosphorylation and inactivation of WCC, effectively shutting down *frq* transcription.

The exposed putative NES on FRQ promotes its export from the nucleus. However, the remaining FRH molecule can either trap FRQ₂:FRH₁ in the nucleus or facilitate its reimport depending on the phosphorylation status and residual NLS activity. Further phosphorylation eventually results in the complete dissociation of FRH, leaving an FRQ₂ species with exposed NESs and no functional NLS. This fully exported FRQ₂ becomes inactive in the cytoplasm and is ultimately degraded, completing the feedback loop. WCC dephosphorylation then resets the system for the next circadian cycle, ensuring robust rhythm regulation.

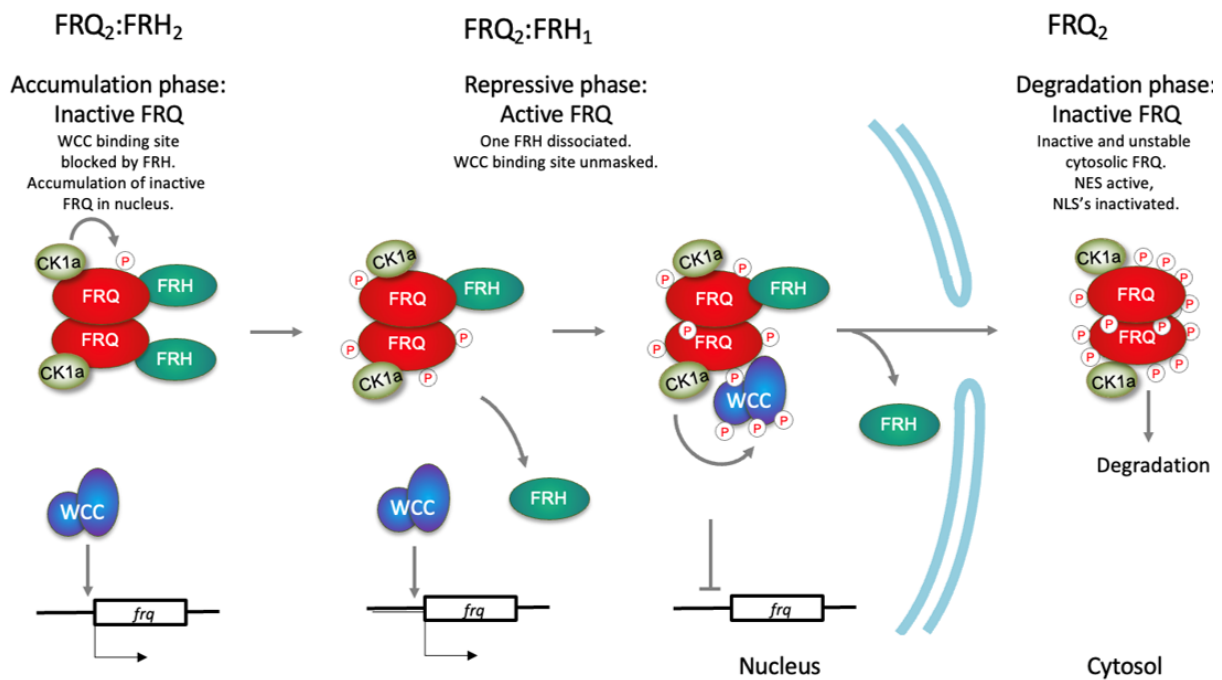


Figure 5.6: Model of our current understanding of the modulation of FRQ by CK1a and FRH

Newly synthesized, unphosphorylated FRQ forms a nuclear heterotetramer with an FRQ₂:FRH₂ stoichiometry, facilitated by its nuclear localization through its three NLSs and partially through FRH. FRH stabilizes FRQ in the nucleus by masking its NES and blocking the binding sites for the White Collar Complex (WCC), rendering FRQ₂:FRH₂ inactive and preventing negative feedback on WCC. As a result, WCC remains active, promoting *frq* transcription and leading to the accumulation of inactive FRQ₂:FRH₂. Slow phosphorylation of FRQ by CK1a inactivates its NLSs and triggers the dissociation of FRH. Due to the stochastic nature of FRQ phosphorylation, FRH dissociates asymmetrically, forming a transient FRQ₂:FRH₁ species. The FRQ subunit that has lost FRH becomes active and can bind WCC, allowing CK1a to phosphorylate and inactivate

WCC, shutting down *frq* transcription. The exposed NES in FRQ prompts nuclear export of FRQ₂:FRH₁, although the remaining FRH molecule can either trap it in the nucleus or promote its reimport depending on the phosphorylation status and activity of the NLSs. Further phosphorylation leads to the dissociation of the second FRH molecule, leaving an FRQ₂ species with two exposed NESs and no functional NLS. This fully exported FRQ₂ becomes inactive in the cytosol and is degraded, closing the feedback loop. WCC dephosphorylation initiates the next circadian cycle, ensuring robust rhythm regulation.

5.7 Conclusion and outlook

The use of a transient system to investigate the interactions within the circadian clock complex provides a novel framework for studying the FFC complex components. This method proved instrumental in this research, allowing for the identification of new regulatory factors influencing the circadian clock's modulation. This approach facilitated the development of a model in which FRQ transitions between two different functional states through phosphorylation. FRH stabilizes medium-phosphorylated FRQ until sufficient phosphorylation disrupts the interaction. Furthermore, FRH inhibits the premature interaction between WCC and FRQ during the initial phase, effectively delaying WCC deactivation by FRQ. My initial findings found using a cellular model could be verified in *Neurospora*. This highlights the system's utility for circadian clock research. However, additional studies are essential to obtain a more complete understanding of the mechanisms governing the circadian clock. An example for this is to answer at which point of FRQ phosphorylation the switches occur which would further validate our model.

I successfully reconstructed aspects of the *Neurospora* circadian clock within a transient cellular system, achieving co-transfection of FRQ, FRH, and WCC to study their interactions. This allowed for valuable insights into these core clock components. However, attempts to co-transfect the entire FFC complex alongside CK1a and WCC did not yet yield conclusive results, highlighting the current limitations of this system. Further investigation is therefore needed to pinpoint the exact timing at which FRQ binds to WCC and inactivates this transcription factor, marking the closure of the circadian feedback loop.

During the investigation of the NLSs of FRQ, several additional findings emerged, including the identification of a third NLS (NLS3) in *Neurospora*. Similar to NLS2,

NLS3 does not appear to be essential for the functionality of the circadian clock in the same way as NLS1. However, the presence of three NLSs raises intriguing questions about their roles. It would be particularly interesting to further explore whether these NLSs are involved in the dimerization or self-interaction of FRQ.

A deeper investigation into NLS1 has clarified why this specific nuclear localization signal is essential for FRQ functionality. Deletion of NLS1 leads to an arrhythmic circadian clock due to disturbing the dimerization process of FRQ, highlighting its importance. However, a targeted mutation within NLS1 that inactivates its localization function while maintaining the region's overall charge revealed that it is the charge, rather than the localization function, that is critical for FRQ's structural integrity. This suggests that NLS1 contributes to protein stabilization, possibly through self-interaction or FRH-mediated stabilization. Studying additional mutants could provide further insight into how FRQ maintains its functional state and how the activity of the NLSs might be modulated through phosphorylation.

Despite extensive research, the identification of a putative NES in the C-terminal region of FRQ remains elusive. Further studies are needed to clarify whether FRQ indeed contains an NES and whether FRH can mask this NES, or if FRH influences the equilibrium by anchoring FRQ in the nucleus through direct binding.

Moreover, a detailed examination of the stoichiometric relationship between FRH and FRQ could offer valuable insights into the regulation of the negative feedback mechanism in the circadian clock. Investigating similarities between mammalian and fungal circadian clocks could also enhance our understanding of circadian regulation across species. Notably, despite extensive research, no definitive interaction site between FRQ and WCC has been identified, indicating that multiple factors may facilitate their interaction, warranting further study.

6. References

- Akashi, M., Tsuchiya, Y., Yoshino, T. and Nishida, E. (2002). "Control of intracellular dynamics of mammalian period proteins by casein kinase I epsilon (CKIepsilon) and CKIdelta in cultured cells." *Mol Cell Biol* 22(6): 1693-1703.
- Alberti, S., Gladfelter, A. and Mittag, T. (2019). "Considerations and Challenges in Studying Liquid-Liquid Phase Separation and Biomolecular Condensates." *Cell* 176(3): 419-434.
- Allmang, C., Kufel, J., Chanfreau, G., Mitchell, P., Petfalski, E. and Tollervy, D. (1999). "Functions of the exosome in rRNA, snoRNA and snRNA synthesis." *The EMBO journal* 18(19): 5399-5410.
- Andreani, T. S., Itoh, T. Q., Yildirim, E., Hwangbo, D. S. and Allada, R. (2015). "Genetics of Circadian Rhythms." *Sleep Med Clin* 10(4): 413-421.
- Aronson, B. D., Johnson, K. A., Loros, J. J. and Dunlap, J. C. (1994). "Negative feedback defining a circadian clock: autoregulation of the clock gene *frequency*." *Science* 263(5153): 1578-1584.
- Aschoff, J. (1954). "Zeitgeber der tierischen Tagesperiodik." *Naturwissenschaften* 41(3): 49-56.
- Aschoff, J. (1965). "Circadian Rhythms in Man." *Science* 148(3676): 1427-1432.
- Aschoff, J. (1981). *Freerunning and Entrained Circadian Rhythms. Biological Rhythms.* J. Aschoff. Boston, MA, Springer US: 81-93.
- Aslanidis, C., de Jong, P. J. and Schmitz, G. (1994). "Minimal length requirement of the single-stranded tails for ligation-independent cloning (LIC) of PCR products." *PCR Methods Appl* 4(3): 172-177.
- Baker, C. L., Kettenbach, A. N., Loros, J. J., Gerber, S. A. and Dunlap, J. C. (2009). "Quantitative Proteomics Reveals a Dynamic Interactome and Phase-Specific Phosphorylation in the Neurospora Circadian Clock." *Molecular Cell* 34(3): 354-363.
- Baker, C. L., Loros, J. J. and Dunlap, J. C. (2012). "The circadian clock of *Neurospora crassa*." *FEMS Microbiology Reviews* 36(1): 95-110.
- Ballario, P., Talora, C., Galli, D., Linden, H. and Macino, G. (1998). "Roles in dimerization and blue light photoresponse of the PAS and LOV domains of *Neurospora crassa* white collar proteins." *Mol Microbiol* 29(3): 719-729.
- Ballario, P., Vittorioso, P., Magrelli, A., Talora, C., Cabibbo, A. and Macino, G. (1996). "White collar-1, a central regulator of blue light responses in *Neurospora*, is a zinc finger protein." *The EMBO journal* 15(7): 1650-1657.
- Banani, S. F., Lee, H. O., Hyman, A. A. and Rosen, M. K. (2017). "Biomolecular condensates: organizers of cellular biochemistry." *Nat Rev Mol Cell Biol* 18(5): 285-298.
- Beadle, G. W. and Tatum, E. L. (1941). "Genetic Control of Biochemical Reactions in *Neurospora*." *Proc Natl Acad Sci U S A* 27(11): 499-506.
- Bell-Pedersen, D., Garceau, N. and Loros, J. J. (1996). "Circadian rhythms in fungi." *Journal of Genetics* 75(3): 387-401.
- Benko, S., Magalhaes, J. G., Philpott, D. J. and Girardin, S. E. (2010). "NLRC5 limits the activation of inflammatory pathways." *J Immunol* 185(3): 1681-1691.

- Berson, D. M., Dunn, F. A. and Takao, M. (2002). "Phototransduction by retinal ganglion cells that set the circadian clock." *Science* 295(5557): 1070-1073.
- Bhadra, U., Thakkar, N., Das, P. and Pal Bhadra, M. (2017). "Evolution of circadian rhythms: from bacteria to human." *Sleep Med* 35: 49-61.
- Boehning, M., Dugast-Darzacq, C., Rankovic, M., Hansen, A. S., Yu, T., Marie-Nelly, H., McSwiggen, D. T., Kokic, G., Dailey, G. M., Cramer, P., Darzacq, X. and Zweckstetter, M. (2018). "RNA polymerase II clustering through carboxy-terminal domain phase separation." *Nat Struct Mol Biol* 25(9): 833-840.
- Boeynaems, S., Alberti, S., Fawzi, N. L., Mittag, T., Polymenidou, M., Rousseau, F., Schymkowitz, J., Shorter, J., Wolozin, B., Van Den Bosch, L., Tompa, P. and Fuxreiter, M. (2018). "Protein Phase Separation: A New Phase in Cell Biology." *Trends Cell Biol* 28(6): 420-435.
- Bunger, M. K., Wilsbacher, L. D., Moran, S. M., Clendenin, C., Radcliffe, L. A., Hogenesch, J. B., Simon, M. C., Takahashi, J. S. and Bradfield, C. A. (2000). "Mop3 is an essential component of the master circadian pacemaker in mammals." *Cell* 103(7): 1009-1017.
- Bünning, E. (1959). Tagesperiodische Bewegungen. *Physiology of Movements / Physiologie der Bewegungen: Part 1 Movements due to Mechanical and Electrical Stimuli and to Radiations / Teil 1 Bewegungen durch Einflüsse Mechanischer und Elektrischer Natur Sowie durch Strahlungen.* L. Baillaud, Banbury, G. H., Brauner, L., Bünning, E., Clayton, R. K., Galston, A. W. et al. Berlin, Heidelberg, Springer Berlin Heidelberg: 579-656.
- Carmel, G., Leichus, B., Cheng, X., Patterson, S. D., Mirza, U., Chait, B. T. and Kuret, J. (1994). "Expression, purification, crystallization, and preliminary x-ray analysis of casein kinase-1 from *Schizosaccharomyces pombe*." *Journal of Biological Chemistry* 269(10): 7304-7309.
- Cesbron, F., Brunner, M. and Diernfellner, A. C. (2013). "Light-dependent and circadian transcription dynamics in vivo recorded with a destabilized luciferase reporter in *Neurospora*." *PLoS ONE* 8(12): e83660.
- Cha, J., Chang, S. S., Huang, G., Cheng, P. and Liu, Y. (2008). "Control of WHITE COLLAR localization by phosphorylation is a critical step in the circadian negative feedback process." *The EMBO journal* 27(24): 3246-3255.
- Cha, J., Yuan, H. and Liu, Y. (2011). "Regulation of the Activity and Cellular Localization of the Circadian Clock Protein FRQ*." *Journal of Biological Chemistry* 286(13): 11469-11478.
- Cha, J., Zhou, M. and Liu, Y. (2015). "Mechanism of the *Neurospora* circadian clock, a FREQUENCY-centric view." *Biochemistry* 54(2): 150-156.
- Chen, C. H., Dunlap, J. C. and Loros, J. J. (2010). "Neurospora illuminates fungal photoreception." *Fungal Genet Biol* 47(11): 922-929.
- Cheng, P., He, Q., He, Q., Wang, L. and Liu, Y. (2005). "Regulation of the *Neurospora* circadian clock by an RNA helicase." *Genes Dev* 19(2): 234-241.
- Cheng, P., Yang, Y., Gardner, K. H. and Liu, Y. (2002). "PAS Domain-Mediated WC-1/WC-2 Interaction Is Essential for Maintaining the Steady-State Level of WC-1 and the Function of Both Proteins in Circadian Clock and Light Responses of *Neurospora*." *Molecular and Cellular Biology* 22(2): 517-524.

- Cheng, P., Yang, Y., Heintzen, C. and Liu, Y. (2001). "Coiled-coil domain-mediated FRQ-FRQ interaction is essential for its circadian clock function in *Neurospora*." *The EMBO journal* 20(1-2): 101-108.
- Cheng, P., Yang, Y., Wang, L., He, Q. and Liu, Y. (2003). "WHITE COLLAR-1, a Multifunctional Neurospora Protein Involved in the Circadian Feedback Loops, Light Sensing, and Transcription Repression of *wc-2* " *Journal of Biological Chemistry* 278(6): 3801-3808.
- Cheong, J. K. and Virshup, D. M. (2011). "Casein kinase 1: Complexity in the family." *Int J Biochem Cell Biol* 43(4): 465-469.
- Collett, M. A., Garceau, N., Dunlap, J. C. and Loros, J. J. (2002). "Light and clock expression of the *Neurospora* clock gene *frequency* is differentially driven by but dependent on WHITE COLLAR-2." *Genetics* 160(1): 149-158.
- Conrad, K. S., Hurley, J. M., Widom, J., Ringelberg, C. S., Loros, J. J., Dunlap, J. C. and Crane, B. R. (2016). "Structure of the frequency-interacting RNA helicase: a protein interaction hub for the circadian clock." *The EMBO journal* 35(15): 1707-1719.
- Crosthwaite, S. K., Dunlap, J. C. and Loros, J. J. (1997). "Neurospora *wc-1* and *wc-2*: transcription, photoresponses, and the origins of circadian rhythmicity." *Science* 276(5313): 763-769.
- de la Cruz, J., Kressler, D. and Linder, P. (1999). "Unwinding RNA in *Saccharomyces cerevisiae*: DEAD-box proteins and related families." *Trends Biochem Sci* 24(5): 192-198.
- de Mairan, J. (1729). "Observation Botanique." *Histoire de l'Académie Royale des Sciences*: 35-36.
- Degli-Innocenti, F. and Russo, V. E. (1984). "Isolation of new white collar mutants of *Neurospora crassa* and studies on their behavior in the blue light-induced formation of protoperithecia." *Journal of Bacteriology* 159(2): 757-761.
- Diernfellner, A. C., Querfurth, C., Salazar, C., Hofer, T. and Brunner, M. (2009). "Phosphorylation modulates rapid nucleocytoplasmic shuttling and cytoplasmic accumulation of *Neurospora* clock protein FRQ on a circadian time scale." *Genes Dev* 23(18): 2192-2200.
- Diernfellner, A. C. R. and Brunner, M. (2020). "Phosphorylation Timers in the *Neurospora crassa* Circadian Clock." *J Mol Biol* 432(12): 3449-3465.
- Dodd, A. N., Salathia, N., Hall, A., Kévei, E., Tóth, R., Nagy, F., Hibberd, J. M., Millar, A. J. and Webb, A. A. (2005). "Plant circadian clocks increase photosynthesis, growth, survival, and competitive advantage." *Science* 309(5734): 630-633.
- Dunlap, J. C. (1999). "Molecular Bases for Circadian Clocks." *Cell* 96(2): 271-290.
- Dunlap, J. C. and Loros, J. J. (2018). "Just-So Stories and Origin Myths: Phosphorylation and Structural Disorder in Circadian Clock Proteins." *Mol Cell* 69(2): 165-168.
- Edgar, R. S., Green, E. W., Zhao, Y., van Ooijen, G., Olmedo, M., Qin, X., Xu, Y., Pan, M., Valekunja, U. K., Feeney, K. A., Maywood, E. S., Hastings, M. H., Baliga, N. S., Mellow, M., Millar, A. J., Johnson, C. H., Kyriacou, C. P., O'Neill, J. S. and Reddy, A. B. (2012). "Peroxiredoxins are conserved markers of circadian rhythms." *Nature* 485(7399): 459-464.
- Eide, E. J., Vielhaber, E. L., Hinz, W. A. and Virshup, D. M. (2002). "The circadian regulatory proteins BMAL1 and cryptochromes are substrates of casein kinase Iepsilon." *J Biol Chem* 277(19): 17248-17254.

- Eide, E. J., Woolf, M. F., Kang, H., Woolf, P., Hurst, W., Camacho, F., Vielhaber, E. L., Giovanni, A. and Virshup, D. M. (2005). "Control of mammalian circadian rhythm by CKIepsilon-regulated proteasome-mediated PER2 degradation." *Mol Cell Biol* 25(7): 2795-2807.
- Erdos, G., Pajkos, M. and Dosztanyi, Z. (2021). "IUPred3: prediction of protein disorder enhanced with unambiguous experimental annotation and visualization of evolutionary conservation." *Nucleic Acids Res* 49(W1): W297-W303.
- Etchegaray, J. P., Machida, K. K., Noton, E., Constance, C. M., Dallmann, R., Di Napoli, M. N., DeBruyne, J. P., Lambert, C. M., Yu, E. A., Reppert, S. M. and Weaver, D. R. (2009). "Casein kinase 1 delta regulates the pace of the mammalian circadian clock." *Mol Cell Biol* 29(14): 3853-3866.
- Feldman, J. F. and Hoyle, M. N. (1973). "Isolation of circadian clock mutants of *Neurospora crassa*." *Genetics* 75(4): 605-613.
- Fischer, W. W., Hemp, J. and Valentine, J. S. (2016). "How did life survive Earth's great oxygenation?" *Current Opinion in Chemical Biology* 31: 166-178.
- Flotow, H., Graves, P. R., Wang, A. Q., Fiol, C. J., Roeske, R. W. and Roach, P. J. (1990). "Phosphate groups as substrate determinants for casein kinase I action." *Journal of Biological Chemistry* 265(24): 14264-14269.
- French-Pacheco, L., Rosas-Bringas, O., Segovia, L. and Covarrubias, A. A. (2022). "Intrinsically disordered signaling proteins: Essential hub players in the control of stress responses in *Saccharomyces cerevisiae*." *PLoS ONE* 17(3): e0265422.
- Froehlich, A. C., Loros, J. J. and Dunlap, J. C. (2003). "Rhythmic binding of a WHITE COLLAR-containing complex to the frequency promoter is inhibited by FREQUENCY." *Proceedings of the National Academy of Sciences* 100(10): 5914-5919.
- Fueller, J., Herbst, K., Meurer, M., Gubicza, K., Kurtulmus, B., Knopf, J. D., Kirrmaier, D., Buchmuller, B. C., Pereira, G., Lemberg, M. K. and Knop, M. (2020). "CRISPR-Cas12a-assisted PCR tagging of mammalian genes." *J Cell Biol* 219(6).
- Fulcher, L. J. and Sapkota, G. P. (2020). "Functions and regulation of the serine/threonine protein kinase CK1 family: moving beyond promiscuity." *Biochem J* 477(23): 4603-4621.
- Fuzik, J., Zeisel, A., Máté, Z., Calvigioni, D., Yanagawa, Y., Szabó, G., Linnarsson, S. and Harkany, T. (2016). "Integration of electrophysiological recordings with single-cell RNA-seq data identifies neuronal subtypes." *Nat Biotechnol* 34(2): 175-183.
- Galagan, J. E., Calvo, S. E., Borkovich, K. A., Selker, E. U., Read, N. D., Jaffe, D., FitzHugh, W., Ma, L. J., Smirnov, S., Purcell, S., Rehman, B., Elkins, T., Engels, R., Wang, S., Nielsen, C. B., Butler, J., Endrizzi, M., Qui, D., Ianakiev, P., Bell-Pedersen, D., Nelson, M. A., Werner-Washburne, M., Selitrennikoff, C. P., Kinsey, J. A., Braun, E. L., Zelter, A., Schulte, U., Kothe, G. O., Jedd, G., Mewes, W., Staben, C., Marcotte, E., Greenberg, D., Roy, A., Foley, K., Naylor, J., Stange-Thomann, N., Barrett, R., Gnerre, S., Kamal, M., Kamvysselis, M., Mauceli, E., Bielke, C., Rudd, S., Frishman, D., Krystofova, S., Rasmussen, C., Metzenberg, R. L., Perkins, D. D., Kroken, S., Cogoni, C., Macino, G., Catcheside, D., Li, W., Pratt, R. J., Osmani, S. A., DeSouza, C. P., Glass, L., Orbach, M. J., Berglund, J. A., Voelker, R., Yarden, O., Plamann, M., Seiler, S., Dunlap, J., Radford, A., Aramayo, R., Natvig, D. O., Alex, L. A., Mannhaupt, G., Ebbole, D. J., Freitag, M., Paulsen, I., Sachs, M. S., Lander, E. S., Nusbaum, C. and Birren, B. (2003). "The genome sequence of the filamentous fungus *Neurospora crassa*." *Nature* 422(6934): 859-868.

- Gardner, G. F. and Feldman, J. F. (1980). "The *frq* locus in *Neurospora crassa*: a key element in circadian clock organization." *Genetics* 96(4): 877-886.
- Gardner, M. J., Hubbard, K. E., Hotta, C. T., Dodd, A. N. and Webb, A. A. (2006). "How plants tell the time." *Biochem J* 397(1): 15-24.
- Gooch, V. D., Mehra, A., Larrondo, L. F., Fox, J., Touroutoutoudis, M., Loros, J. J. and Dunlap, J. C. (2008). "Fully codon-optimized luciferase uncovers novel temperature characteristics of the *Neurospora* clock." *Eukaryot Cell* 7(1): 28-37.
- Görl, M., Mero, M., Huttner, B., Johnson, J., Roenneberg, T. and Brunner, M. (2001). "A PEST-like element in FREQUENCY determines the length of the circadian period in *Neurospora crassa*." *The EMBO journal* 20(24): 7074-7084.
- Graves, P. R. and Roach, P. J. (1995). "Role of COOH-terminal phosphorylation in the regulation of casein kinase I delta." *J Biol Chem* 270(37): 21689-21694.
- Guo, J., Cheng, P. and Liu, Y. (2010). "Functional Significance of FRH in Regulating the Phosphorylation and Stability of *Neurospora* Circadian Clock Protein FRQ " *Journal of Biological Chemistry* 285(15): 11508-11515.
- Guo, J., Cheng, P., Yuan, H. and Liu, Y. (2009). "The exosome regulates circadian gene expression in a posttranscriptional negative feedback loop." *Cell* 138(6): 1236-1246.
- Gustafson, C. L. and Partch, C. L. (2015). "Emerging models for the molecular basis of mammalian circadian timing." *Biochemistry* 54(2): 134-149.
- Harding, R. W. and Turner, R. V. (1981). "Photoregulation of the Carotenoid Biosynthetic Pathway in Albino and White Collar Mutants of *Neurospora crassa*." *Plant Physiology* 68(3): 745-749.
- He, Q., Cha, J., He, Q., Lee, H. C., Yang, Y. and Liu, Y. (2006). "CKI and CKII mediate the FREQUENCY-dependent phosphorylation of the WHITE COLLAR complex to close the *Neurospora* circadian negative feedback loop." *Genes Dev* 20(18): 2552-2565.
- He, Q., Cheng, P., Yang, Y., He, Q., Yu, H. and Liu, Y. (2003). "FWD1-mediated degradation of FREQUENCY in *Neurospora* establishes a conserved mechanism for circadian clock regulation." *The EMBO journal* 22(17): 4421-4430.
- He, Q., Cheng, P., Yang, Y., Wang, L., Gardner, K. H. and Liu, Y. (2002). "White Collar-1, a DNA Binding Transcription Factor and a Light Sensor." *Science* 297(5582): 840-843.
- He, Q. and Liu, Y. (2005). "Degradation of the *Neurospora* circadian clock protein FREQUENCY through the ubiquitin-proteasome pathway." *Biochem Soc Trans* 33(Pt 5): 953-956.
- Hilleren, P. J. and Parker, R. (2003). "Cytoplasmic degradation of splice-defective pre-mRNAs and intermediates." *Mol Cell* 12(6): 1453-1465.
- Hirano, A., Fu, Y. H. and Ptáček, L. J. (2016). "The intricate dance of post-translational modifications in the rhythm of life." *Nat Struct Mol Biol* 23(12): 1053-1060.
- Horowitz, N. H. (1991). "Fifty years ago: the *Neurospora* revolution." *Genetics* 127(4): 631-635.
- Houseley, J., LaCava, J. and Tollervey, D. (2006). "RNA-quality control by the exosome." *Nat Rev Mol Cell Biol* 7(7): 529-539.

- Huang, G., Chen, S., Li, S., Cha, J., Long, C., Li, L., He, Q. and Liu, Y. (2007). "Protein kinase A and casein kinases mediate sequential phosphorylation events in the circadian negative feedback loop." *Genes Dev* 21(24): 3283-3295.
- Hurley, J. M., Dasgupta, A., Emerson, J. M., Zhou, X., Ringelberg, C. S., Knabe, N., Lipzen, A. M., Lindquist, E. A., Daum, C. G., Barry, K. W., Grigoriev, I. V., Smith, K. M., Galagan, J. E., Bell-Pedersen, D., Freitag, M., Cheng, C., Loros, J. J. and Dunlap, J. C. (2014). "Analysis of clock-regulated genes in *Neurospora* reveals widespread posttranscriptional control of metabolic potential." *Proc Natl Acad Sci U S A* 111(48): 16995-17002.
- Hurley, Jennifer M., Larrondo, Luis F., Loros, Jennifer J. and Dunlap, Jay C. (2013). "Conserved RNA Helicase FRH Acts Nonenzymatically to Support the Intrinsically Disordered *Neurospora* Clock Protein FRQ." *Molecular Cell* 52(6): 832-843.
- Inouye, S. T. and Kawamura, H. (1979). "Persistence of circadian rhythmicity in a mammalian hypothalamic "island" containing the suprachiasmatic nucleus." *Proc Natl Acad Sci U S A* 76(11): 5962-5966.
- Jacobus, A. P. and Gross, J. (2015). "Optimal cloning of PCR fragments by homologous recombination in *Escherichia coli*." *PLoS ONE* 10(3): e0119221.
- Jankowski, M. S., Griffith, D., Shastry, D. G., Pelham, J. F., Ginell, G. M., Thomas, J., Karande, P., Holehouse, A. S. and Hurley, J. M. (2024). "Disordered clock protein interactions and charge blocks turn an hourglass into a persistent circadian oscillator." *Nature Communications* 15(1): 3523.
- Johnson, A. E., Chen, J. S. and Gould, K. L. (2013). "CK1 is required for a mitotic checkpoint that delays cytokinesis." *Curr Biol* 23(19): 1920-1926.
- Kato, Y., Kawamoto, T., Fujimoto, K. and Noshiro, M. (2014). DEC1/STRA13/SHARP2 and DEC2/SHARP1 Coordinate Physiological Processes, Including Circadian Rhythms in Response to Environmental Stimuli. Current Topics in Developmental Biology. R. Taneja, Academic Press. 110: 339-372.
- Knippschild, U., Gocht, A., Wolff, S., Huber, N., Lohler, J. and Stoter, M. (2005). "The casein kinase 1 family: participation in multiple cellular processes in eukaryotes." *Cell Signal* 17(6): 675-689.
- Knippschild, U., Milne, D. M., Campbell, L. E., DeMaggio, A. J., Christenson, E., Hoekstra, M. F. and Meek, D. W. (1997). "p53 is phosphorylated in vitro and in vivo by the delta and epsilon isoforms of casein kinase 1 and enhances the level of casein kinase 1 delta in response to topoisomerase-directed drugs." *Oncogene* 15(14): 1727-1736.
- Kondo, T., Strayer, C. A., Kulkarni, R. D., Taylor, W., Ishiura, M., Golden, S. S. and Johnson, C. H. (1993). "Circadian rhythms in prokaryotes: luciferase as a reporter of circadian gene expression in cyanobacteria." *Proc Natl Acad Sci U S A* 90(12): 5672-5676.
- Konopka, R. J. and Benzer, S. (1971). "Clock Mutants of *Drosophila melanogaster*." *Proceedings of the National Academy of Sciences* 68(9): 2112-2116.
- Kume, K., Zylka, M. J., Sriram, S., Shearman, L. P., Weaver, D. R., Jin, X., Maywood, E. S., Hastings, M. H. and Reppert, S. M. (1999). "mCRY1 and mCRY2 are essential components of the negative limb of the circadian clock feedback loop." *Cell* 98(2): 193-205.
- LaCava, J., Houseley, J., Saveanu, C., Petfalski, E., Thompson, E., Jacquier, A. and Tollervey, D. (2005). "RNA degradation by the exosome is promoted by a nuclear polyadenylation complex." *Cell* 121(5): 713-724.

- Laemmli, U. K. (1970). "Cleavage of Structural Proteins during the Assembly of the Head of Bacteriophage T4." *Nature* 227(5259): 680-685.
- Larrondo, L. F., Olivares-Yanez, C., Baker, C. L., Loros, J. J. and Dunlap, J. C. (2015). "Circadian rhythms. Decoupling circadian clock protein turnover from circadian period determination." *Science* 347(6221): 1257-1277.
- Lauinger, L., Diernfellner, A., Falk, S. and Brunner, M. (2014). "The RNA helicase FRH is an ATP-dependent regulator of CK1 α in the circadian clock of *Neurospora crassa*." *Nature Communications* 5(1): 3598.
- Lee, K., Loros, J. J. and Dunlap, J. C. (2000). "Interconnected Feedback Loops in the *Neurospora* Circadian System." *Science* 289(5476): 107-110.
- Li, M. Z. and Elledge, S. J. (2007). "Harnessing homologous recombination in vitro to generate recombinant DNA via SLIC." *Nat Methods* 4(3): 251-256.
- Li, Q., Peng, X., Li, Y., Tang, W., Zhu, J. a., Huang, J., Qi, Y. and Zhang, Z. (2019). "LLPSDB: a database of proteins undergoing liquid-liquid phase separation in vitro." *Nucleic Acids Research* 48(D1): D320-D327.
- Linden, H. (2002). "A White Collar Protein Senses Blue Light." *Science* 297(5582): 777-778.
- Liu, G., Park, Y. J. and Abraham, E. (2008). "Interleukin-1 receptor-associated kinase (IRAK) -1-mediated NF-kappaB activation requires cytosolic and nuclear activity." *FASEB J* 22(7): 2285-2296.
- Liu, H. and Naismith, J. H. (2008). "An efficient one-step site-directed deletion, insertion, single and multiple-site plasmid mutagenesis protocol." *BMC Biotechnol* 8: 91.
- Liu, Y., Loros, J. and Dunlap, J. C. (2000). "Phosphorylation of the *Neurospora* clock protein FREQUENCY determines its degradation rate and strongly influences the period length of the circadian clock." *Proc Natl Acad Sci U S A* 97(1): 234-239.
- Lorentzen, E. and Conti, E. (2006). "The exosome and the proteasome: nano-compartments for degradation." *Cell* 125(4): 651-654.
- Loros, J. J. and Feldman, J. F. (1986). "Loss of temperature compensation of circadian period length in the *frq-9* mutant of *Neurospora crassa*." *J Biol Rhythms* 1(3): 187-198.
- Loros, J. J., Richman, A. and Feldman, J. F. (1986). "A recessive circadian clock mutation at the *frq* locus of *Neurospora crassa*." *Genetics* 114(4): 1095-1110.
- Lowrey, P. L. and Takahashi, J. S. (2004). "Mammalian circadian biology: elucidating genome-wide levels of temporal organization." *Annu Rev Genomics Hum Genet* 5: 407-441.
- Luo, C., Loros, J. J. and Dunlap, J. C. (1998). "Nuclear localization is required for function of the essential clock protein FRQ." *The EMBO journal* 17(5): 1228-1235.
- Lupas, A., Van Dyke, M. and Stock, J. (1991). "Predicting coiled coils from protein sequences." *Science* 252(5009): 1162-1164.
- Malzahn, E., Ciprianidis, S., Káldi, K., Schafmeier, T. and Brunner, M. (2010). "Photoadaptation in *Neurospora* by competitive interaction of activating and inhibitory LOV domains." *Cell* 142(5): 762-772.

- Marzoll, D., Serrano, F. E., Diernfellner, A. C. R. and Brunner, M. (2022a). "*Neurospora* casein kinase 1a recruits the circadian clock protein FRQ via the C-terminal lobe of its kinase domain." *FEBS Lett* 596(15): 1881-1891.
- Marzoll, D., Serrano, F. E., Shostak, A., Schunke, C., Diernfellner, A. C. R. and Brunner, M. (2022b). "Casein kinase 1 and disordered clock proteins form functionally equivalent, phospho-based circadian modules in fungi and mammals." *Proc Natl Acad Sci U S A* 119(9).
- Merrow, M. W., Garceau, N. Y. and Dunlap, J. C. (1997). "Dissection of a circadian oscillation into discrete domains." *Proc Natl Acad Sci U S A* 94(8): 3877-3882.
- Mitchell, P. and Tollervey, D. (2000). "Musing on the structural organization of the exosome complex." *Nat Struct Biol* 7(10): 843-846.
- Mohr, G., Del Campo, M., Mohr, S., Yang, Q., Jia, H., Jankowsky, E. and Lambowitz, A. M. (2008). "Function of the C-terminal domain of the DEAD-box protein Mss116p analyzed *in vivo* and *in vitro*." *J Mol Biol* 375(5): 1344-1364.
- Moore, R. Y. and Eichler, V. B. (1972). "Loss of a circadian adrenal corticosterone rhythm following suprachiasmatic lesions in the rat." *Brain Res* 42(1): 201-206.
- Nelson, M. A., Morelli, G., Carattoli, A., Romano, N. and Macino, G. (1989). "Molecular cloning of a *Neurospora crassa* carotenoid biosynthetic gene (albino-3) regulated by blue light and the products of the white collar genes." *Mol Cell Biol* 9(3): 1271-1276.
- Nguyen Ba, A. N., Pogoutse, A., Provart, N. and Moses, A. M. (2009). "NLStradamus: a simple Hidden Markov Model for nuclear localization signal prediction." *BMC Bioinformatics* 10: 202.
- O'Neill, J. S. and Reddy, A. B. (2011). "Circadian clocks in human red blood cells." *Nature* 469(7331): 498-503.
- Olmedo, M., Ruger-Herreros, C. and Corrochano, L. M. (2010). "Regulation by blue light of the fluffy gene encoding a major regulator of conidiation in *Neurospora crassa*." *Genetics* 184(3): 651-658.
- Pelham, J. F., Dunlap, J. C. and Hurley, J. M. (2020). "Intrinsic disorder is an essential characteristic of components in the conserved circadian circuit." *Cell Commun Signal* 18(1): 181.
- Peng, Z., Yan, J., Fan, X., Mizianty, M. J., Xue, B., Wang, K., Hu, G., Uversky, V. N. and Kurgan, L. (2015). "Exceptionally abundant exceptions: comprehensive characterization of intrinsic disorder in all domains of life." *Cell Mol Life Sci* 72(1): 137-151.
- Pittendrigh, C. S. (1960). "Circadian rhythms and the circadian organization of living systems." *Cold Spring Harb Symp Quant Biol* 25: 159-184.
- Putnam, A. A. and Jankowsky, E. (2013). "DEAD-box helicases as integrators of RNA, nucleotide and protein binding." *Biochim Biophys Acta* 1829(8): 884-893.
- Querfurth, C., Diernfellner, A. C., Gin, E., Malzahn, E., Hofer, T. and Brunner, M. (2011). "Circadian conformational change of the *Neurospora* clock protein FREQUENCY triggered by clustered hyperphosphorylation of a basic domain." *Mol Cell* 43(5): 713-722.
- Ramos-Garcia, S. L., Roberson, R. W., Freitag, M., Bartnicki-Garcia, S. and Mourino-Perez, R. R. (2009). "Cytoplasmic bulk flow propels nuclei in mature hyphae of *Neurospora crassa*." *Eukaryot Cell* 8(12): 1880-1890.

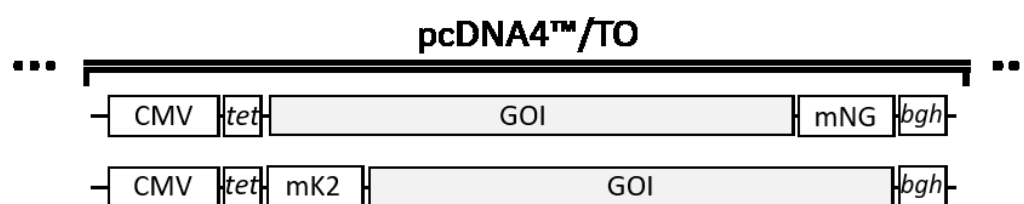
- Reischl, S. and Kramer, A. (2011). "Kinases and phosphatases in the mammalian circadian clock." *FEBS Letters* 585(10): 1393-1399.
- Reischl, S., Vanselow, K., Westermark, P. O., Thierfelder, N., Maier, B., Herzog, H. and Kramer, A. (2007). "Beta-TrCP1-mediated degradation of PERIOD2 is essential for circadian dynamics." *J Biol Rhythms* 22(5): 375-386.
- Rudolph, M. G. and Klostermeier, D. (2015). "When core competence is not enough: functional interplay of the DEAD-box helicase core with ancillary domains and auxiliary factors in RNA binding and unwinding." *Biol Chem* 396(8): 849-865.
- Salomon, M., Christie, J. M., Knieb, E., Lempert, U. and Briggs, W. R. (2000). "Photochemical and mutational analysis of the FMN-binding domains of the plant blue light receptor, phototropin." *Biochemistry* 39(31): 9401-9410.
- Sartor, F., Xu, X., Popp, T., Dodd, A. N., Kovács Á, T. and Merrow, M. (2023). "The circadian clock of the bacterium *B. subtilis* evokes properties of complex, multicellular circadian systems." *Sci Adv* 9(31): eadh1308.
- Sato, T. K., Yamada, R. G., Ukai, H., Baggs, J. E., Miraglia, L. J., Kobayashi, T. J., Welsh, D. K., Kay, S. A., Ueda, H. R. and Hogenesch, J. B. (2006). "Feedback repression is required for mammalian circadian clock function." *Nat Genet* 38(3): 312-319.
- Schafmeier, T., Diernfellner, A., Schafer, A., Dintsis, O., Neiss, A. and Brunner, M. (2008). "Circadian activity and abundance rhythms of the *Neurospora* clock transcription factor WCC associated with rapid nucleo-cytoplasmic shuttling." *Genes Dev* 22(24): 3397-3402.
- Schafmeier, T. and Diernfellner, A. C. (2011). "Light input and processing in the circadian clock of *Neurospora*." *FEBS Lett* 585(10): 1467-1473.
- Schafmeier, T., Haase, A., Kaldi, K., Scholz, J., Fuchs, M. and Brunner, M. (2005). "Transcriptional feedback of *Neurospora* circadian clock gene by phosphorylation-dependent inactivation of its transcription factor." *Cell* 122(2): 235-246.
- Schafmeier, T., Kaldi, K., Diernfellner, A., Mohr, C. and Brunner, M. (2006). "Phosphorylation-dependent maturation of *Neurospora* circadian clock protein from a nuclear repressor toward a cytoplasmic activator." *Genes Dev* 20(3): 297-306.
- Schitteck, B. and Sinnberg, T. (2014). "Biological functions of casein kinase 1 isoforms and putative roles in tumorigenesis." *Mol Cancer* 13: 231.
- Shi, M., Collett, M., Loros, J. J. and Dunlap, J. C. (2010). "FRQ-interacting RNA helicase mediates negative and positive feedback in the *Neurospora* circadian clock." *Genetics* 184(2): 351-361.
- Shirogane, T., Jin, J., Ang, X. L. and Harper, J. W. (2005). "SCFbeta-TRCP controls clock-dependent transcription via casein kinase 1-dependent degradation of the mammalian period-1 (Per1) protein." *J Biol Chem* 280(29): 26863-26872.
- Solt, L. A., Kojetin, D. J. and Burris, T. P. (2011). "The REV-ERBs and RORs: molecular links between circadian rhythms and lipid homeostasis." *Future Med Chem* 3(5): 623-638.
- Songyang, Z., Lu, K. P., Kwon, Y. T., Tsai, L. H., Filhol, O., Cochet, C., Brickey, D. A., Soderling, T. R., Bartleson, C., Graves, D. J., DeMaggio, A. J., Hoekstra, M. F., Blenis, J., Hunter, T. and Cantley, L. C. (1996). "A structural basis for substrate specificities of protein Ser/Thr kinases: primary sequence

- preference of casein kinases I and II, NIMA, phosphorylase kinase, calmodulin-dependent kinase II, CDK5, and Erk1." *Mol Cell Biol* 16(11): 6486-6493.
- Stephan, F. K. and Zucker, I. (1972). "Circadian Rhythms in Drinking Behavior and Locomotor Activity of Rats Are Eliminated by Hypothalamic Lesions." *Proceedings of the National Academy of Sciences* 69(6): 1583-1586.
- Suelmann, R., Sievers, N. and Fischer, R. (1997). "Nuclear traffic in fungal hyphae: *in vivo* study of nuclear migration and positioning in *Aspergillus nidulans*." *Mol Microbiol* 25(4): 757-769.
- Sun, H., Huang, Y., Mei, S., Xu, F., Liu, X., Zhao, F., Yin, L., Zhang, D., Wei, L., Wu, C., Ma, S., Wang, J., Cen, S., Liang, C., Hu, S. and Guo, F. (2021). "A Nuclear Export Signal Is Required for cGAS to Sense Cytosolic DNA." *Cell Rep* 34(1): 108586.
- Swartz, T. E., Corchnoy, S. B., Christie, J. M., Lewis, J. W., Szundi, I., Briggs, W. R. and Bogomolni, R. A. (2001). "The photocycle of a flavin-binding domain of the blue light photoreceptor phototropin." *J Biol Chem* 276(39): 36493-36500.
- Talora, C., Franchi, L., Linden, H., Ballario, P. and Macino, G. (1999). "Role of a white collar-1–white collar-2 complex in blue-light signal transduction." *The EMBO journal* 18(18): 4961-4968.
- Tang, C. T., Li, S., Long, C., Cha, J., Huang, G., Li, L., Chen, S. and Liu, Y. (2009). "Setting the pace of the *Neurospora* circadian clock by multiple independent FRQ phosphorylation events." *Proc Natl Acad Sci U S A* 106(26): 10722-10727.
- Tariq, D., Maurici, N., Bartholomai, B. M., Chandrasekaran, S., Dunlap, J. C., Bah, A. and Crane, B. R. (2024). "Phosphorylation, disorder, and phase separation govern the behavior of Frequency in the fungal circadian clock." *eLife* 12.
- Tataroğlu, Ö., Lauinger, L., Sancar, G., Jakob, K., Brunner, M. and Diernfellner, A. C. (2012). "Glycogen synthase kinase is a regulator of the circadian clock of *Neurospora crassa*." *J Biol Chem* 287(44): 36936-36943.
- Tatavosian, R., Kent, S., Brown, K., Yao, T., Duc, H. N., Huynh, T. N., Zhen, C. Y., Ma, B., Wang, H. and Ren, X. (2019). "Nuclear condensates of the Polycomb protein chromobox 2 (CBX2) assemble through phase separation." *J Biol Chem* 294(5): 1451-1463.
- Tsvetkov, P., Asher, G., Paz, A., Reuven, N., Sussman, J. L., Silman, I. and Shaul, Y. (2008). "Operational definition of intrinsically unstructured protein sequences based on susceptibility to the 20S proteasome." *Proteins* 70(4): 1357-1366.
- van Hoof, A., Lennertz, P. and Parker, R. (2000). "Yeast exosome mutants accumulate 3'-extended polyadenylated forms of U4 small nuclear RNA and small nucleolar RNAs." *Mol Cell Biol* 20(2): 441-452.
- Vogel, H. J. (1956). "A Convenient Growth Medium for *Neurospora crassa*." *Microbial Genetics Bulletin*(13): 42-47.
- Wang, B. and Dunlap, J. C. (2023). "Domains required for the interaction of the central negative element FRQ with its transcriptional activator WCC within the core circadian clock of *Neurospora*." *J Biol Chem* 299(7): 104850.
- Wang, B., Kettenbach, A. N., Zhou, X., Loros, J. J. and Dunlap, J. C. (2019). "The Phospho-Code Determining Circadian Feedback Loop Closure and Output in *Neurospora*." *Mol Cell* 74(4): 771-784 e773.

- Wang, B., Zhou, X., Loros, J. J. and Dunlap, J. C. (2015a). "Alternative Use of DNA Binding Domains by the *Neurospora* White Collar Complex Dictates Circadian Regulation and Light Responses." *Mol Cell Biol* 36(5): 781-793.
- Wang, B., Zhou, X., Loros, J. J. and Dunlap, J. C. (2015b). "Alternative Use of DNA Binding Domains by the *Neurospora* White Collar Complex Dictates Circadian Regulation and Light Responses." *Molecular and Cellular Biology* 36(5): 781-793.
- Ward, J. J., Sodhi, J. S., McGuffin, L. J., Buxton, B. F. and Jones, D. T. (2004). "Prediction and functional analysis of native disorder in proteins from the three kingdoms of life." *J Mol Biol* 337(3): 635-645.
- Warren, E. J., Allen, C. N., Brown, R. L. and Robinson, D. W. (2003). "Intrinsic light responses of retinal ganglion cells projecting to the circadian system." *Eur J Neurosci* 17(9): 1727-1735.
- Wijnen, H. and Young, M. W. (2006). "Interplay of circadian clocks and metabolic rhythms." *Annu Rev Genet* 40: 409-448.
- Winogradoff, D., John, S. and Aksimentiev, A. (2020). "Protein unfolding by SDS: the microscopic mechanisms and the properties of the SDS-protein assembly." *Nanoscale* 12(9): 5422-5434.
- Woelfle, M. A., Ouyang, Y., Phanvijhitsiri, K. and Johnson, C. H. (2004). "The adaptive value of circadian clocks: an experimental assessment in cyanobacteria." *Curr Biol* 14(16): 1481-1486.
- Xu, R. M., Carmel, G., Sweet, R. M., Kuret, J. and Cheng, X. (1995). "Crystal structure of casein kinase-1, a phosphate-directed protein kinase." *The EMBO journal* 14(5): 1015-1023.
- Ye, J., Osborne, A. R., Groll, M. and Rapoport, T. A. (2004). "RecA-like motor ATPases--lessons from structures." *Biochim Biophys Acta* 1659(1): 1-18.
- Yin, L., Wu, N. and Lazar, M. A. (2010). "Nuclear receptor Rev-erb α : a heme receptor that coordinates circadian rhythm and metabolism." *Nucl Recept Signal* 8: e001.
- Zemp, I., Wandrey, F., Rao, S., Ashiono, C., Wyler, E., Montellese, C. and Kutay, U. (2014). "CK1delta and CK1epsilon are components of human 40S subunit precursors required for cytoplasmic 40S maturation." *J Cell Sci* 127(Pt 6): 1242-1253.
- Zhang, G., Wang, Z., Du, Z. and Zhang, H. (2018). "mTOR Regulates Phase Separation of PGL Granules to Modulate Their Autophagic Degradation." *Cell* 174(6): 1492-1506.e1422.
- Zheng, B., Albrecht, U., Kaasik, K., Sage, M., Lu, W., Vaishnav, S., Li, Q., Sun, Z. S., Eichele, G., Bradley, A. and Lee, C. C. (2001). "Nonredundant roles of the mPer1 and mPer2 genes in the mammalian circadian clock." *Cell* 105(5): 683-694.

7. Appendix

A



B

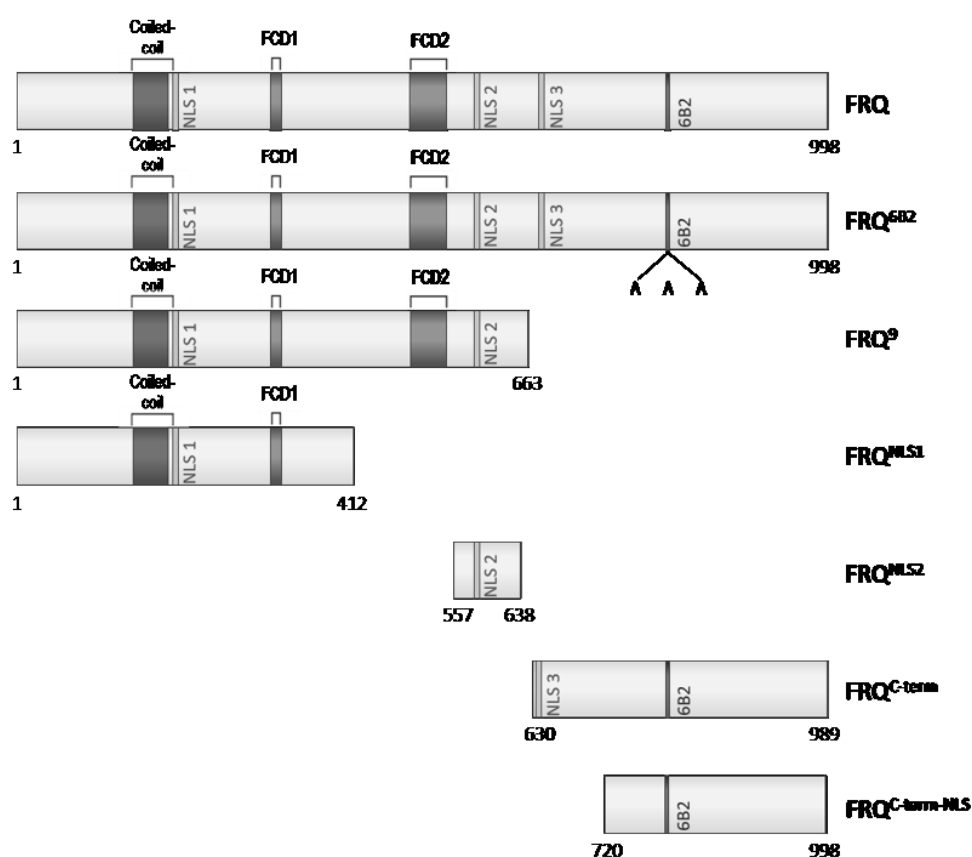


Figure S1: Overview of constructs

(A) Schematic of pcDNA Expression Vectors: The gene of interest (GOI) is driven by a CMV promoter with a TET operator. Tags include either a C-terminal mNeonGreen (mNG; (Fueller et al. 2020)) or an N-terminal mKate2 (mK2), followed by the 3'-UTR of the Bovine Growth Hormone Gene (*bgh*).

(B) Schematic of FRQ Constructs: Key features include the coiled-coil dimerization domain, predicted NLSs, FRQ-CK1 α interaction domains 1 and 2, and the 6B2 region required for FRH binding. The FRQ^{6B2} mutant substitutes residues 774-776 (DHF) with AAA. Proteins are tagged N-terminally with mK2 or C-terminally with mNG.

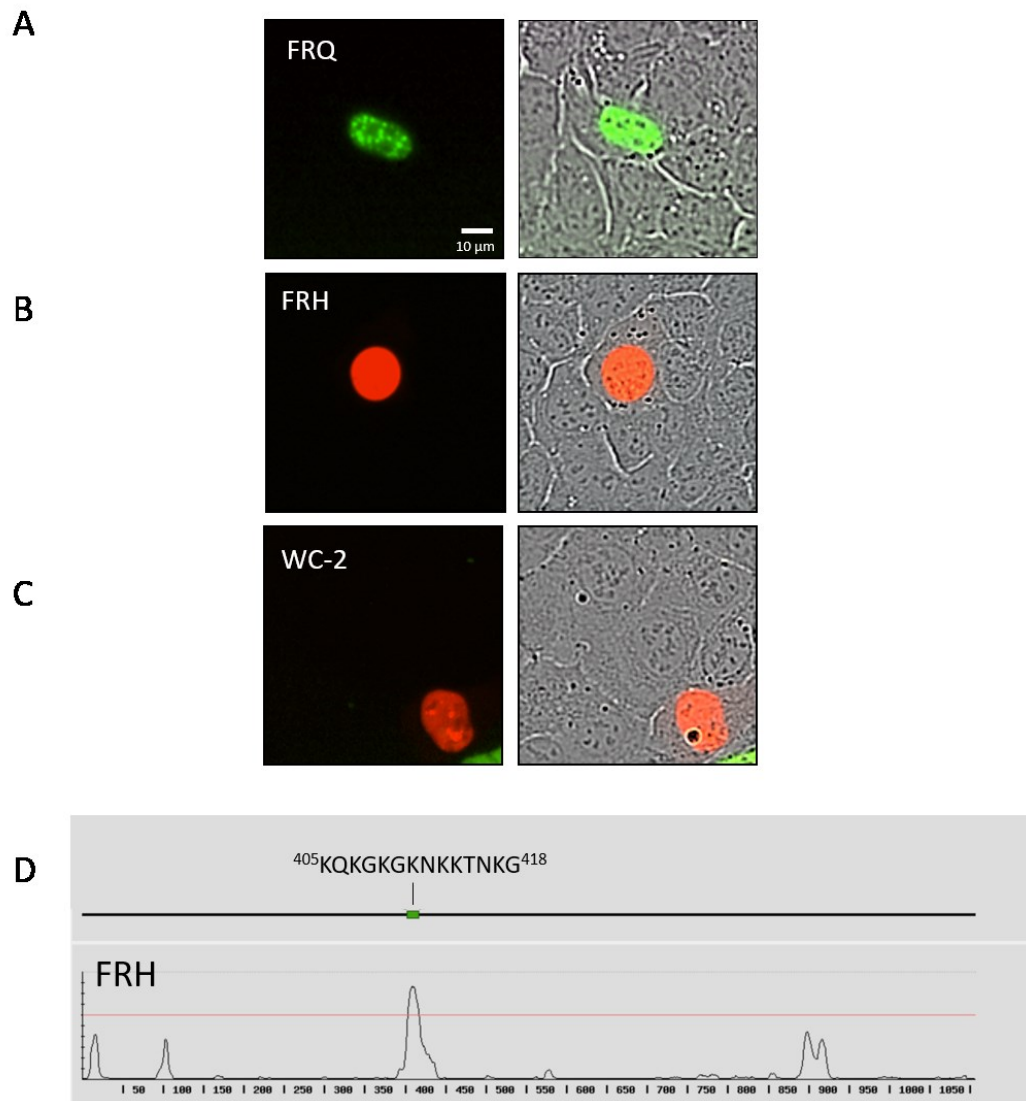


Figure S2: Subcellular localization of FRH

(A) Transient expression of FRQ-mNG (25 ng) with unlabeled FRQ (50 ng) in U2OStx cells. Microscopy image taken by Incucyte SX1 using a 20X objective; Scale bar= 10μm.

(B) FRH-mNG (50 g) is localized in the nucleus of U2OStx cells. Microscopy image taken by Incucyte SX1 using a 20X objective; Scale bar= 10μm.

(C) mK2-WC-2 (50 ng) shown with higher expression, which then shows a higher amount of dissolved WC-2 in the nucleus. Microscopy image taken by Incucyte SX1 using a 20X objective; Scale bar= 10μm.

(D) Prediction of FRH NLS by NLStradamus (Nguyen Ba et al. 2009) in FRH. The predicted NLS (aa 405-418) is not resolved in the crystal structure (PDB2XGJ; Figure 1.6) and predicted to be unfolded (AF: Q873J5-F1).

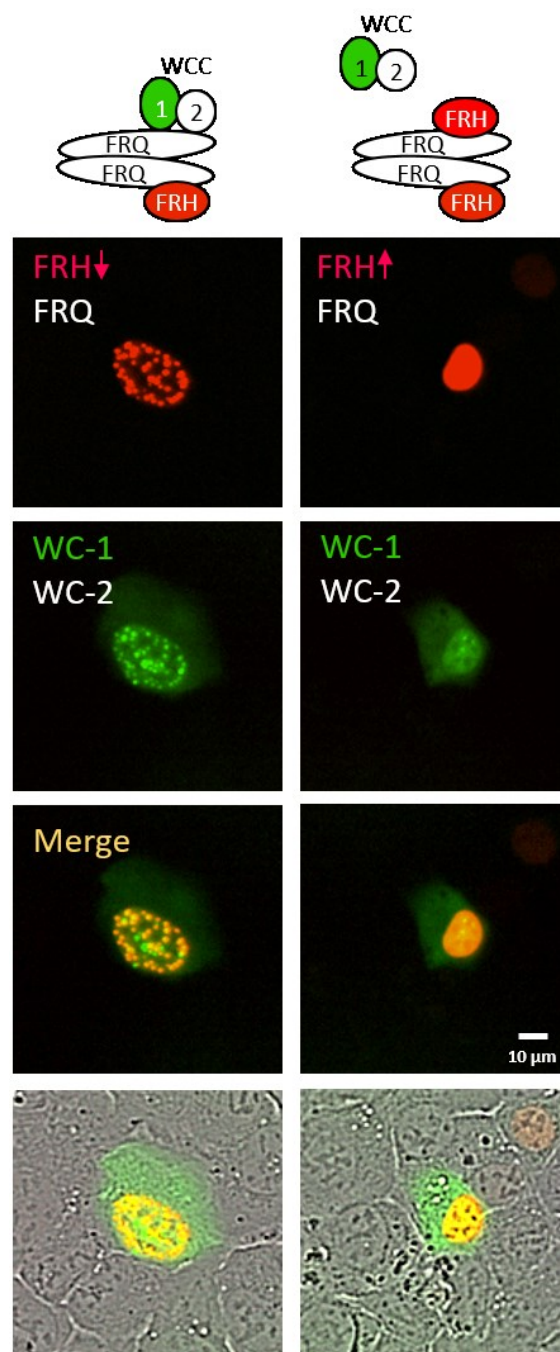


Figure S3: **Saturating amounts of FRH interfere with binding of FRQ to WCC**

Top: Schematics depict the interactions of fluorescently tagged (green and red) and untagged (white) proteins.

Left: Co-expression of FRQ (50 ng) and sub-saturating amounts of mK2-FRH (12.5 ng) with WC-1-mNG (50 ng) and untagged WC-2 (25 ng). FRQ, mK2-FRH and WC-1-mNG co-localize in nuclear foci.

Right: Co-expression of FRQ (40 ng) and saturating amounts of mK2-FRH (80 ng) with WC-1-mNG (50) and untagged WC-2 (25 ng). MK2-FRH is dispersed in the nucleus and WCC forms nuclear foci.

This Figure is a replicate of Figure 4.3.1 with swapped fluorescent tag combinations.

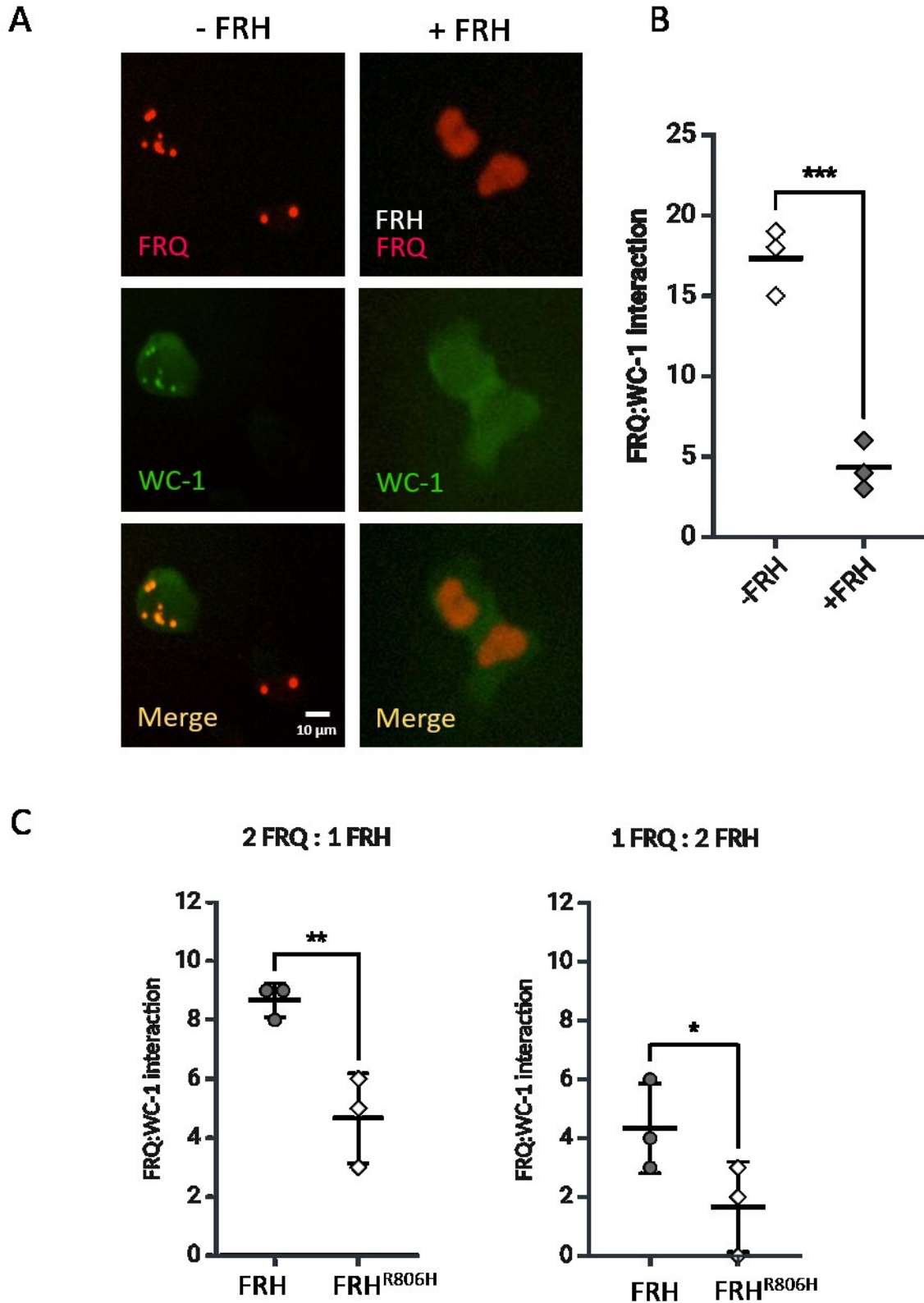


Figure S4 continued: FRH and FRH^{R806H} compete with the binding of WC-1 to FRQ

The image on the left shows FRQ forming nuclear foci, with WC-1-mNG enriched in those nuclear foci, indicating an interaction. On the right, mK2-FRQ foci are dissolved by saturating FRH amounts and WC-1-mNG is localized to the cytosol. There is no indication of interaction between mK2-FRQ and WC-1-mNG.

(B) Evaluation of A. The localization of WC-1 was analyzed and cells counted. n=3 x 20 cells. *** : p < 0.001.

(C) Left: 2 FRQ : 1 FRH. Co-expression of mK2-FRQ (40 ng) and mNG-WC-1 (50 ng) with non-saturating amounts (20 ng) of either untagged FRH or FRH^{R806H}. Interaction of mK2-FRQ with WC-1-mNG was evaluated by counting cells displaying nuclear enrichment of WC-1-mNG. 20 cells each from three independent experiments were evaluated. Unpaired t-test, **: p < 0.007. Microscopy pictures are not shown, since the phenotype of the cells is identical to A.

Right: 1 FRQ : 2 FRH. Co-expression of mK2-FRQ (40 ng) and mNG-WC-1 (50 ng) with saturating amounts (80 ng) of either untagged FRH or FRH^{R806H}. n = 3 x 20 cells. *: p < 0.049.

Figure S5 (on next page): CK1a phosphorylates FRQ, FRQ^{6B2} and FRQ⁹ in U2OStx cells over the course of time

Replicates of Western blot analysis of mK2-FRQ, mK2-FRQ^{6B2} and mK2-FRQ⁹ co-expressed with and without CK1a in U2OStx cells after 4h and 14h post induction with DOX. n=3.

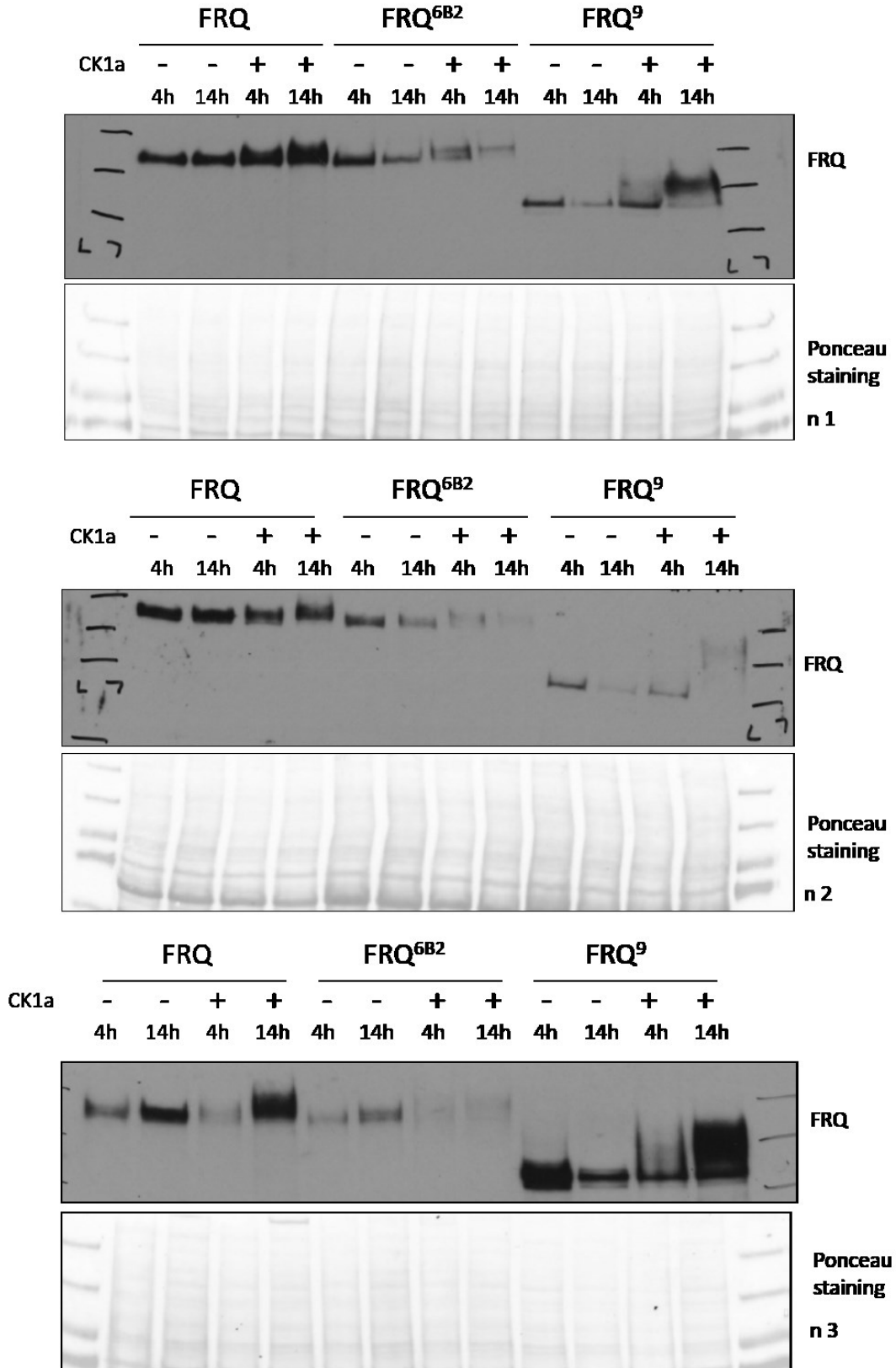


Figure legend on previous page

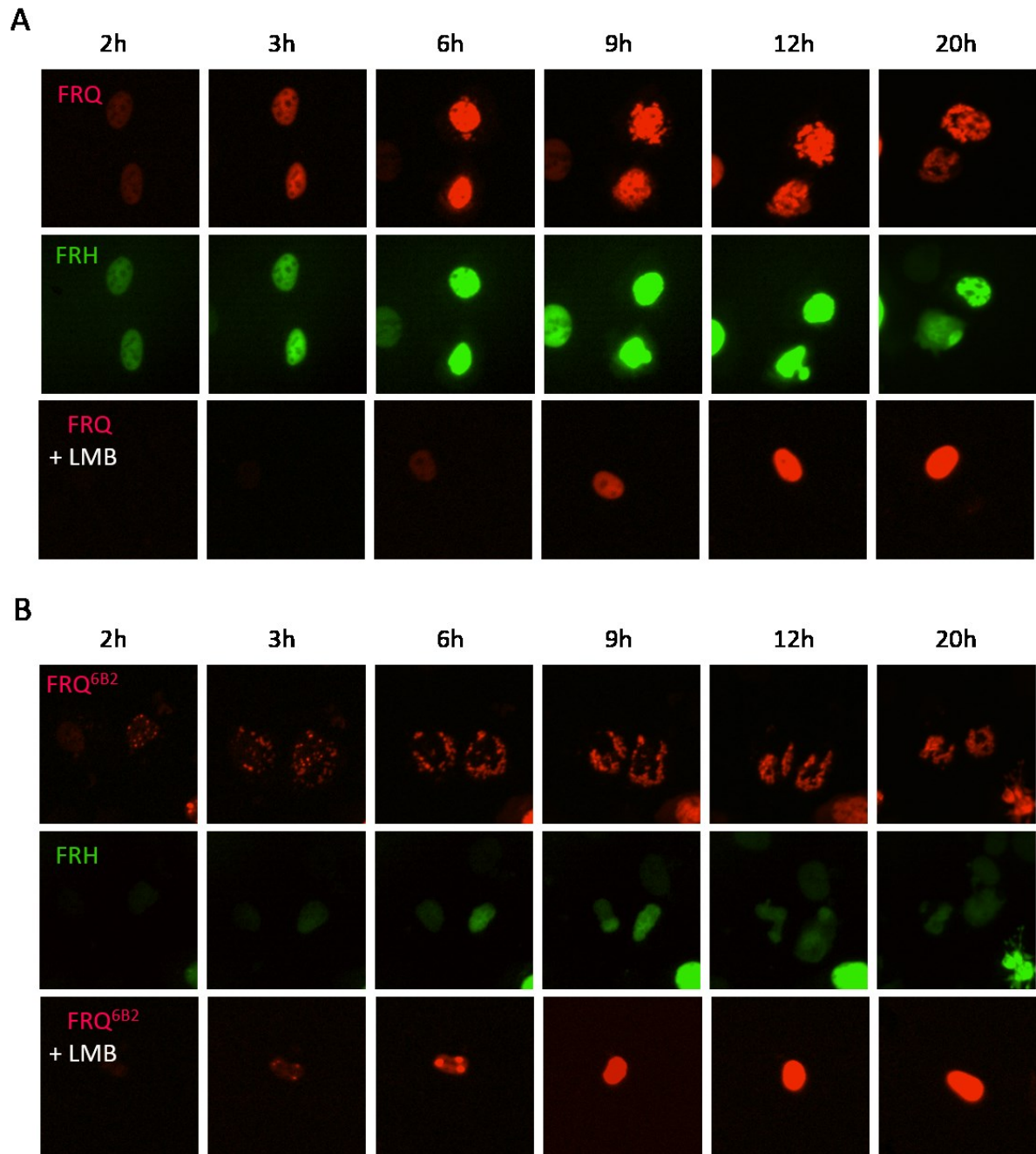


Figure continues on next page

C

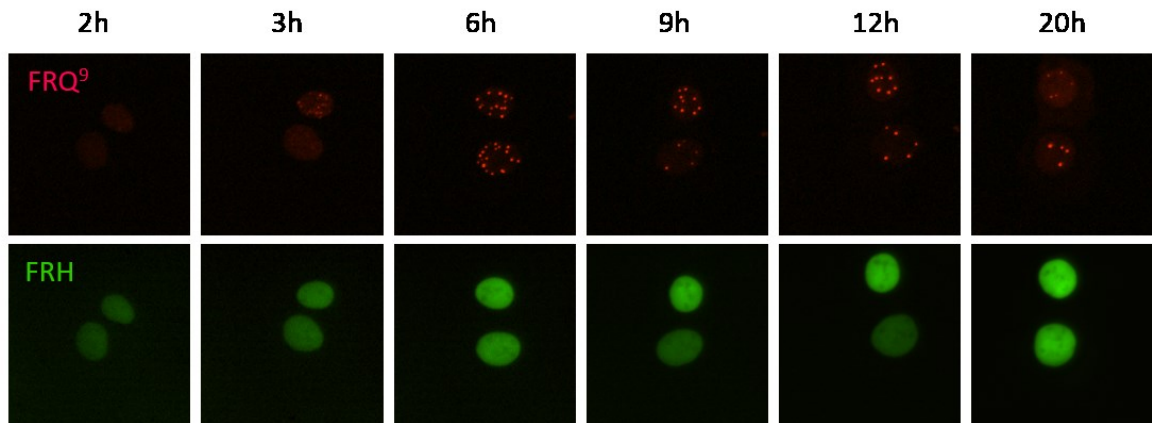


Figure S6: **Phosphorylation of FRQ by CK1a triggers its dissociation from FRH and nuclear export**

(A), (B) and (C): Co-expression of (A) mK2-FRQ, (B) mK2-FRQ^{6B2} or (C) mK2-FRQ⁹ with FRH-mNG and untagged CK1a between 2 to 20 h post induction with DOX. LMB was added when indicated. Data are identical to Figure 4.5.1b, but show separate panels for the mK2-tagged FRQ versions and FRH-mNG.

A

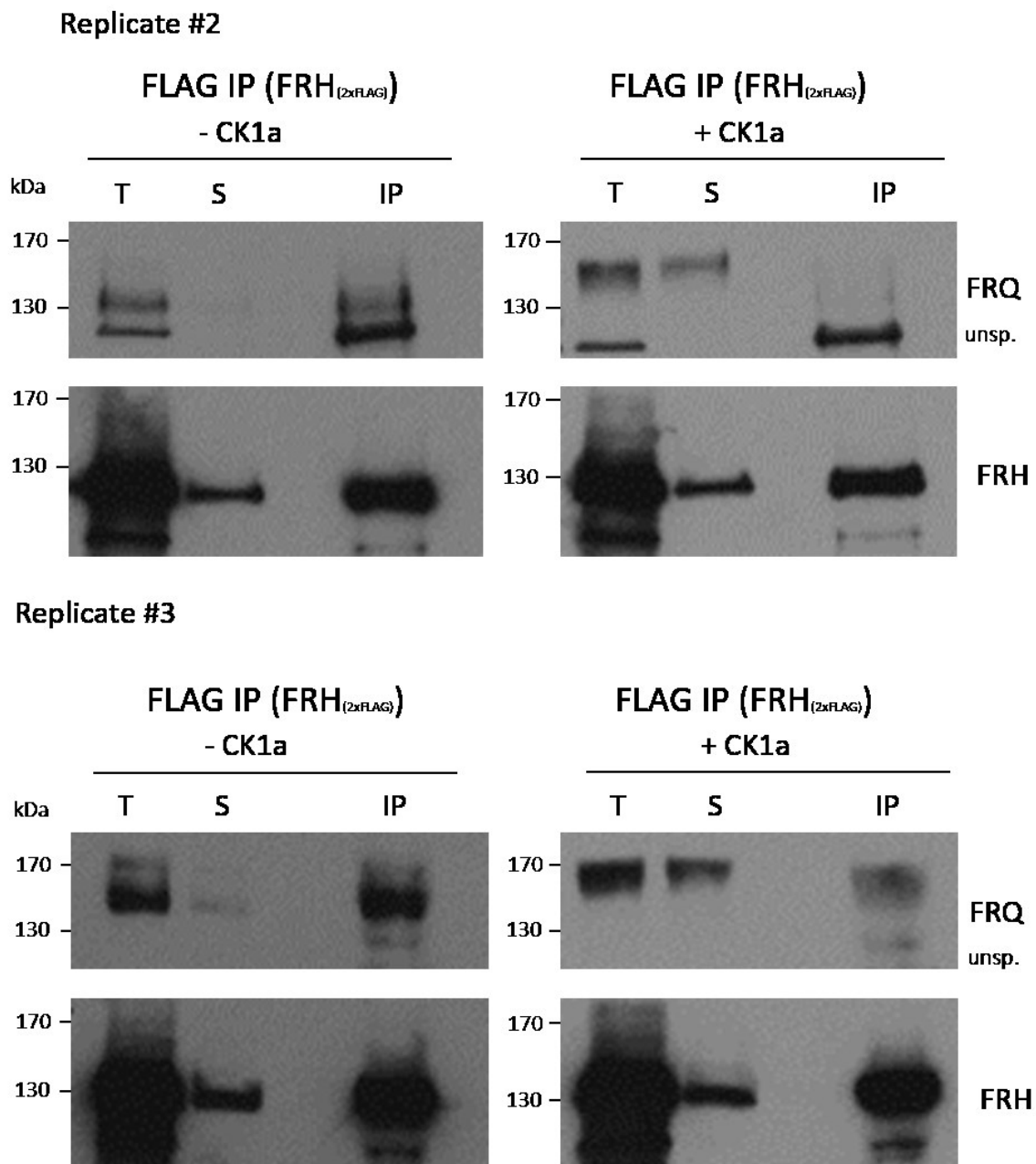


Figure S7: Phosphorylation of FRQ by CK1a triggers its dissociation from FRH
 Replicates of FLAG-FRH-IP from native *Neurospora* whole cell lysates (Figure 4.5.2a), showing co-IP of hypo- but not hyperphosphorylated FRQ.